

5-2017

ANDROGEN RECEPTOR AND PROSTATE CANCER CELL HETEROGENEITY

Qu Deng

Follow this and additional works at: https://digitalcommons.library.tmc.edu/utgsbs_dissertations



Part of the [Cancer Biology Commons](#), and the [Neoplasms Commons](#)

Recommended Citation

Deng, Qu, "ANDROGEN RECEPTOR AND PROSTATE CANCER CELL HETEROGENEITY" (2017). *The University of Texas MD Anderson Cancer Center UTHealth Graduate School of Biomedical Sciences Dissertations and Theses (Open Access)*. 744.

https://digitalcommons.library.tmc.edu/utgsbs_dissertations/744

This Dissertation (PhD) is brought to you for free and open access by the The University of Texas MD Anderson Cancer Center UTHealth Graduate School of Biomedical Sciences at DigitalCommons@TMC. It has been accepted for inclusion in The University of Texas MD Anderson Cancer Center UTHealth Graduate School of Biomedical Sciences Dissertations and Theses (Open Access) by an authorized administrator of DigitalCommons@TMC. For more information, please contact digitalcommons@library.tmc.edu.

ANDROGEN RECEPTOR AND PROSTATE CANCER CELL HETEROGENEITY

by

Qu Deng, B.Med.Sci.

APPROVED:

Dean Tang, M.D., Ph.D.

Advisory Professor

Mark Bedford, Ph.D.

Taiping Chen, Ph.D.

Sharon Dent, Ph.D.

Rick Finch, Ph.D.

APPROVED:

Dean, The University of Texas

MD Anderson Cancer Center UTHHealth Graduate School of Biomedical Sciences

ANDROGEN RECEPTOR AND PROSTATE CANCER CELL HETEROGENEITY

A

THESIS

Presented to the Faculty of

The University of Texas

MD Anderson Cancer Center UTHealth

Graduate School of Biomedical Sciences

in Partial Fulfillment

of the Requirements

for the Degree of

DOCTOR OF PHILOSOPHY

by

Qu Deng, B.Med.Sci.

Houston, Texas

May 2017

DEDICATION

To my parents for their endless love, support and encouragement

ACKNOWLEDGEMENTS

At the end of this most rewarding journey of my life, I would like to express my heartfelt gratitude towards everyone who helped me and contributed to my development. My mentor, Dr. Dean Tang, has been the best mentor I could ask for. I thank him for seeing my potentials to be a scientist before anyone else did. I thank for his trust in me to answer one of the most challenging questions in the field. I thank for his knowledge and patience in mentoring my PhD study. I thank for his encouragement and guidance when I felt lost. The professional lessons that Dr. Tang has bestowed on me are invaluable to my career to come.

I thank Dr. Mark Bedford, Dr. Shawn Bratton, Dr. Taiping Chen, Dr. Sharon Dent, Dr. Rick Finch, Dr. Feng Wang-Johanning, Dr. David Mitchell and Dr. Xuetong Shen for serving on my committees and providing insightful feedback on my research with their outstanding knowledge and experience.

I thank Dr. Xin Liu, who is so kind and patient to teach me all basic scientific procedures and to help me initiate my thesis research. I thank Dr. Can Liu for being the best friend of mine and for the joy and happiness we had together in Science Park. I also thank Dr. Kiera Rycaj for reviewing my thesis. I thank all the current and past Tang lab members who have worked together with me for the friendship and constant support. I thank all my colleagues in Science Park and Roswell Park Cancer Institute. Special thanks also go to Ms. Cindy Morgan, Ms. Judene Bliss and the IT departments in Science Park and Roswell Park Cancer Institute for setting up the videoconference defense.

Finally, I thank my parents for their endless love and support. I thank Ms. Yixin Zang for her love and companion, and for being the cheerleader of my life.

ANDROGEN RECEPTOR AND PROSTATE CANCER CELL HETEROGENEITY

Qu Deng, B.Med.Sci.

Advisory Professor: Dean Tang, M.D., Ph.D.

Androgen receptor (AR) plays an important role in prostate cancer (PCa) development and has been the main therapeutic target in advanced PCa. AR expression is heterogeneous in both primary PCa and castration resistant prostate cancer (CRPC). However, the functional significance of AR heterogeneity in regulating PCa biology and response to androgen/AR-targeted therapies remains unclear. The overarching hypothesis for my Ph.D is that **AR heterogeneity contributes to PCa development, progression, and therapy resistance**. A more specific postulate is that PCa cells expressing AR (i.e, AR⁺) and PCa cells expressing little AR (i.e, AR^{-/lo}) possess intrinsically distinct biological and tumorigenic properties as well as sensitivities to AR-targeting therapies. Here I tested my hypothesis by generating RFP-tagged AR⁺ LNCaP clones with zinc finger nucleases (ZFNs) and isogenic AR knockout (AR-KO) LNCaP clones with CRISPR-cas9 technology. With the novel genetically matched clones, we demonstrate that the AR⁺ and AR-KO clonal LNCaP cells manifest contrasting tumor-regenerating capacities and responses to castration and AR antagonists. Specifically, AR⁺ LNCaP cells are highly tumorigenic in androgen-dependent (AD) environment and are exquisitely sensitive to androgen-deprivation therapy (ADT). On the contrary, AR-KO LNCaP cells possess high tumor-initiating and tumor-propagating capabilities in androgen-ablated environment. Further, AR-KO LNCaP cells are resistant to the current AR antagonist enzalutamide. Thus, our study links AR heterogeneity to distinct castration

and enzalutamide responses and suggests the urgency in developing novel therapeutics to target AR^{-/-} PCa cells/clones.

TABLE OF CONTENTS

APPROVAL PAGE	i
TITLE PAGE.....	ii
DEDICATION	iii
ACKNOWLEDGEMENTS.....	iv
ABSTRACT.....	vi
TABLE OF CONTENTS	viii
LIST OF ILLUSTRATIONS.....	xi
ABBREVIATIONS.....	xiv
Chapter 1. Introduction.....	1
1.1. Cancer stem cells and tumor heterogeneity.....	2
1.2. Prostate cancer stem cells (PCSCs).....	6
1.3. Androgen receptor (AR) heterogeneity in prostate cancer.....	10
1.4. PCSCs in primary and untreated PCa: AR negativity and signaling mechanisms.....	21
1.5. PCSCs in CRPC might be AR ⁺ or AR ⁻	26
1.6. AR and PCSCs in PCa metastasis	30
1.7. Clinical implications and perspectives.....	32
Chapter 2. Build AR reporter systems by using PSA and AR promoters.....	35
2.1. Introduction	36
2.2. Materials and methods.....	39

2.3. Results	43
2.3.1. Identify AR ^{-/-} LNCaP clones using the PSAP-eGFP lentivector.....	43
2.3.2. Establish ARP-RFP reporters to separate AR ⁺ and AR ^{-/-} PCa cells	49
2.4. Discussion	54
Chapter 3. Build AR-tagging clones with Zinc Finger Nucleases (ZFNs)	56
3.1. Introduction	57
3.2. Materials and methods.....	61
3.3. Results	68
3.3.1. Design an AR tracking model in PCa cells with ZFNs	68
3.3.2. ZFN14-mediated AR tagging in K562 cells.....	74
3.3.3. ZFN14-mediated AR tagging in LNCaP cells	77
3.3.4. ZFN14-mediated AR tagging in PC3 cells	86
3.4. Discussion	88
Chapter 4. Generate AR Knockout (KO) PCa cell clones using CRISPR-cas9 technique.....	90
4.1. Introduction	91
4.2. Materials and methods.....	93
4.3. Results	96
4.3.1. Design efficient gRNAs to target human AR in LNCaP cells	96
4.3.2. Establish AR-KO LNCaP cell clones	99
4.3.3. Characterize AR functions in the AR-KO clones	102
4.4. Discussion.....	105

Chapter 5. Functional and molecular studies in isogenic AR⁺ and AR-KO LNCaP cells.....	107
5.1. Introduction	108
5.2. Materials and methods.....	110
5.3. Results	114
5.3.1. AR ⁺ cells are more tumorigenic in androgen-proficient environment.....	114
5.3.2. AR-KO LNCaP cells are resistant to castration and highly tumorigenic in castrated mice	120
5.3.3. AR-KO LNCaP cells are resistant to Enzalutamide	127
5.4. Discussion	134
Bibliography.....	138
Vita.....	162

LIST OF ILLUSTRATIONS

Figure 1-1 Unified model of clonal evolution and cancer stem cells	5
Figure 1-2 A hypothetical model of tumorigenic heterogeneity of human PCa cells	9
Figure 1-3 Genomic organization of the AR gene and overall domain structure of the AR protein.....	15
Figure 1-4 Heterogeneous and discordant PSA and AR protein expression in PCa	16
Figure 1-5 Heterogeneous and discordant PSA and AR protein expression in PCa	17
Figure 1-6 AR and PSA protein expression in CRPC	19
Figure 1-7 Heterogeneous and discordant AR and PSA protein expression in PCa cell models in both AD and AI conditons.	20
Figure 1-8 PCSCs in untreated/primary PCa.	25
Figure 1-9 Hypothetical PCSCs in CRPC	29
Figure 2-1 PSAP-GFP lentivector	38
Figure 2-2 AR ^{-/-} LNCaP cell population is enriched in the PSA ^{-/-} cell population.....	45
Figure 2-3 Single cell cloning of the GFP ⁺ and GFP ^{-/-} LNCaP cells	46
Figure 2-4 AR and PSA expression in the clones	47
Figure 2-5 AR and PSA mRNA expression levels in the clones	48
Figure 2-6 AR promoter fragments and luciferase report assays.....	51
Figure 2-7 ARP-DsRed reporter studies in LNCaP cells.	52
Figure 2-8 ARPs in pLVX-DD-tdTomato lentiviral reporter system.	53
Figure 3-1 Stucture and design of ZFNs, and the outcome of genome editing using programmable nucleases	59
Figure 3-2 ZFNs and the donor structure map	62

Figure 3-3 Cel-1 assay and junction PCR	67
Figure 3-4 workflow of generating AR-tagging clones with ZFNs.	69
Figure 3-5 AR tagging strategy	70
Figure 3-6 Consensus sequence at the AR C terminal region in 4 human PCa cell lines.	71
Figure 3-7 ZFN candidates for AR targeting	72
Figure 3-8 Donor plasmid verification.....	73
Figure 3-9 Cutting efficiency of ZFN14 in K562 cells	75
Figure 3-10 AR tagging system in K562 cells	76
Figure 3-11 Cutting efficiency of ZFN14 in LNCaP cells	80
Figure 3-12 Alternative ZFNs and donor plasmid modifications.....	81
Figure 3-13 The AR tagging system in LNCaP cells	82
Figure 3-14 Genotyping of the RFP clones	83
Figure 3-15 Characterizations of the AR-tagged clones	84
Figure 3-16 AR siRNA knockdown in RFP ⁺ clones	85
Figure 3-17 The AR tagging system in PC3 cells.....	87
Figure 4-1 Schematic of the RNA-guided Cas9 nuclease.....	92
Figure 4-2 General strategies to generate AR-KO LNCaP clones using the CRISPR-cas9 system	97
Figure 4-3 AR-KO with CRISPR-cas9 in bulk LNCaP cells.....	98
Figure 4-4 Screening of AR-KO clones	100
Figure 4-5 Genotype of the AR-KO clones.....	101
Figure 4-6 Attenuated AR signaling in AR-KO clones.....	103
Figure 4-7 Lower AR activity and blunted DHT responses in AR-KO cells.	104

Figure 5-1 AR ⁺ cells possess higher clonal and sphere-forming abilities in androgen-proficient conditions than AR-KO cells	116
Figure 5-2 AR ⁺ LNCaP cells are more proliferative than the isogenic AR-KO cells in androgen-proficient conditions.	117
Figure 5-3 AR ⁺ cells are more tumorigenic in intact NOD-SCID and NSG mice compared to isogenic AR-KO LNCaP cells.	118
Figure 5-4 AR ⁺ LNCaP cells are more tumorigenic in testosterone-supplemented NSG mice than isogenic AR-KO cells.	119
Figure 5-5 AR-KO LNCaP cells are more tumorigenic than AR ⁺ cells in castrated hosts.	123
Figure 5-6 AR-KO LNCaP cells are more tumorigenic than AR ⁺ LNCaP cells in the same castrated NSG mice	124
Figure 5-7 The dynamics of AR-KO and AR ⁺ LNCaP cells in animals with different systemic androgen levels	126
Figure 5-8 AR-KO LNCaP clonal cells form more clones and spheres than the clonally derived AR ⁺ LNCaP cells under Enzalutamide treatment.	129
Figure 5-9 AR-KO LNCaP clonal cells are resistant to Enzalutamide treatment <i>in vitro</i>	130
Figure 5-10 AR-KO LNCaP cells are resistant to Enzalutamide treatment <i>in vivo</i>	132

ABBREVIATIONS

μL	microliter
ml	milliliter
μg	microgram
kg	kilogram
mg	milligram
μM	micromolar
nM	nanomolar
ACD	Asymmetric Cell Division
AD	Androgen Dependent
ADT	Androgen Deprivation Therapy
AR	Androgen Receptor
ARE	AR Responsive Elements
ARP	AR Promoter
BAT	Bipolar Androgen Therapy
CARN	Castration-Resistant Nkx3.1-expressing cells
CRISPR-cas9	Clustered Regularly Interspaced Short Palindromic Repeats- CRISPR-associated 9
CRPC	Castration-Resistant Prostate Cancer
CSC	Cancer Stem Cell
DBD	DNA Binding Domain
DHT	Dihydrotestosterone
DSB	Double Strand Break

EMT	Epithelial-to-Mesenchymal Transition
ESC	Embryonic Stem Cells
FACS	Fluorescence-Activated Cell Sorting
FFPE	Formalin-Fixed Paraffin-Embedded
GR	Glucocorticoid Receptor
GnRH	Gonadotropin-Releasing Hormone
HDR	Homology-Directed Repair
HPCa	Human Prostate Cancer
HR	Homologous Recombination
HSC	Hematopoietic Stem Cell
IHC	Immunohistochemistry
IF	Immunofluorescence
i.p.	intraperitoneal injection
KO	Knock Out
LBD	Ligand-Binding Domain
MET	Mesenchymal-Epithelial Transition
MOI	Multiplicity of Infection
NHEJ	Non-homologous End Joining
NOD/SCID	Non-Obese Diabetic/Severe Combined Immunodeficiency
NSG	NOD/SCID-IL2R $\gamma^{-/-}$ mice
NTD	NH2-Terminal Domain
PAM	Protospacer Adjacent Motif
PCa	Prostate Cancer
PCSC	Prostate Cancer Stem Cell

PSA	Prostate Specific Antigen
PSAP	PSA Promoter
s.c.	subcutaneous
sgRNA	single guide RNA
SP	Side Population
TALEN	Transcription Activator Like Effector Nucleases
t.i.w.	three times a week
TMA	Tissue Microarray
ZFN	Zinc-Finger Nuclease

Chapter 1. Introduction

This chapter is based on two published works: Deng, Q. and Tang, D.G., *Androgen receptor and prostate cancer stem cells: biological mechanisms and clinical implications*. Endocrine-Related Cancer, 2015. 22(6): p. T209-20. [1]. And Liu, X., Chen, X., Rycak, K., Chao, H.P., Deng, Q., Jeter, C., Liu, C., Honorio, S., Li, H., Davis, T., Suraneni, M., Laffin, B., Qin, J., Li, Q., Yang, T., Whitney, P., Shen, J., Huang, J., and Tang, D.G., *Systematic dissection of phenotypic, functional, and tumorigenic heterogeneity of human prostate cancer cells*. Oncotarget, 2015. 6(27): p. 23959-86. [2]

No permission is required.

1.1. Cancer stem cells and tumor heterogeneity

Clonal evolution, driven by genetic instability in cancer cells, generates cellular heterogeneity within tumors. These genetically heterogeneous cellular clones are in persistent evolution during disease progression and clinical treatment, wherein subclones with advantageous survival attributes such as drug resistance, become dominate and survive (Figure1-1; top). This mode of progression results in extensive branching evolution, which can subsequently lead to variable numbers of clonal cell expansions that define multifocal cancer. The multifocal and heterogeneous nature of prostate cancer (PCa) has hindered efforts to understand tumor cell clonality, and the origin of PCa remains controversial. High-resolution genome technologies have led to data supporting independent tumor origins as well as a monoclonal origin of multifocal PCa. In support of the former, recent genome-wide DNA sequencing of multifocal PCa revealed the existence of multiple independent clonal expansions within each patient [3]. Even morphologically normal regions of the prostate possessed as many as ten genetic mutations, with several shared by cancer samples within the same patient, suggesting these clones existed prior to the formation of the distinct cancer lineages. The recent use

of next generation sequencing has led to an expansion in our understanding of the complex genetic basis of PCa. Genetic alterations, such as TMPRSS2-ERG fusion and PTEN deletion within tumor clones, have been shown to activate critical signaling pathways such as ERG and PI3K, thus driving clonal evolution in patients with “high-risk” primary PCa [4]. In an effort to identify genomic alterations that characterize a monoclonal origin of a lethal metastatic cell clone in a patient with CRPC (castration-resistant prostate cancer), authors of a recent study found that during 17 years of tumor progression, only the tumor clones with *PTEN*, *P53* and *SPOP* (Speckle-type POZ protein) mutations gained additional genetic alterations and gave rise to lethal metastatic tumors [5]. Surprisingly, the lethal clone (defined by the presence of the same *PTEN*, *P53*, and *SPOP* mutations) in this patient was found to arise from a morphologically low-grade (Gleason 3) tumor focus instead of from the predominant Gleason 4 tumor foci. Whole-genome exome sequencing in 50 lethal, and heavily pre-treated metastatic CRPCs also confirmed the monoclonal origin of lethal CRPC [6]. Regardless of origin, these examples highlight the importance of genetically-driven clonal evolution in driving PCa progression.

Additionally, there is also strong evidence that tumor cells within a genetically identical clone possess different tumorigenic abilities and, in most cases, are organized in a hierarchical manner [7-9] (Figure1-1; bottom). Sitting at the apex of this tumorigenic hierarchy, in untreated tumors, is the small subset of stem-like cancer cells, or cancer stem cells (CSCs) that possess high self-renewal and differentiation ability. In other words, CSCs can sustain an established tumor clone through unlimited self-renewal and maintain intraclonal heterogeneity through generating both tumorigenic and less or non-tumorigenic cancer cells. Similar to normal hematopoietic stem cells (HSCs), which are

among the best-understood adult stem cells, the best-characterized CSCs are CSCs in leukemia or leukemic stem cells [8]. Like HSCs, LSCs are undifferentiated lacking the expression of lineage differentiation markers. Subsequent studies have led to the identification of CSCs in multiple human solid tumors and a common phenotypic feature appears to be the lack of differentiation markers and regulators [7-9].

In a strict sense, CSCs in human tumors are defined as a population of cancer cells, when prospectively purified from patient tumors, xenografts, and even long-term cultures, can regenerate and also indefinitely propagate human tumors in immune-deficient mice. In reality, CSC properties of a candidate population of human tumor cells are best assessed by performing limiting dilution tumor-regeneration assays combined with serial tumor transplantations and cell biological (e.g., clonal in 2D; clonogenic in 3D; sphere formation; single-cell division and differentiation; etc) as well as molecular (e.g., RNA-Seq and ChIP-Seq) characterizations [10]. The tumor cell population that can initiate or regenerate tumors at low cell doses is considered to be tumor-initiating or tumor-regenerating cells while the tumor cell population that can long-term propagate human xenograft tumors is called tumor-propagating cells [10]. Unfortunately, many of the reported CSC populations do not fully satisfy this strict definition. For example, some studies only utilized cell lines to perform in vitro assays without tumor experiments, whereas others only performed tumor experiments without carrying out further serial transplantations. Such deficiencies have created confusion and disbelief in the field of CSCs. Nevertheless, recent lineage tracing studies in genetically driven mouse model tumors (i.e., glioblastoma, and intestinal and skin tumors) have provided definitive evidence for CSCs [10].

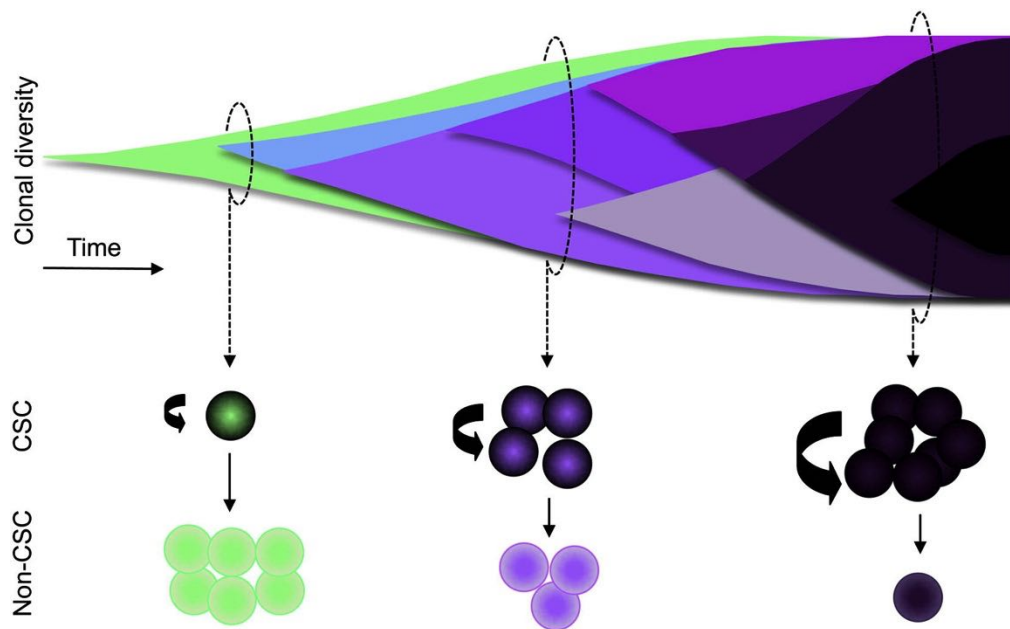


Figure 1-1 Unified model of clonal evolution and cancer stem cells

This figure is reproduced from Kreso, A. and Dick, J.E., *Evolution of the cancer stem cell model*. Cell Stem Cell, 2014. **14**(3): p. 275-91. [8] with permission of Cell Stem Cell license Number 3963820933777.

Acquisition of favorable mutations can result in clonal expansion of the founder cell. In parallel, another cell may gain a different mutation that allows it to form a new subclone. Over time, genetic mutations accumulate and subclones evolve in parallel. The bottom panel shows that it may be that CSCs are not static entities but can evolve over the lifetime of a cancer as genetic changes can influence CSC frequency. Some subclones may contain a steep developmental hierarchy (left), where only few self-renewing CSCs exist among a large number of non-CSCs. Other subclones (middle) may contain an intermediate hierarchy, where the number of CSCs is relatively high but a hierarchy still exists. Some subclones may have the genetic alterations that confer high self-renewal potential, where most cells are tumorigenic, as frequently observed in advanced and treatment-failed clinical tumors. In this scenario, applying the CSC concept to such homogeneous subclones is not warranted because most cells can self-renew and few non-CSC progeny are generated. [8]

1.2. Prostate cancer stem cells (PCSCs)

The CSC model helps explain the generation of tumor cell heterogeneity from the viewpoint of stem cell maturation and differentiation. PCa is well known to be a highly heterogeneous malignancy, with each tumor harboring many tumor clones [3, 5]. Therefore, evidence supporting the existence of PCSC populations does not come as a surprise [11, 12] (Figure 1-2). PCSCs are defined, more or less, using a spectrum of classical *in vitro* and *in vivo* assays used to define CSCs (see above). *In vitro*, PCSCs preferentially express stem cell and CSC-associated molecules, self-renewal genes (e.g., Bmi-1, Stat3, Nanog, Sox2, Oct4) and possess high clonal and clonogenic capacities. *In vivo*, PCSCs possess higher tumor-initiating and serial tumor-propagating activities than non-PCSCs in immunodeficient mice [11-13]. Three papers, published in 2005, simultaneously provided the earliest proof-of-principle evidence for PCSCs: 1) the Side Population (SP) in the LAPC9 human xenografts was enriched in tumor-initiating cells [14]; 2) ABCG2, a surface pump protein normally involved in cellular detoxification, mediated efflux of androgen in putative PCSCs [15]; and 3) the CD44⁺α2β1⁺CD133⁺ PCa cells from patient prostate tumors possessed high clonogenic survivability in methylcellulose [16].

Our lab, since 2002, has been employing and developing a variety of experimental strategies to elucidate the cellular basis and molecular regulation of PCa cell heterogeneity in an effort to link PCa cell heterogeneity to therapy resistance and tumor relapse (Figure 1-2). Virtually all of our PCSC studies have been based on tumor-regeneration and, in many cases, serial tumor transplantation assays. Using the SP analysis, we were the first to provide evidence that the SP in certain PCa xenograft models is enriched in tumor-regenerating and tumor-propagating cells and thus satisfies

the strict definition of CSCs [14]. Using cell surface markers, our systematic studies have provided convincing evidence that the CD44 high-expressing (i.e., CD44⁺) PCa cell population in most, though not all, PCa models we have studied, is significantly enriched in PCSCs with enhanced tumor-regenerating, tumor-propagating, and metastatic capacities [2, 17-19]. Using holoclone assays, we have shown that the PCa cell holoclones, like stem cell-enriched primary keratinocyte holoclones, possess long-term tumor-propagating CSC properties [20]. Using lentiviral-mediated lineage tracing, we have demonstrated that the phenotypically undifferentiated PCa cell population that lacks the expression of PSA (i.e., PSA^{-lo}), harbors self-renewing long-term tumor-propagating PCSCs, which express stem cell genes and epigenetic profiles, can undergo authentic asymmetric cell division, and are intrinsically refractory to castration treatments [2, 7].

Similar to the heterogeneity of CSC populations observed in other tumor systems [7], the heterogeneous PCSC pool contains CSC subsets with distinct tumor-regenerating and tumor-propagating capabilities [2], supporting evidence of different PCSC populations reported by others [16, 21-24]. Akin to the undifferentiated nature of LSCs and other CSCs [7], a common phenotypic trait reported in PCSC populations is the lack of expression of differentiation regulators and markers such as AR (see below), PSA [7], and MHC molecules [21].

One of the major unresolved questions related to PCSCs is whether subpopulations of PCa cells purified from primary patient tumors or CRPCs, truly possess hardcore CSC properties such as the ability to regenerate tumors at the single-cell level and/or support serial tumor transplantations. Although patient tumor or early PDX (patient-derived xenograft) derived cells have been shown, in many experimental settings, to possess certain CSC properties (especially in vitro), the answer to this

question has remained unknown mainly due to the current technical difficulties in recapitulating human PCa development in immunodeficient mice [12].

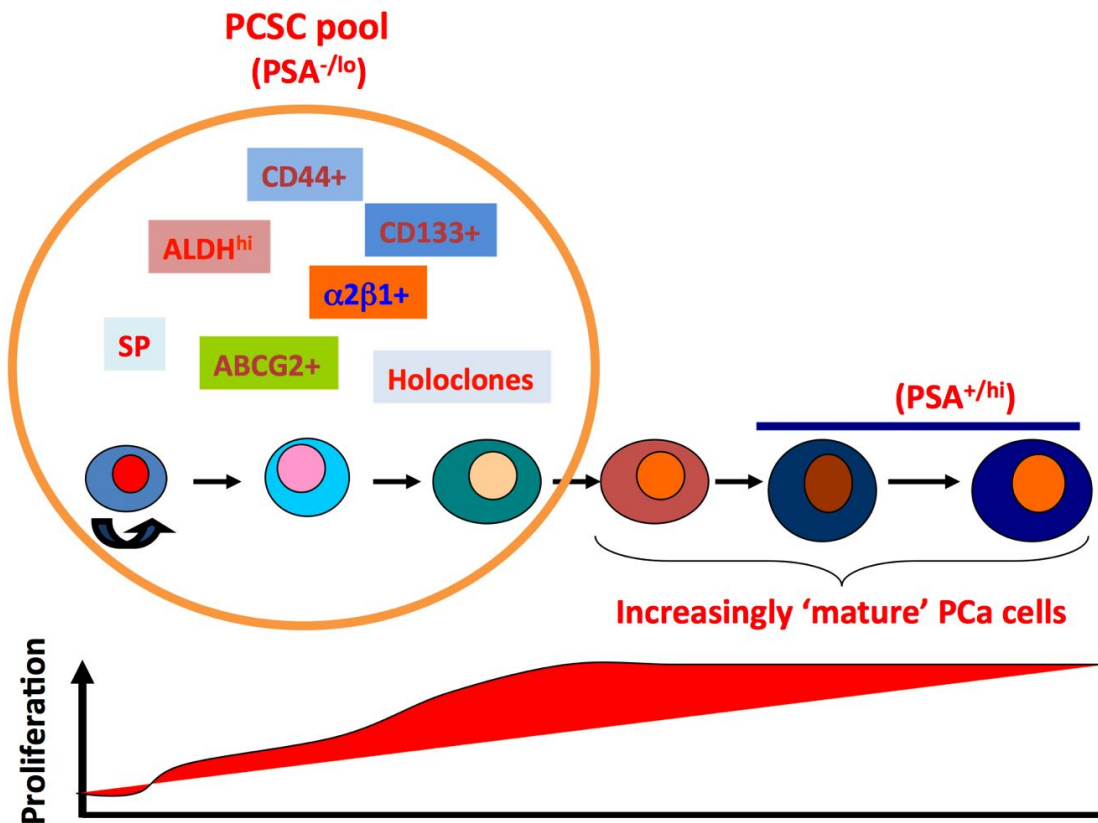


Figure 1-2 A hypothetical model of tumorigenic heterogeneity of human PCa cells

This figure is reproduced from Liu, X., Chen, X., Rycaj, K., Chao, H.P., Deng, Q., Jeter, C., Liu, C., Honorio, S., Li, H., Davis, T., Suraneni, M., Laffin, B., Qin, J., Li, Q., Yang, T., Whitney, P., Shen, J., Huang, J., and Tang, D.G., *Systematic dissection of phenotypic, functional, and tumorigenic heterogeneity of human prostate cancer cells*. Oncotarget, 2015. **6**(27): p. 23959-86. [2] with permission of Oncotarget

Prostate tumors contain a spectrum of cancer cells at different stages of differentiation (marked by cells of varying colors and sizes). Undifferentiated ($PSA^{-/lo}$) PCa cells are quiescent (thus low proliferative index; below) and can undergo assymetric cell division (ACD) developing into differentiated (PSA^{+}) cells. The $PSA^{-/lo}$ PCa cells possess long-term tumor-propagating activity. Importantly, the $PSA^{-/lo}$ PCa cell population is still heterogeneous containing tumorigenic subsets including the castration-resistant cells. In contrast, fully differentiated (PSA^{+}) PCa cells, despite being highly proliferative (thus high proliferative index, below), only undergo symmetric cell division and possess more limited tumor-propagating capabilities.[2]

1.3. Androgen receptor (AR) heterogeneity in prostate cancer

AR is a master regulator of normal prostate differentiation and development. Human *AR* gene, located on chromosome Xq11-12, encodes a protein with four functional domains: the NH₂-terminal domain (NTD), the DNA binding domain (DBD), the hinge domain and the ligand-binding domain (LBD) (Figure 1-3). The AR protein is expressed in the luminal cell layer of the prostatic glands, and AR signaling critically regulates development, differentiation, and maintenance of the prostate as documented in both human and animal studies. Somatic mutations of the *AR* gene lead to malfunction of AR and androgen insensitivity syndrome in human, in which 46 XY individuals present female phenotype and the prostate is absent [25]. The *AR* NTD knockout male mice all have small immature testes and lack secondary reproductive organs [26].

Simanainen *et. al.* [27] established an *AR* exon 3 knockout mouse model and observed under-developed prostate in the male mice with delayed structural and functional differentiation of the prostate epithelium. Increased proliferation in the *AR* deficient epithelium was also observed [27]. In another prostate-specific AR knockout mouse model, Wu *et. al.* [28] also reported increased proliferation and less differentiation of the epithelium. These genetic studies suggest that AR promotes prostate differentiation and suppresses epithelium proliferation in the mature prostate; in this manner, AR signaling maintains the homeostasis and relative dormancy of mature prostate epithelium. Consistent with this pro-differentiation role of AR, prostate epithelial-specific *AR* knockout promoted TRAMP tumor development, providing genetic evidence for the tumor-suppressive function of AR [29].

Somewhat paradoxically, however, AR expression is frequently overexpressed in PCa and, in fact, AR is thought to be required for prostate tumorigenesis and hence,

targeting AR and AR signaling has long been a therapeutic strategy. Androgen-deprivation therapy (ADT) aims to block androgen synthesis (e.g., Abiraterone) or AR functions (e.g., bicalutamide, Enzalutamide). Nevertheless, AR expression has been observed to be heterogeneous in primary, and in particular, in treatment-failed patient tumors.

Ruizeveld de Winter *et. al.* [30] examined AR expression via immunohistochemistry (IHC) staining in 26 primary PCa, and found that 7 cases presented considerable heterogeneity in AR expression as well as a decrease in the proportion of AR-expressing cells in more aggressive tumors. Similar AR IHC staining by Masai *et. al.* [31] revealed that AR expression correlated inversely with grade. Also, Chodak *et. al.* [32] analyzed AR expression in 57 untreated PCa and observed that AR content was significantly higher in differentiated tumors compared to that of poorly differentiated tumors. Immunofluorescence (IF) analysis of AR and PSA proteins in 11 untreated primary patient tumors in our lab showed that both AR⁺ and AR⁻ subpopulations of PCa cells could be identified in all samples, although, as expected, the AR⁺PSA⁺ PCa cells represented the major subpopulation (Figure 1-4 and 1-5). The AR⁻ PCa cells in primary (untreated) PCa samples represented ~5 - 30% of the total (Figure 1-4D) [2]. Overall, these and many other studies suggest that, although AR⁻ cells may not constitute the dominant cell population in treatment naïve tumors, all primary prostate tumors nevertheless harbor both AR⁺ and AR⁻ cells and clones.

AR heterogeneity in hormone-refractory PCa has been observed since the early 1990's. van der Kwast *et. al.* [33] examined AR expression in CRPC and found that in 13/17 tumors, over 80% of the tumor cells were AR⁺. However, 3 tumors showed a considerable heterogeneity in AR expression and in 1 sample, nearly all tumor cells

appeared AR^{-lo}. Sadi *et. al.* [34] observed similar AR heterogeneity in needle biopsy specimens of 17 patients with Stage D PCa. Ruizeveld de Winter *et. al.* [35] examined AR expression in locally progressive CRPC and found that less differentiated PCa cells tended towards diminished AR expression. Computer qualification of nuclear AR levels in PCa patient samples showed that the AR concentration per cell was significantly more heterogeneous in poor responders [36]. AR expression varies in metastases as well. Shah *et. al.* [37] investigated AR expression via IHC staining in metastatic lesions of 30 CRPC patients who underwent warm autopsy, and observed wide variations in AR expression between tumor samples. Specifically, 31% (83 of 265) of metastatic samples had <50% AR⁺ cells and 41.5% (100/265) metastases had <10% AR⁺ cells. Five patient metastases had <1% AR⁺ cells [37]. Similarly, Davis *et. al.* [38] reported that both AR⁺ cells and AR staining intensity decreased in metastatic CRPC cells compared with benign tissues or untreated PCa. Of note, two commonly used PCa cell lines, Du145 and PC3, which were derived from brain and bone metastasis, respectively, and possess high tumorigenic and metastatic capacities, lack AR expression. ARCaP cells, derived from the ascites fluid of a disseminated CRPC, express little AR [39]. Bone metastases MDA PCa 118a/118b also completely lack AR (and PSA) expression [40].

My colleagues and I analyzed AR and PSA protein expression in 23 CRPC samples including 20 samples (CRPC1–20) (Figure 1-6A) in a tissue microarray (TMA) and 3 regular CRPC (CRPC21–23) samples (Figure 1-6B). AR expression showed wide variability in these CRPC samples. For example, CRPC5 and CRPC12 showed increased AR expression and an increase in AR⁺ PCa cells compared to untreated PCa; but many CRPC samples (e.g., CRPC9, 16, and 20–23) significantly lacked AR⁺ PCa cells (Figure 1-6). Furthermore, in all AR⁺ CRPC samples, AR⁻ PCa cells could be

readily identified, e.g., in CRPC8 and CRPC2 and CRPC7. In sharp contrast to AR expression patterns, the majority of the 23 CRPC samples lacked appreciable PSA expression and PSA⁺ PCa cells (Figure 1-6). Only one sample (CRPC12) was found to have concordant AR and PSA expression and only CRPC19 (the patient was treated with Lupron for ~2 weeks) expressed high intratumoral PSA (Figure 1-6 B). The IHC studies in this CRPC cohort indicate that AR heterogeneity is more prominent in CRPC than primary PCa, but PSA^{-/lo} PCa cells (which can be AR⁺ or AR⁻) are enriched in CRPC patient samples [2].

Subsequently, we investigated the relative abundance of the 4 subtypes of PCa cells (i.e., AR⁺/PSA⁺, AR⁺/PSA⁻, AR⁻/PSA⁺, AR⁻/PSA⁻) in 3 AD (androgen-dependent) and AI (androgen-independent) PCa xenograft models (LNCaP, LAPC4 and LAPC9) [7]. In all 3 models, the AI tumors were highly enriched in PSA^{-/lo} PCa cells (Figure 1-7). In LNCaP AD tumors, ~80% of the cells were AR⁺PSA⁺ and the other 3 subtypes of cells represented the minority (Figure 1-7, A and B). In contrast, the LNCaP AI tumors showed greatly reduced AR⁺PSA⁺ cells and dramatically increased PSA^{-/lo} (AR⁺PSA^{-/lo} and AR⁻PSA^{-/lo}) cells (Figure 1-7, A and B). Similarly, PSA^{-/lo} PCa cells were significantly increased in LAPC4 (Figure 1-7, C) and LAPC9 (not shown) AI tumors. Interestingly, in LAPC4 AI tumors, most AR localized to the cytoplasm (Figure 1-7, C).

Similar AR heterogeneity has also been observed in prostatic-specific transgenic mouse models. In ARR₂Pb driven c-Myc (i.e., Hi-Myc) model [41], the residual tumors five months post-castration expressed low and heterogeneous levels of cytoplasmic AR compared to the intact mice. These castration-resistant Hi-Myc tumor cells were also quiescent as confirmed by negative Ki67 staining [41]. In prostate-specific *Pten*-deleted mouse prostate, although most tumor cells expressed AR after 10 weeks' castration, the

expression level was weaker and more diffuse compared to the hormonally intact prostate [42].

AR heterogeneity in CRPCs has a genetic basis. Recent sequencing efforts in a cohort comprised of 150 patients with metastatic CRPC suggested that genetic alterations of AR (mutations, amplifications) become enriched in CRPCs (~63% patients) compared to those in untreated tumors [43]. In addition to mutations in *AR* itself, alterations of members in the AR signaling pathway were also observed in metastatic CRPCs, including *FOXA1* and *NCOR1/2*, among others. Similarly, by comparing 50 lethal CRPCs and 11 primary PCa, Grasso *et. al.* [6] identified mutations in *FOXA1* and *MLL2* in CRPCs that likely change the AR signaling in treatment-failed tumors.

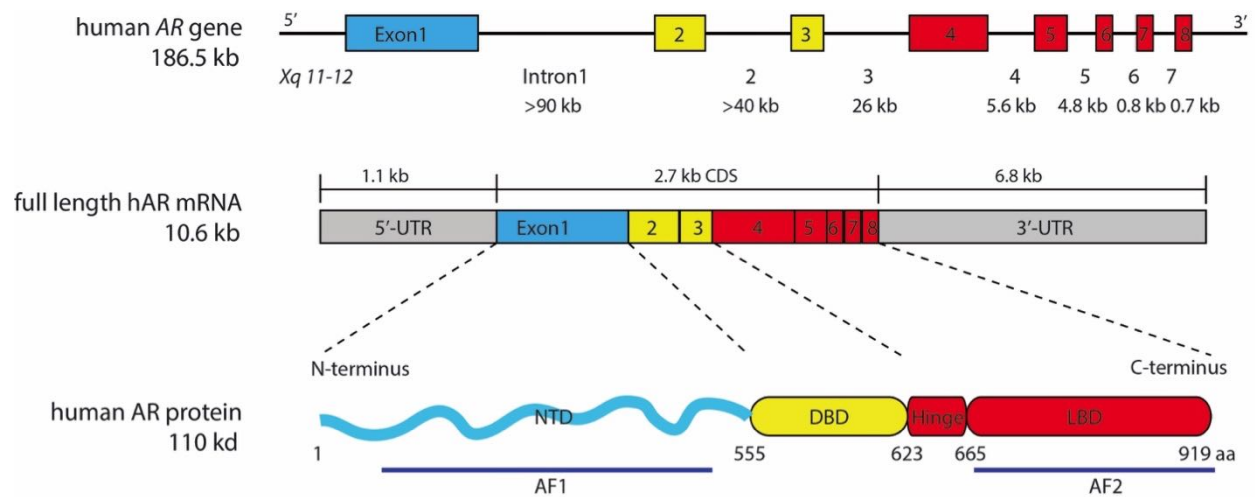


Figure 1-3 Genomic organization of the AR gene and overall domain structure of the AR protein.

This figure is reproduced from Deng, Q. and Tang, D.G., *Androgen receptor and prostate cancer stem cells: biological mechanisms and clinical implications*. Endocrine-Related Cancer, 2015. 22(6): p. T209-20. [1] with the permission of Endocrine-Related Cancer.

The AR gene, located on the long arm of X chromosome and spanning 186.5 kb, It contains eight exons interrupted by introns of various lengths (indicated below). The AR transcript is 10.6 kb with exon 1 coding for the N-terminus domain (NTD), exons 2 and 3 the DNA binding domain (DBD) and exons 4-8 the hinge and Ligand binding domain (LBD). The full-length AR protein contains 919 amino acids, consisting of a very flexible NTD and constant DBD, hinge domain and LBD. The constitutively active AF1 domain is located in the NTD and the LBD consists of the AF2 domain. [1]

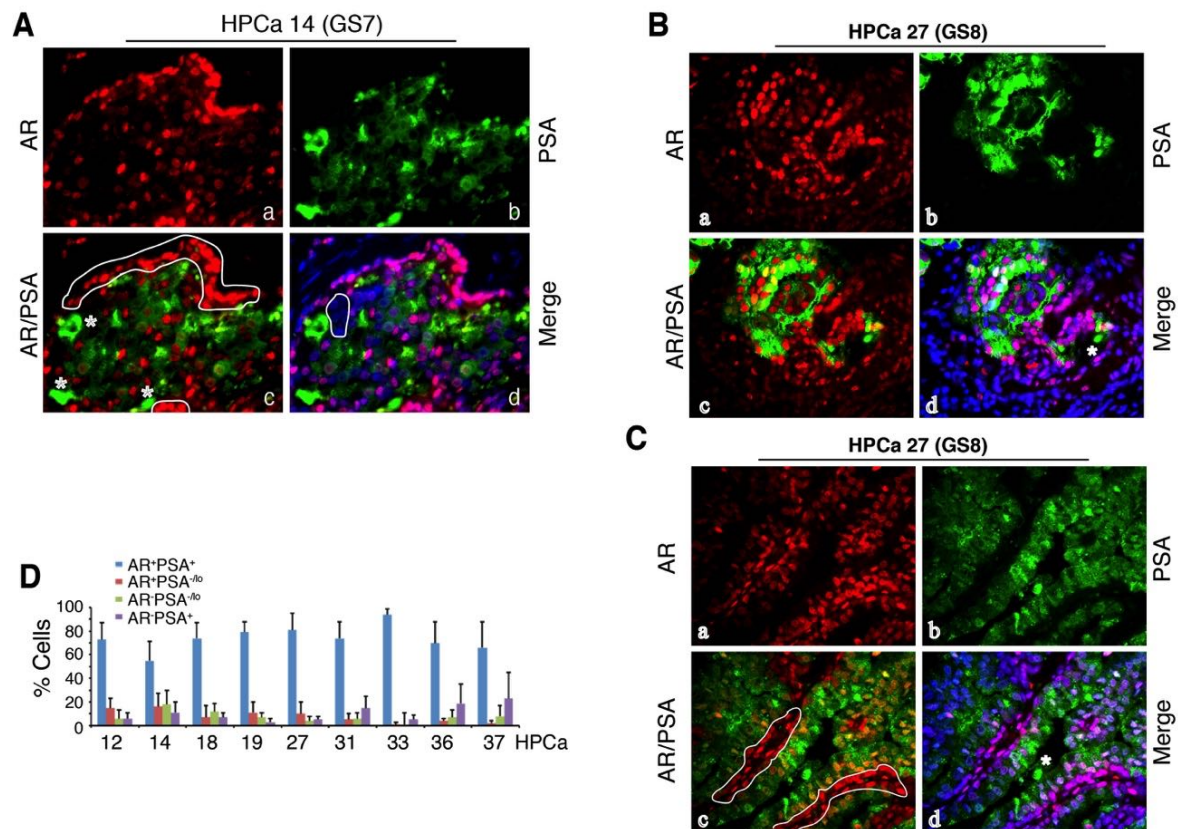


Figure 1-4 Heterogeneous and discordant PSA and AR protein expression in PCa

This figure is adapted from Liu, X., Chen, X., Rycaj, K., Chao, H.P., Deng, Q., Jeter, C., Liu, C., Honorio, S., Li, H., Davis, T., Suraneni, M., Laffin, B., Qin, J., Li, Q., Yang, T., Whitney, P., Shen, J., Huang, J., and Tang, D.G., *Systematic dissection of phenotypic, functional, and tumorigenic heterogeneity of human prostate cancer cells*. *Oncotarget*, 2015. **6**(27): p. 23959-86. [2] with permission of Oncotarget

Representative immunofluorescence images ($\times 400$) illustrating heterogeneous and discordant PSA and AR protein expression in HPCa 14 (A) and HPCa 27 (B, C) and quantification of 4 subpopulations of PCa cells in the 9 HPCa samples (D).

In **A**, AR⁺PSA⁺ PCa cells are marked by red nuclei and green cytoplasm, AR⁺PSA^{-/lo} cells by red alone (panel c, white circled areas), AR⁻PSA⁺ cells by green alone (panel c, asterisks), and AR⁻PSA^{-/lo} cells by being negative (or low) for both red and green staining (panel d, white circled area).

B-C. In HPCa 27, AR⁺PSA⁻ cells are quite abundant in this sample (Bc, red alone cells; Cc, white circled area). Rare AR⁻PSA⁺ cells can be seen by green staining alone (Cd, white asterisk). AR⁻PSA⁻ cells are negative or low for both red and green staining (Ad and Bd, cells positive for DAPI only). [2]

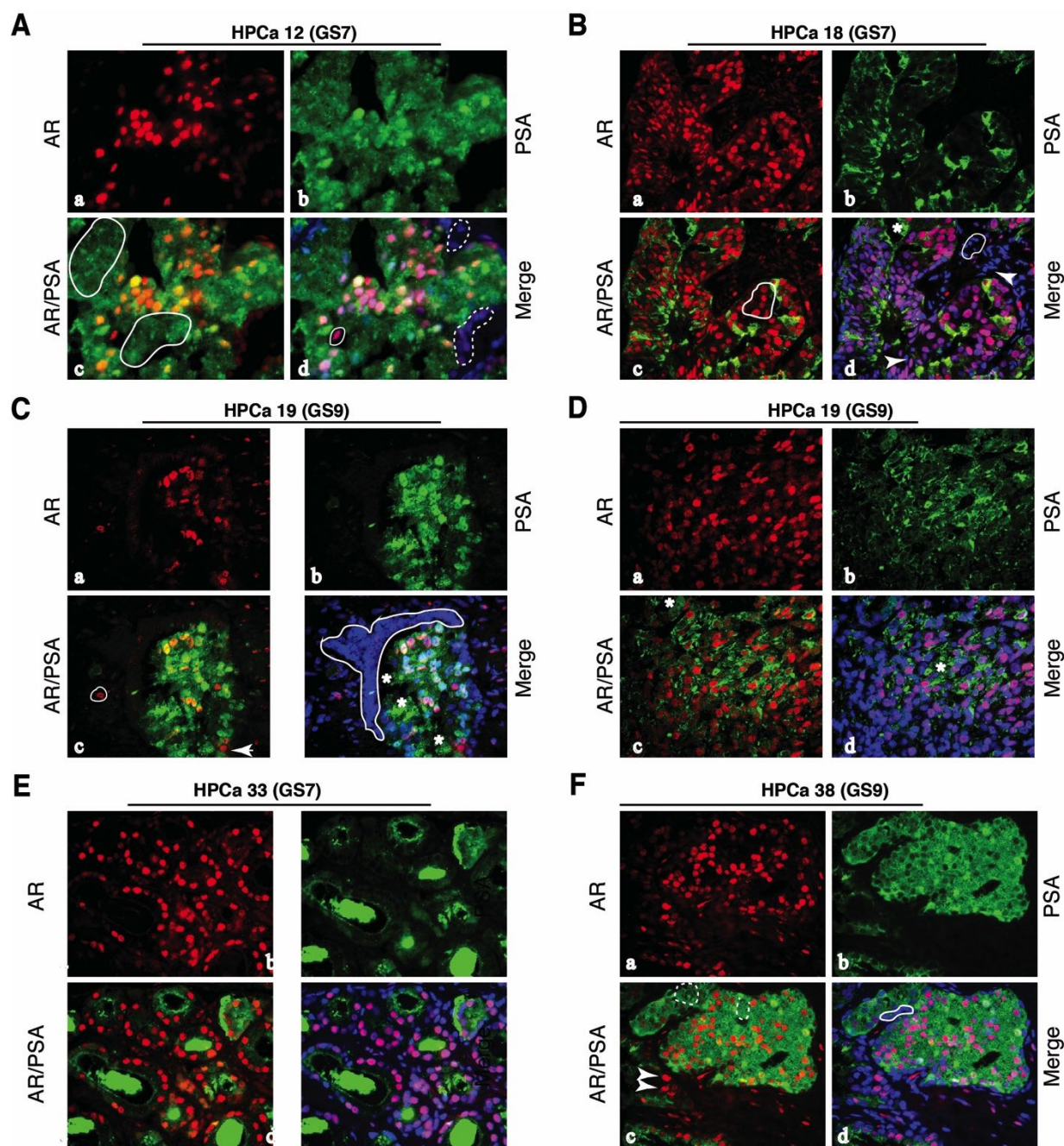


Figure 1-5 Heterogeneous and discordant PSA and AR protein expression in PCa

This figure is adapted from Liu, X., Chen, X., Rycaj, K., Chao, H.P., Deng, Q., Jeter, C., Liu, C., Honorio, S., Li, H., Davis, T., Suraneni, M., Laffin, B., Qin, J., Li, Q., Yang, T., Whitney, P., Shen, J., Huang, J., and Tang, D.G., *Systematic dissection of phenotypic, functional, and tumorigenic heterogeneity of human prostate cancer cells*. Oncotarget, 2015. **6**(27): p. 23959-86. [2] with permission of Oncotarget.

A. Representative immunofluorescence images ($\times 400$) illustrating 4 subpopulations of PCa cells in HPCa 12. Although most cells are AR⁺PSA⁺ PCa cells marked by red nuclei

and green cytoplasm, AR⁻PSA⁺ cells can be seen by green staining alone (panel c, white circled areas), AR⁺PSA⁻ cells by red staining alone (panel d, one white circled area), and AR⁻PSA⁻ cells by being negative or low for both red and green staining (panel d, dashed white circled areas).

B. Representative immunofluorescence images (×400) illustrating 4 subpopulations of PCa cells in HPCa 18. AR⁺PSA⁻ cells are identified by red staining alone (panel c, white circled area), AR⁻PSA⁺ cells by green staining alone (panel d, white asterisk), and AR⁻PSA⁻ cells by being negative or low for both colors (panel d, white circled area and white arrowheads).

C-D. Representative immunofluorescence images (×400) illustrating 4 subpopulations of PCa cells in HPCa19. AR⁺PSA⁻ cells are identified by red staining alone (Cc, white circled area and white arrow), AR⁻PSA⁺ cells are by green staining alone (Cd and Dc-d, white asterisks), and AR⁻PSA⁻ cells are by being negative (or low staining) for both colors (Cd, white circled area).

E. Representative immunofluorescence images (×400) of AR and PSA staining in HPCa33. This Gleason 7 tumor manifests numerous small glands in which PSA⁺ secretions can be observed in the lumen. There are many AR⁺PSA⁻ cells (Cc, cells with red nuclei alone) and AR⁻PSA⁻ cells (Cd, cells low or negative for both red and green signals).

F. Representative immunofluorescence images (×400) illustrating 4 subpopulations of PCa cells in HPCa38. AR⁺PSA⁺ cells are marked by red nuclei and green cytoplasm (panel c), AR⁺PSA⁻ cells by red staining alone (panel c, white arrowheads), AR⁻PSA⁺ cells by green staining alone (panel c, white dashed circled cells), and AR⁻PSA⁻ cells by being negative or low for both red and green staining (panel d, white circled area and many single DAPI-positive cells) [2]

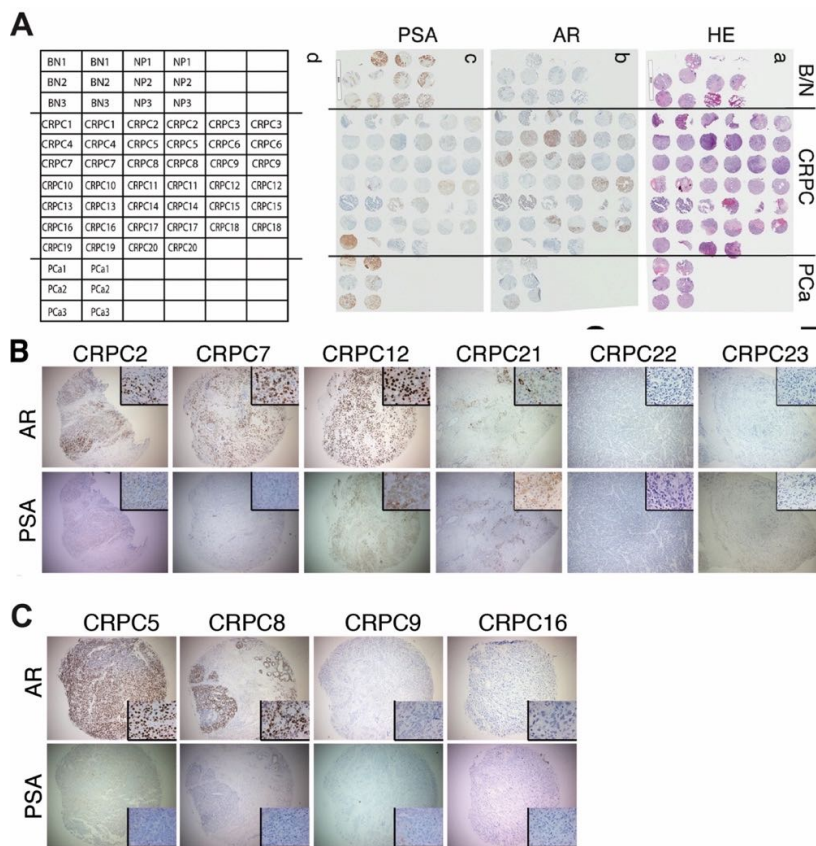


Figure 1-6 AR and PSA protein expression in CRPC

This figure is adapted from Liu, X., Chen, X., Rycaj, K., Chao, H.P., Deng, Q., Jeter, C., Liu, C., Honorio, S., Li, H., Davis, T., Suraneni, M., Laffin, B., Qin, J., Li, Q., Yang, T., Whitney, P., Shen, J., Huang, J., and Tang, D.G., *Systematic dissection of phenotypic, functional, and tumorigenic heterogeneity of human prostate cancer cells*. *Oncotarget*, 2015. **6**(27): p. 23959-86. [2] with permission of Oncotarget.

A. AR and PSA protein expression in 20 CRPC patient samples on a TMA. Shown on right are HE (a) and AR (b) and PSA (c) IHC images of the TMA and below the TMA grid (d). The 20 CRPC samples are in the middle (demarcated by two vertical lines whereas several benign/normal prostate and PCa samples are shown on the top and bottom, respectively). All samples were cut in duplicate. NP, normal prostate (i.e., no cancer); BN, benign prostate from patients with PCa; PCa, hormone-naïve prostate cancer. CRPC1–13, PCa patients treated with castration (mostly bicalutamide) and eventually failed after months to years; CRPC14–17, patients failed both radiation and hormonal therapies; CRPC18, the patient failed radiation and cryotherapy; CRPC19, the patient with advanced PCa treated with Lupron for 2 weeks; CRPC20, the patient received 4 months of Lupron treatment plus 2 months of Casodex.

B-C. IHC analysis of AR and PSA in TMA samples. Shown are 11 CRPC samples illustrating prominent loss of PSA, heterogeneous expression of AR, and discordant AR and PSA expression (insets: 400×). CRPC21 – CRPC23 were 3 separate patient CRPC samples not included in the TMA. [2]

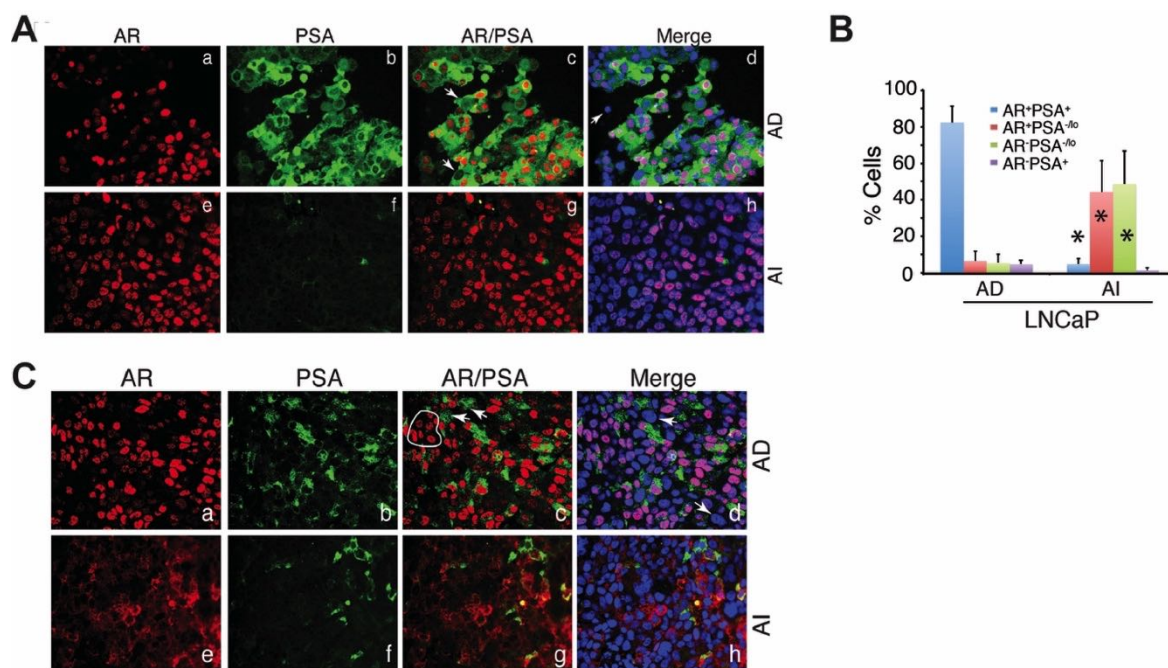


Figure 1-7 Heterogeneous and discordant AR and PSA protein expression in PCa cell models in both AD and AI conditons.

This figure is adapted from Liu, X., Chen, X., Rycaj, K., Chao, H.P., Deng, Q., Jeter, C., Liu, C., Honorio, S., Li, H., Davis, T., Suraneni, M., Laffin, B., Qin, J., Li, Q., Yang, T., Whitney, P., Shen, J., Huang, J., and Tang, D.G., *Systematic dissection of phenotypic, functional, and tumorigenic heterogeneity of human prostate cancer cells*. *Oncotarget*, 2015. **6**(27): p. 23959-86. [2] with permission of Oncotarget.

A. Double immunofluorescence staining of AR and PSA in AD vs. AI LNCaP xenograft tumors. Arrows indicate AR⁻PSA⁺ (c) or AR⁻PSA^{-/lo} (d) cells. Note significantly increased PSA^{-/lo} LNCaP cells in the AI tumor (f). Shown are representative immunofluorescence images (original magnification; ×400).

B. Quantification of the 4 subtypes of PCa cells in AD and AI LNCaP xenograft tumors. A total of 809 and 907 cells were counted from several AD and AI tumors, respectively. *P < 0.001 in AI compared in AD tumors.

C. Double immunofluorescence staining of AR and PSA in AD vs. AI LAPC4 xenograft tumors. In panel c, the white circle indicates several AR⁺PSA^{-/lo} cells and arrows indicate AR⁻PSA⁺ cells. In panel d, arrows point to AR⁻PSA^{-/lo} cells. Note significantly increased PSA^{-/lo} LAPC4 cells in the AI tumor (f). Shown are representative immunofluorescence images (original magnification; ×400). [2]

1.4. PCSCs in primary and untreated PCa: AR negativity and signaling mechanisms

The preceding discussions highlight the presence of AR⁻ PCa cells in untreated PCa [2]. This is an important point as AR⁻ PCa cells are expected to be unresponsive to AR-targeting therapies. This is consistent with reports that androgen-independent PCa cells pre-exist in primary tumors, which may be selected for during ADT [2, 44, 45]. Interestingly, AR expression is often low or undetectable in many reported PCSC populations in untreated PCa models or primary tumors (Figure 1-8). For example, CD44⁺α2β1⁺CD133⁺ cells purified from seven human tumor samples [16], ABCG2⁺ putative PCSCs [15], and CD44⁺ cells in several PCa xenografts [18] were all shown to be AR⁻. In fact, AR⁻CD44⁺ PCSCs had the ability to differentiate, at the clonal level, into AR⁺CD44⁻ cells [18]. Gu *et. al.* [46] also showed that HPET cells (human prostate epithelial cells immortalized by overexpressing hTERT) expressed stem cell molecules such as CD44 and Nanog, could regenerate three prostate epithelial cell types, and were AR negative. Miki *et. al.* [23] demonstrated mutually exclusive expression patterns of CD133 and AR via IHC staining in 16 clinical specimens. Rajasekhar *et. al.* [24] reported both AR and PSA negativity in the TRA-1-60⁺CD151⁺ and CD166⁺ PCSC population, which possessed high tumorigenic ability and could generate differentiated AR⁺ and PSA⁺ tumors *in vivo*. Docetaxel-resistant PCSCs that lacked the expression of MHC molecules were also negative for AR and PSA [21]. Likewise, the PSA^{-/lo} PCSC population was shown to be enriched in AR⁻ PCa cells [2, 7]. These and many other studies [1] suggest that PCSCs in primary and untreated tumors are generally AR⁻; in other words, AR⁻ (and PSA⁻) cells are highly enriched in primary and/or untreated PCSC populations (Figure 1-8). Alternatively, loss of AR expression has been shown to

promote PCSC generation through STAT3 signaling [47]. It remains to be seen whether the AR⁺ and/or AR⁻ PCa cells in untreated/primary PCa possess distinct self-renewal, tumor-propagating properties and drug sensitivities as these two populations of PCa cells have not been prospectively separated, purified, and compared.

PCSCs in untreated PCas remain AR⁻ presumably because these cells are simply less differentiated. Alternatively, molecules such as ABCG2 are preferentially expressed in PCSCs [15], which mediate efflux of androgens leading to the degradation of ligand-less AR in PCSCs. We have shown, via serial tumor-transplantation assays and analysis of asymmetric cell divisions using clonal and time-lapse analyses, that several PCSC populations (e.g., SP, CD44⁺, ABCG2⁺, and PSA^{-lo}) have self-renewal ability [2, 7, 14, 18]. A fraction of PSA^{-lo} PCa cells can undergo authentic asymmetric cell division regenerating a PSA^{-lo} daughter cell as well as a differentiated PSA⁺ cell, which subsequently undergoes rapid proliferation [2, 7]. Self-renewal is a shared property for both normal stem cells and CSCs, and, not surprisingly, many molecules and pathways that regulate self-renewal in normal stem cells have been reported to operate in PCSCs (Figure 1-8). For example, we have shown that NANOG is preferentially expressed in several PCSC populations and is important for CSC properties, as its knockdown severely impairs tumor regeneration [48]. In contrast, inducible expression of NANOG alone is sufficient to reprogram bulk cancer cells into stem-like cancer cells with enhanced tumor-regenerating and tumor-propagating activities [49]. Our results suggest that certain pluripotency molecules may also be functionally important for PCSC self-renewal and other properties. In support, several other studies have similarly implicated OCT4 and SOX2 in conferring PCSC activities [50, 51]. Interestingly, reciprocal relationships between AR and NANOG/OCT4/SOX2 have been noted in these studies.

Hedgehog (HH) and WNT signaling often act together and play important roles in regulating self-renewal. The importance of WNT/ β -catenin signaling is illustrated by the observations that treatment of LNCaP and C4-2 cells with WNT-3a increased their sphere formation rate and size, with increased nuclear β -catenin accumulation [52]. Although the AR antagonist, bicalutamide, reduced the sphere size, the sphere formation rate did not change, thus suggesting a role of WNT signaling in PCSC self-renewal independent from AR [52]. Bmi-1 acts down-stream of HH, and has been shown to be necessary for HH induced self-renewal in several populations of normal stem cells as well as CSCs [53-55]. Lukacs *et. al.* [56] investigated the effects of Bmi-1 loss in the presence of over-activated Wnt signaling on murine prostate stem cells (PSCs) and demonstrated that Bmi-1 expression was required for Wnt pathway to modulate self-renewal in the PSCs. In addition, several other signaling molecules and pathways may also be involved in regulating PCSCs. For example, PTEN/PI3K/AKT pathway has been reported to be essential for PCSC proliferation independent of AR status [22].

E-twenty-six (Ets)-related gene (ERG), which is essential for adult HSC maintenance and self-renewal during stress-induced hematopoiesis [57-59], is deregulated in most PCa through the most common genetic event, the TMPRESS2-ERG fusion [60-62]. TMPRSS2-ERG expression is associated with a relative increase in clonogenic PCa cells [63]. Interestingly, although the expression of TMPRESS2-ERG fusion gene is expected to occur in AR⁺ PCa cells due to the TMPRESS2 regulation by AR, recent evidence suggests that the TMPRESS2-ERG fusion protein may also be expressed in the AR⁻ PCSCs. Polson and colleagues [64] demonstrated that in CD133⁺ α 2 β 1⁺ primary tumor cells with stem cell properties, TMPRSS2-ERG and AR expression was not necessarily concordant. While most of the marker-positive cells were

AR negative, they expressed ERG at both RNA and protein levels, which may help maintain PCSC properties such as self-renewal in the marker positive cells [64].

Taken together, the above discussions indicate that many well-known signaling molecules and pathways can regulate and confer CSC properties in AR⁻ PCSCs [11, 12]. These molecules and pathways represent obvious therapeutic targets, and therapeutics targeting these PCSC-specific signaling nodes could, in principle, be utilized in conjunction with the ADT regimens.

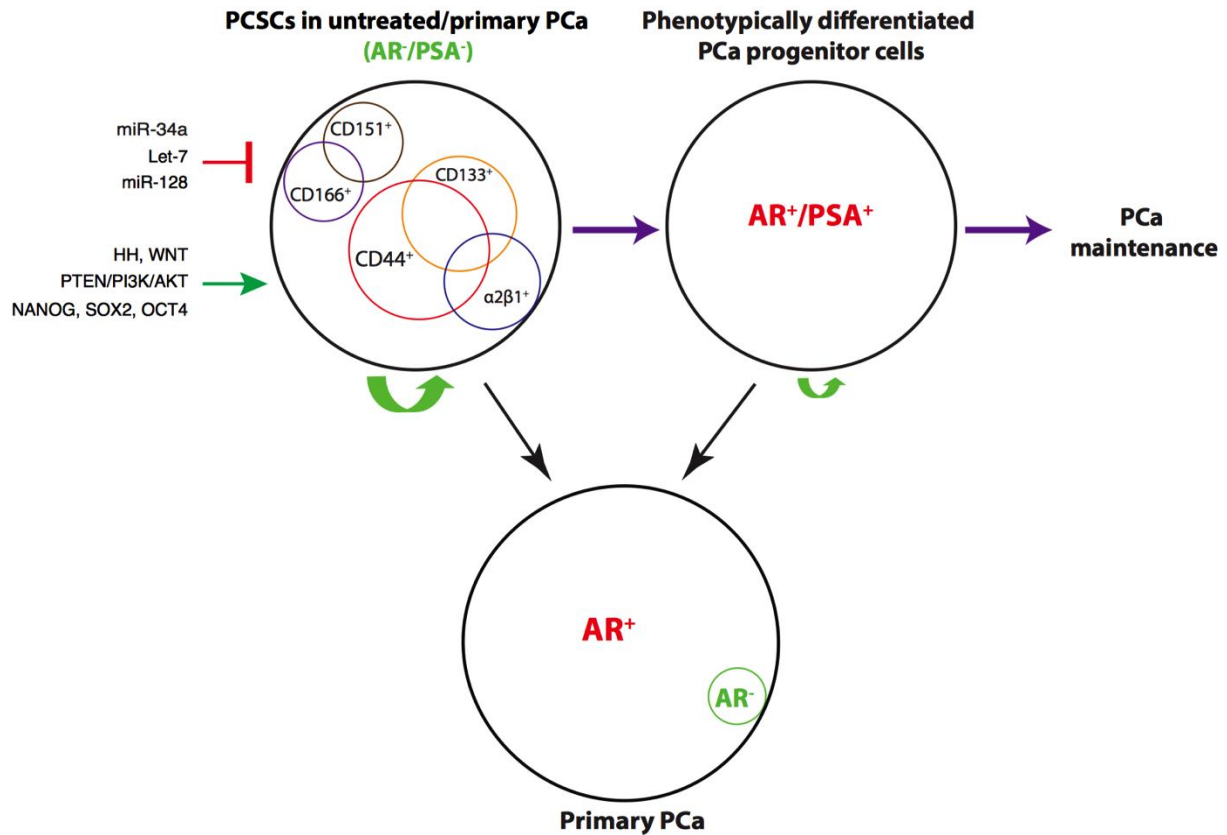


Figure 1-8 PCSCs in untreated/primary PCa.

This figure is reproduced from [Deng, Q. and Tang, D.G., *Androgen receptor and prostate cancer stem cells: biological mechanisms and clinical implications*. Endocrine-Related Cancer, 2015. 22\(6\): p. T209-20. \[1\]](#) with the permission of Endocrine-Related Cancer.

Primary PCa contains AR⁺ PCa cells as the majority with the AR⁻ PCa cells being the minority (below). Depicted on top (left) are several representative PCSC populations reported in primary PCa and untreated prostate tumor models, which are mostly AR⁻ and PSA⁻ but have the capacity to differentiate into more mature, AR⁺/PSA⁺ PCa cells (right). The PSA^{-/lo} PCSC population has unlimited self-renewal potential (indicated by a large green arrow) whereas differentiated AR⁺/PSA⁺ PCa progenitors cells have more limited self-renewal activity (indicated by a small green arrow) [2, 7]. The PCSCs can be positively regulated through HH (Hedgehog), WNT and PTEN signaling pathways, as well as by transcription factors such as NANOG/SOX2/OCT4. On the other hand, several miRNAs including miR-34a, let-7, and miR-128 have been reported to negatively regulate PCSCs. [1]

1.5. PCSCs in CRPC might be AR⁺ or AR⁻

It is well appreciated that AR heterogeneity is more pronounced in CRPCs than in primary tumors (see above, [2]) and activation of alternative AR signaling in PCa cells may promote PCa cell proliferation under androgen-deprived environments [65]. What is the cell-of-origin of CRPCs? AR⁺ or AR⁻ PCa cells? As early as 1981, Isaacs and Coffey, working on the Dunning R3327H rat prostatic adenocarcinoma model, proposed that castration selected for androgen-insensitive cells that pre-existed in the untreated tumors [45]. Craft *et. al.* [66], working on the LAPC9 xenograft model, also provided evidence of outgrowth of the androgen-independent clones in the later stages of CRPC development. Fiñones *et. al.* [44] demonstrated androgen-independent PCa cells in untreated early-stage prostate adenocarcinomas. These androgen-independent and androgen-insensitive PCa cells may not necessarily be AR⁻, because PCa cells that overexpress AR and splice variants that lack the LBD may also be insensitive or refractory to androgen ablation. Our recent work provided direct evidence for AR⁻ PCa cells in primary patient tumors [2]. As many PCSCs have been shown to be AR⁻ and to be resistant to castration and other therapeutics [2, 7, 11, 12], it is reasonable to postulate that the AR⁻ PCa cells that pre-exist in untreated tumors could be favored as ‘initiators’ or the cells-of-origin of CRPCs (Figure 1-9). These AR⁻ PCa cells could be expanded upon ADT-induced elimination of AR⁺ cells as well as a result of the de-differentiation of AR⁺ PCa cells (Figure 1-9), much like therapy- or microenvironment-induced de-differentiation of non-CSCs in other tumor systems [7, 8]. As a result, the AR⁻ PCa cells in CRPCs may function as the CSCs for the AR⁻ CRPC clones (Figure 1-9). The best example is the PSA^{-/lo} PCSC population, which has been evinced to possess significant tumor-regenerating and tumor-propagating activities in fully castrated male mice [7]. Germann

et. al. [67] showed that PCa cells expressing stem cell markers such as ALDH1A1 and NANOG became enriched in the BM18 castration model, and castration-resistant stem-like PCa cells had a luminal progenitor phenotype but were negative for AR. Jiao *et. al.* [68] identified a CD166⁺ cell population in both human and mouse CRPCs, which was enriched in basal stem/progenitor cells that were CK5⁺/p63⁺/CK8⁺/AR⁻/TROP2^{hi} and displayed enhanced sphere formation and tissue regeneration abilities. Also, studies on NANOG ([48, 49] and SOX2 [51] have shown that PCa cells expressing these molecules are castration resistant and express relatively low levels of AR. These observations raise the possibility that the AR⁻ PCSCs may gain growth advantages in androgen-deficient environments, leading to distinct AR⁻ clones in CRPC (Figure 1-9).

Despite these observations, most CRPCs clearly also have AR⁺ cells and clones (Figure 1-6 [2]). Although these AR⁺ cells in CRPCs can potentially be derived from the differentiation of AR⁻ PCa cells (Figure 1-9), it is very likely that at least some AR⁺ PCa cells can survive androgen deprivation and function as cells-of-origin as well as CSCs for CRPCs (Figure 1-9). This is plausible as AR⁺ PCa cells in most untreated primary tumors constitute the bulk cell population (Figure 1-9). It is conceivable that due to their abundance, some of these AR⁺ PCa cells, under the selective pressure from androgen deprivation, may selectively gain genetic alterations such as *AR* gene amplification and TMPRSS2-ERG fusion, resulting in expansion of AR⁺ clones (Figure 1-9, right). In the resultant AR⁺ PCa cell clones, AR may still be functioning to regulate both conventional as well as new AR target genes [65]. Regulation of conventional AR targets can be achieved through intratumoral androgen synthesis. Alternatively, AR signaling in the AR⁺ CRPC clones may be executed through ligand-independent AR splice variants and/or AR crosstalks with activated receptors such as EGFR. In fact, there is evidence that

certain AR⁺ cell populations are refractory to castration and can function as the cell-of-origin for PCa in mouse models. Wang *et. al.* [69] showed that castration-resistant Nkx3.1-expressing cells (CARNs) that expressed luminal markers including AR, represented a rare population of androgen-resistant cells in the murine prostate that could function as the cells-of-origin for PCa caused by *Pten* deletion.

Interestingly, expressing wild-type AR at physiological levels in AR⁻ PC3 cells induced growth inhibition [70] whereas knocking down AR in AR-expressing metastatic PCa cells like LNCaP and its derivative C4-2 resulted in growth inhibition, apoptotic cell death and compromised tumor development [71, 72]. The contrasting roles of AR in AR⁻ vs. AR⁺ PCa cell lines imply differential involvement of AR in AR⁺ and AR⁻ PCSCs in CRPCs. Regardless, the phenotype of PCSCs in CRPCs may be context-dependent and both AR⁺ and AR⁻ clones, which possess their own intra-clonal CSCs, likely co-exist in hormone-refractory tumors (Figure 1-9). Clarifying the precise functions of AR⁺ vs. AR⁻ PCSCs in CRPC awaits the development of critical experimental tools that can allow the prospective separation of AR⁺ and AR⁻ CRPC cells.

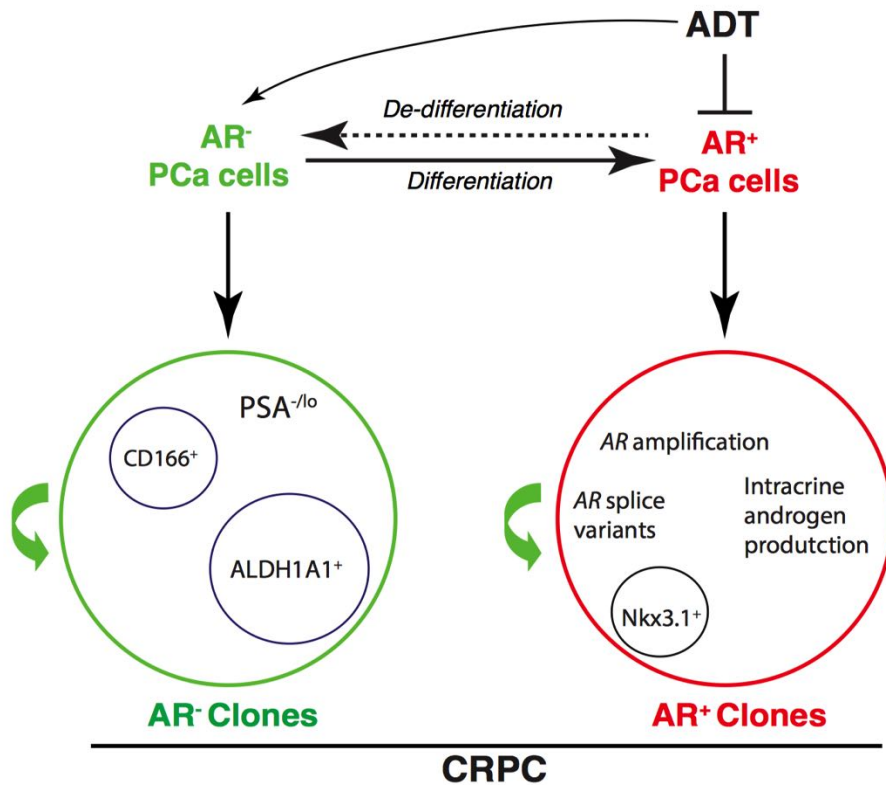


Figure 1-9 Hypothetical PCSCs in CRPC

This figure is reproduced from Deng, Q. and Tang, D.G., *Androgen receptor and prostate cancer stem cells: biological mechanisms and clinical implications*. Endocrine-Related Cancer, 2015. 22(6): p. T209-20. [1] with the permission of Endocrine-Related Cancer.

ADT selectively targets AR⁺ PCa cells and has been shown to enrich AR⁻ PCa cells, which may result from preferential elimination by ADT of AR⁺ cells as well as de-differentiation of AR⁺ PCa cells to AR⁻ cells (top). Clinical CRPCs contain distinct AR⁺ and AR⁻ clones, both of which might contain their own CSCs. In AR⁺ clones, PCSCs could have AR amplification or ligand-independent AR signaling pathways to support the self-renewal in androgen-deprived environment. Several potential CSC subpopulations in AR⁻ and AR⁺ PCa cell clones are indicated. [1]

1.6. AR and PCSCs in PCa metastasis

Metastasis is common in CRPC patients. The acquisition of invasive properties through epithelial-mesenchymal transition (EMT), a normal development process, is crucial for the evolution of a metastatic population [73, 74]. There is accumulating evidence supporting the role of ADT in inducing an EMT in PCa cells [75-80], subsequently endowing PCa cells with CSC traits. Both Tanaka *et. al.* [79] and Jennbacken *et. al.* [76] showed that N-cadherin was upregulated in castration-resistant LNCaP, LAPC4, and LAPC9 xenograft models. Sun *et. al.* [77] interrogated EMT marker expression in mouse and human CRPC samples and observed overall higher levels of mesenchymal markers in CRPC compared to non-castrated samples. They proposed a negative feedback loop model between ZEB1 and AR to explain the ADT-induced EMT. To some extent, AR signaling may be involved in the EMT switching in PCa cells. A study on AR and ZEB2 suggests that AR may function differently between AR⁺ and AR⁻ cell lines [75]. Specifically, ZEB2 expression positively correlated with AR expression in LNCaP cells, but the opposite was observed in PC3 and DU145 cells. In addition, AR splice variants, AR3 and ARv567es, were shown to promote EMT in PCa cells [78, 80].

Not only do CSCs play an important role in tumor initiation and treatment resistance, they may also be involved in distant metastases. Tanaka *et. al.* [79] have shown that castration-resistant, N-cadherin positive PCa cells are enriched in stem cell markers including CD44 and NANOG. Vice versa, Lin⁻CD44⁺CD133⁺Sca-1⁺CD117⁺ mouse PSCs express higher levels of mesenchymal markers N-cadherin and vimentin compared to non-stem cells [77]. On the other hand, EMT may also suppress the stemness in PCa cells [81]. This is not surprising as the mesenchymal-epithelial transition (MET) is equally important and required for metastatic colonization. Research

on the role of MET in PCa metastasis is very limited.

1.7. Clinical implications and perspectives

Studies supporting the potential prognostic role of AR in PCa are controversial, and most evidence suggests that AR is not prognostic in PCa [82-86]. Minner *et. al.* [85] examined the AR expression in more than 2800 treatment-naïve PCa patient samples and observed no significant correlation between AR expression level and the risk of biochemical recurrence. Studies by Fleischmann *et. al.* [82] in 382 lymph node metastases reported that AR is not prognostic in nodal positive PCa, although higher AR does correlate with a larger size of metastases. Despite significant improvements in the ADT efficacy in blocking AR signaling, currently there are no clear correlations between androgen signaling ablation and patient prognosis. A study by Ford *et. al.* [83] in 24 CRPC patients showed that 33% of patients have AR amplification, and patients with AR gene amplification had recurrence five months earlier than those without amplification; however, no statistically significant survival disadvantage was observed in the AR amplified patients. More recently, Lu-Yao *et. al.* [84] performed a median 110-month follow-up study in a cohort consisting of 66,717 PCa patients who underwent primary ADT or conservative management and found that primary ADT was not associated with improved long-term overall or disease-specific patient survival. Furthermore, AR heterogeneity in PCa implies that targeting AR signaling as a monotherapy would be an inefficient approach in preventing disease recurrence.

PCSCs may represent the driving force for tumor progression and metastases. A number of studies have shown that the expression of stem-cell markers has prognostic significance in PCa, as well as other cancer types [87, 88]. Studies on PSA^{-/lo} PCSCs suggest that intratumoral PSA expression is inversely correlated with tumor Gleason score and patient survival [7]. Multiple studies have shown that AR⁻ tumor cells are

enriched in PCSC populations, implicating a pivotal role for PCSCs in ADT resistance. Hence, targeting PCSCs specifically in an adjuvant setting might be helpful in preventing CRPC. Preclinical studies targeting PCSCs have provided promising results. For instance, we have demonstrated that microRNA-34a (miR-34a) potently inhibits PCa progression and metastasis via directly targeting CD44 [19]. We have also reported the suppression of PCSC self-renewal and tumor progression via several other microRNAs including let7b and miR-128 [19, 89, 90]. At the same time, direct inhibition of WNT, PTEN/PI3K/AKT and other cell-signaling pathways has demonstrated tumor suppressive effects via reduction of the PCSC population [11, 91].

Understanding and elucidating the roles of and the interrelationship between AR heterogeneity and PCSCs could offer fresh insight in designing novel therapeutics to target lethal CRPC and metastasis. Recent evidence suggests that in untreated tumors, PCSCs seem to be largely AR⁻ whereas in CRPCs, PCSCs may be either AR⁺ or AR⁻. In other words, both AR⁺ and AR⁻ PCa cell clones co-exist in most CRPCs (Figure 1-9). In principle, PCSCs, whether AR⁺ or AR⁻, are endowed with the fundamental trait of ‘stemness’, which is regulated by unique cohorts of genes, the epigenetic landscape and environmental factors [8]. The development of novel therapeutics that target PCSC ‘stemness’ is imperative, and has the potential, when used in conjunction with ADT, to help prevent tumor recurrence.

Two outstanding questions remain to be addressed: 1) are there intrinsic biological and tumorigenic differences between AR⁺ and AR^{-/lo} PCa cells? 2) How do the two subpopulations of PCa cells respond to the AR targeted therapies? The overarching hypothesis for my thesis research is that **AR heterogeneity contributes to PCa development, progression, and therapy resistance**. To address the above questions

and to test my overarching hypothesis, I propose the following two specific aims of my research are: 1) develop novel genetic tools to separate AR⁺ and AR⁻ PCa cells; and 2) to functionally and molecularly study the isogenic AR⁺ and AR-KO LNCaP cells

Chapter 2. Build AR reporter systems by using PSA and AR promoters

2.1. Introduction

The impact of AR heterogeneity in PCa on cancer biology and therapy response remains to be elucidated mainly due to the lack of tools in separating the AR⁺ and AR⁻ subpopulations of PCa cells. In this chapter, we discuss the development of one method of separating the two populations via construction of an AR reporter systems containing PSA or AR promoters.

LNCaP cells were initially established from a PCa lymph node metastasis, and are the most commonly used PCa cell line with ~7,000 citations in Pubmed. Regular LNCaP cultures contain cells expressing high levels of AR (i.e., AR⁺) and PSA (i.e., PSA⁺) as well as cells expressing little/no AR (i.e., AR^{-/^{lo}}) and PSA (PSA^{-/^{lo}}) [92]. By utilizing a PSA promoter (PSAP) driven enhanced green fluorescence protein (eGFP) in a lentiviral-tracing vector (Figure 2-1, A), we previously separated two phenotypically different but lineage-related (i.e., PSA⁺ and PSA^{-/^{lo}}) subpopulations of PCa cells [7]. Comprehensive cell biological, molecular, and tumor studies revealed that the phenotypically undifferentiated PSA^{-/^{lo}} PCa cell population harbors self-renewing long-term tumor-propagating cells that are intrinsically refractory to castration [7].

The PSAP used in the study [7] was originally derived from a PCa patient with high serum PSA and is highly specific and sensitive for PSA-positive PCa cells [93]. It contains two parts of the full PSA promoter, -4703 to -3904bp and -538bp to -1bp (Figure 2-1, B), which includes 13 of the 22 putative AR response elements (AREs) in the full PSA promoter (Figure 2-1, C). The abundance of AREs makes this an optimal promoter to report canonical AR activity. For this reason, we first attempted to use this PSAP-eGFP lentivector to identify AR⁺ and AR^{-/^{lo}} cells in LNCaP cell system.

At the same time, we constructed four AR promoter (ARP) fragments based on previous functional analysis of the AR promoter [94]. All four AR promoter fragments were active in various PCa cell lines [94]. Similar to our PSA^{-/-} studies, we used the ARPs to drive a Red Fluorescence Protein (RFP) and aimed to report endogenous AR expression in PCa cells. In combination with the PSAP-eGFP system, our goal was to further dissect four phenotypically different subsets of PCa cells: AR⁺/PSA⁺, AR⁻/PSA⁺, AR⁻/PSA⁻ and AR⁺/PSA⁻.

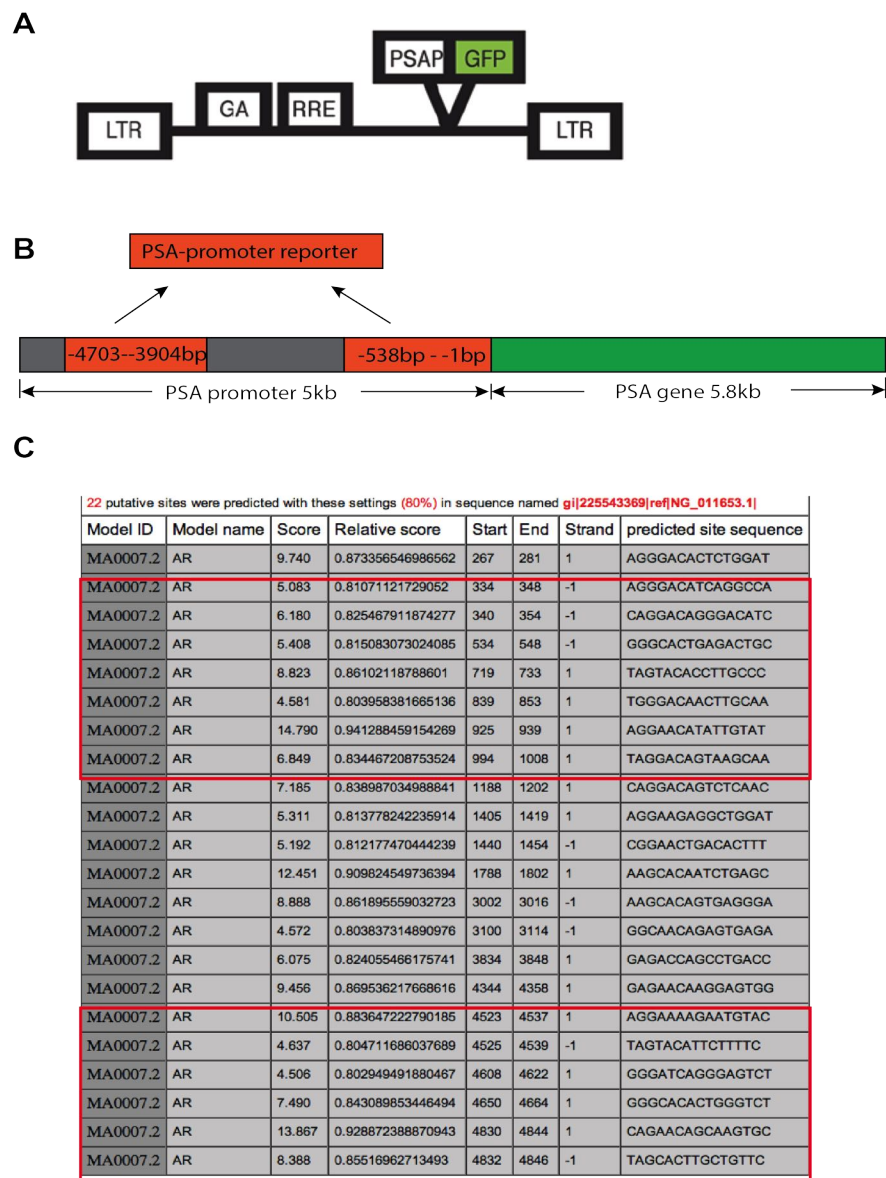


Figure 2-1 PSAP-GFP lentivector

A. The PSAP-eGFP lentivector, in which eGFP is driven by PSAP (PSA promoter). LTR, long-terminal repeat; GA, gag gene; RRE, Rev responsive element.

B. Gene structure of PSA and the full promoter. The red boxes indicate parts contained in the PSAP-eGFP vector.

C. The 22 putative AREs (Androgen-Responsive Elements) predicted by Transcription Binding Sites Prediction (TBSP) program on PSA promoter. The 2 red boxes indicate AREs located in the PSAP of the PSAP-eGFP vector.

2.2. Materials and methods

2.2.1. Cell culture and materials

LNCaP and 293FT packaging cells were obtained from ATCC (Manassas, VA) and Invitrogen (Carlsbad, CA), respectively. LNCaP cells were cultured in RPMI 1640 (Thermo Scientific, MA) supplemented with 10% fetal bovine serum (FBS) (Thermo Scientific, MA) and 100U/ml Penicillin-Streptomycin (PS) (Thermo Scientific, MA). 293FT cells were cultured in DMEM (Thermo Scientific, MA) supplemented with 10% FBS and 100U/ml Penicillin-Streptomycin.

Vectors used include: pGL4.11 [luc2P] Vector (cat# E6661, Promega, Madison, WI); pDsRed-Express-DR (Clontech Laboratories, Inc Mountain View, CA); and pLVX-DD-tdTomato reporter vector and pLVX-DD-tdTomato Control vector (cat# 631753, Clontech Laboratories, Inc., CA).

Antibodies used include: mouse mAb to AR (cat# sc-7305, clone 441; Santa Cruz Biotechnology, Santa Cruz, CA); rabbit mAb to GAPDH (cat# sc-25778, clone FL-335; Santa Cruz Biotech); rabbit pAb to PSA (cat# A0562; Dako, Carpinteria, CA); and AlexaFlour-conjugated secondary antibodies (Invitrogen).

Restriction enzymes used include: XhoI (R0146S, NEB, Ipswich, MA); AgeI (R0552S, NEB, Ipswich, MA); ApaI (R0114S, NEB, Ipswich, MA) BamHI (R0136S, NEB, Ipswich, MA); and HindIII (R0104S, NEB, Ipswich, MA)

The human DNA was amplified using the following primers: 3.5 kb ARP FWD: GGCTTTCCAGAGCAAAGAGC REV: CAGGCTGTGATGATGCGGTA. 1.7kb ARP FWD: GAGCTCTGGACAAAATTGAGCG REV: CAGGCTGTGATGATGCGGTA. 588bp ARP FWD: AGCCCTGGCGCCTAAACCTT REV: GGAGGACAAAGGCAGCCGTCAG. 161bp ARP: FWD: GGAGGCCGGCCCGGTGG REV: TTTCCCTCTGTGCGCCTCCT CTG. qRT-

PCR primers: hAR FWD: TTAGGGCTGGGAAGGGTCTA REV: ATGGGCTTGGGGAGAACCAT. hAR2 FWD: GGAGATGAAGCTTCTGGGTGT REV: GTTGTTCGTGTCCAGCAC. PSA FWD: TCTGCGGCGGTGTTCTG REV: GCCGACCCAGCAAGATCA. GAPDH FWD: AATCCCATCACCATCTTCCA REV: TGGACTCCACGACGTACTCA

2.2.2. Lentiviral infection of LNCaP cells

PSAP-eGFP Lentivirus was produced in 293FT packaging cells and titers were determined by GFP percentage in HT1080 cells. LNCaP cells were infected, generally, at a multiplicity of infection (MOI) of 30 and harvested at least 72 hrs post-infection.

pLVX-ARP-DD-tdTomato lentivirus was packaged with the Lenti X™ packaging kit (cat# 631275, Clontech Laboratories, Inc., CA) in 293FT cells and titers were determined with Lenti-X™ GoStix™ (cat# 631243, Clontech Laboratories, Inc., CA). LNCaP cells were infected at an MOI of 1-2. Infected cells were selected by puromycin (cat# P8833 Sigma-Aldrich, Inc., St. Louis, MO) at 1 µg/ml.

2.2.3. FACS and purification of the PSA⁺ and PSA⁻ LNCaP Cells

At 48-72 hrs post PSAP-GFP infection, LNCaP cells were dissociated into a single-cell suspension using trypsin/EDTA and approximately 5-10 x 10⁶ cells were used for FACS analysis. The top 10% GFP-bright (i.e., PSA⁺) cells were purified out for functional assays as the 'positive' population. Generally, the bottom 2-6% cells (i.e., PSA^{-/lo}) were selected as the 'negative' population. Post-sort analysis (i.e., qRT-PCR) was routinely performed to assess the purity of each population.

2.2.4. Immunofluorescence (IF) microscopy

For PSA and AR double IF staining, cells were plated on poly-lysine-coated glass coverslips and incubated in a mix of mouse monoclonal anti-AR (clone 411, SC-7305, Santa Cruz Technology; 1:200) and rabbit polyclonal anti-PSA (A0526, Carpinteria, CA; 1:5) in PBS containing 0.1% Triton and 5% goat serum for 2 hrs at room temperature (RT). After thorough washing, coverslips were incubated for 60 min with secondary antibodies (Invitrogen) Alexa Fluor 594-conjugated goat anti-mouse IgG (1:1000) and Alexa Fluor 488-conjugated goat anti-rabbit IgG (1:1000) in PBS plus 0.1% Triton and 5% serum, followed by thorough washing. Finally, cells were stained with DAPI (H-1200; Vector Laboratories, Burlingame, CA) for 10 min at RT, and coverslips were mounted with 6 µL ProLong® Gold anti-fade reagent (Invitrogen). Images were acquired within 30 min on an Olympus microscope.

2.2.5. PCR, RT-PCR and qRT-PCR

For PCR, genomic DNA was extracted from 2 million clonally cultured LNCaP cells using the Qiagen Genomic DNA mini kit (cat# 13323, Germantown, MD) and the concentration was measured using a Nanodrop 2000 (Thermo Scientific, Waltham, MA). For each PCR, 500ng of genomic DNA was used. For qRT-PCR, RNA was extracted from 2 million clonal cultured cells using the Qiagen RNeasy Mini Kit (cat# 74104, Germantown, MD), followed by cDNA synthesis using the SuperScript® III One-Step RT-PCR System (cat# 12574018 Thermo Scientific, Waltham, MA). qPCR were performed on an ABI Prism 7900HT (Applied Biosystems, Foster City, CA) with SYBR® Green PCR Master Mix (cat# 4344463 Life tech, Carlsbad, CA).

2.2.6. ARP-RFP reporter constructs and luciferase assays

Four sets of primers were utilized to amplify four distinct sizes of ARP fragments. The PCR products were cloned into pCR™2.1 Vector (cat# K20001 Thermo Scientific, Waltham, MA) for sequencing and subcloning. To construct the ARP-RFP reporter, we cloned the ARP fragments into pDsRed-Express-DR between XhoI and AgeI sites. To construct the pLVX-ARP-DD-tdTomato vector, we subcloned the ARP fragments into the pLVX-DD-tdTomato reporter vector through ApaI and BamHI digestion. For luciferase assays, we cloned the four ARP fragments into pGL4.11 [luc2P] vector (cat# E6661, Promega, Madison, WI) via the enzyme digestion sites: XhoI and HindIII, in order to make the reporters. LNCaP cells were seeded in 24-well plates (3×10^4 cells/well) and co-transfected with 1 µg reporter vectors together with 10 ng Renilla luciferase internal normalization plasmid (phRL-CMV). The ratio of firefly to Renilla luciferase activity was determined with a dual luciferase assay (cat# E1910, Promega, Madison, WI) 48 hrs later.

2.3. Results

2.3.1. Identify AR^{-/-} LNCaP clones using the PSAP-eGFP lentivector

Infection of LNCaP cells with the PSAP-GFP lentivector at an MOI of 30 led to an almost 100% infected population of cells, indicating that GFP positivity faithfully reports the endogenous PSA expression [7]. All PSA⁺ (i.e., GFP⁺) LNCaP cells expressed high nuclear AR, whereas only ~30% PSA^{-/-} (i.e., GFP^{-/-}) LNCaP cells had strong nuclear AR (Figure 2-2) [2]. The same is true in LAPC9 and LAPC4 cells. These observations suggest that the PSA^{-/-} PCa cell population is heterogeneous with respect to AR expression, but are enriched with AR⁻ cells LNCaP population. By exploiting this PSAP-GFP model, we expect to select for AR⁻ clones based on PSA expression.

By FACS sorting and limiting dilution, we selected and cultured multiple GFP^{-/-} and GFP⁺ single cell clones. Consistent with previous work [7], we observed that GFP⁺ LNCaP cells universally developed into homogeneous GFP⁺ clones (Type I) (Figure 2-3, A). In contrast GFP^{-/-} LNCaP cells developed into Type II (mixed GFP⁺/GFP^{-/-} clones) or Type III (100% GFP^{-/-} clones) (Figure 2-3, B). In six weeks, we established 24 GFP^{-/-} LNCaP single cell clones and several GFP⁺ LNCaP clones as the AR⁺ control group.

AR and PSA expression of these clones was assessed via IF staining (Figure 2-4). PSA staining was much lower in GFP^{-/-} clones compared to the control clone, IA1, and bulk LNCaP cells. However, AR staining remained heterogeneous within each GFP^{-/-} and GFP⁺ clone. Moreover, all clones contained approximately 60% AR^{hi} cells, as did the bulk LNCaP cells. We further characterized AR and PSA mRNA expression between clones via qRT-PCR (Figure 2-5). PSA mRNA expression varied in that 11 out of 23 (47%) clones exhibited lower PSA compared to the control clone, whereas clone IIB12, IIB17, and IIB27 expressed significantly higher PSA. Overall, AR mRNA expression

corresponded with PSA mRNA expression ($R^2 = 0.61$). Lower levels of AR mRNA were observed in 16 out of the 24 clones (66%) compared to the control IA1 clone, indicating that GFP^{-lo} LNCaP clones were indeed enriched in AR^{lo} cells. Nevertheless, use of this PSAP-GFP lentivector was unsuccessful in establishing homogeneous AR^{-lo} LNCaP clones.

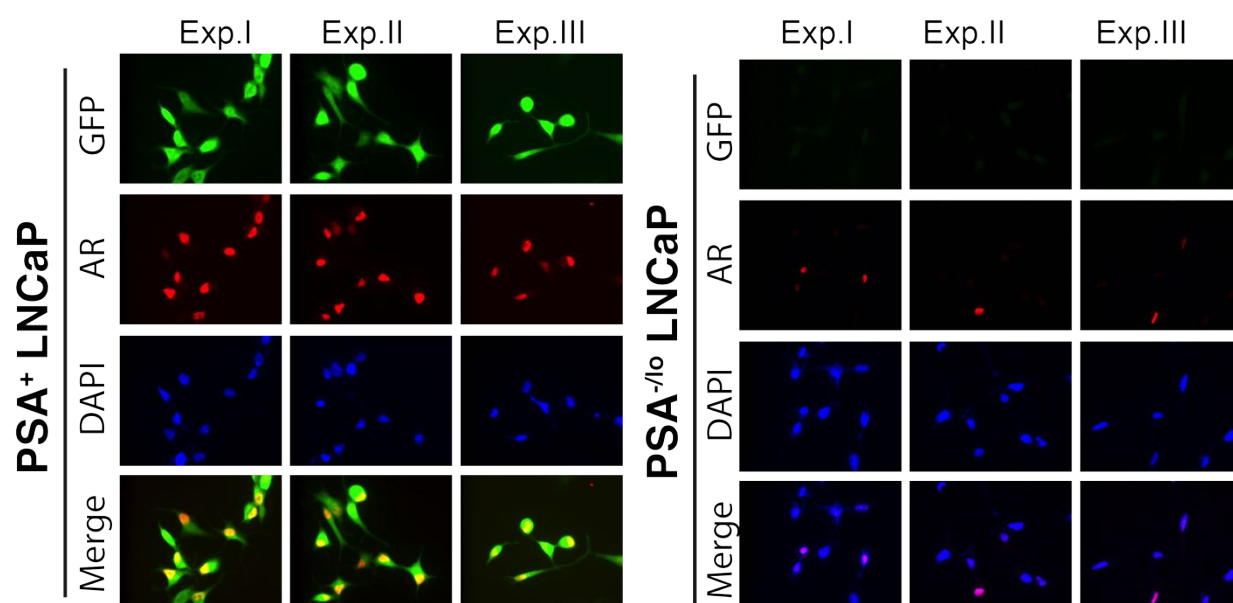


Figure 2-2 AR^{-/-} LNCaP cell population is enriched in the PSA^{-/-} cell population

This figure was adapted from Liu, X. *et. al.* 2015 [2]. No permission required.

GFP⁺ (i.e., PSA⁺) LNCaP cells expressed high levels of nuclear AR whereas GFP^{-/-} (PSA^{-/-}) LNCaP cells were negative or weakly positive for nuclear AR. Shown are three representative fields (×400) of purified GFP⁺ (left) and GFP⁻ (right) LNCaP cells stained for AR and DAPI, representing three independent sorts.

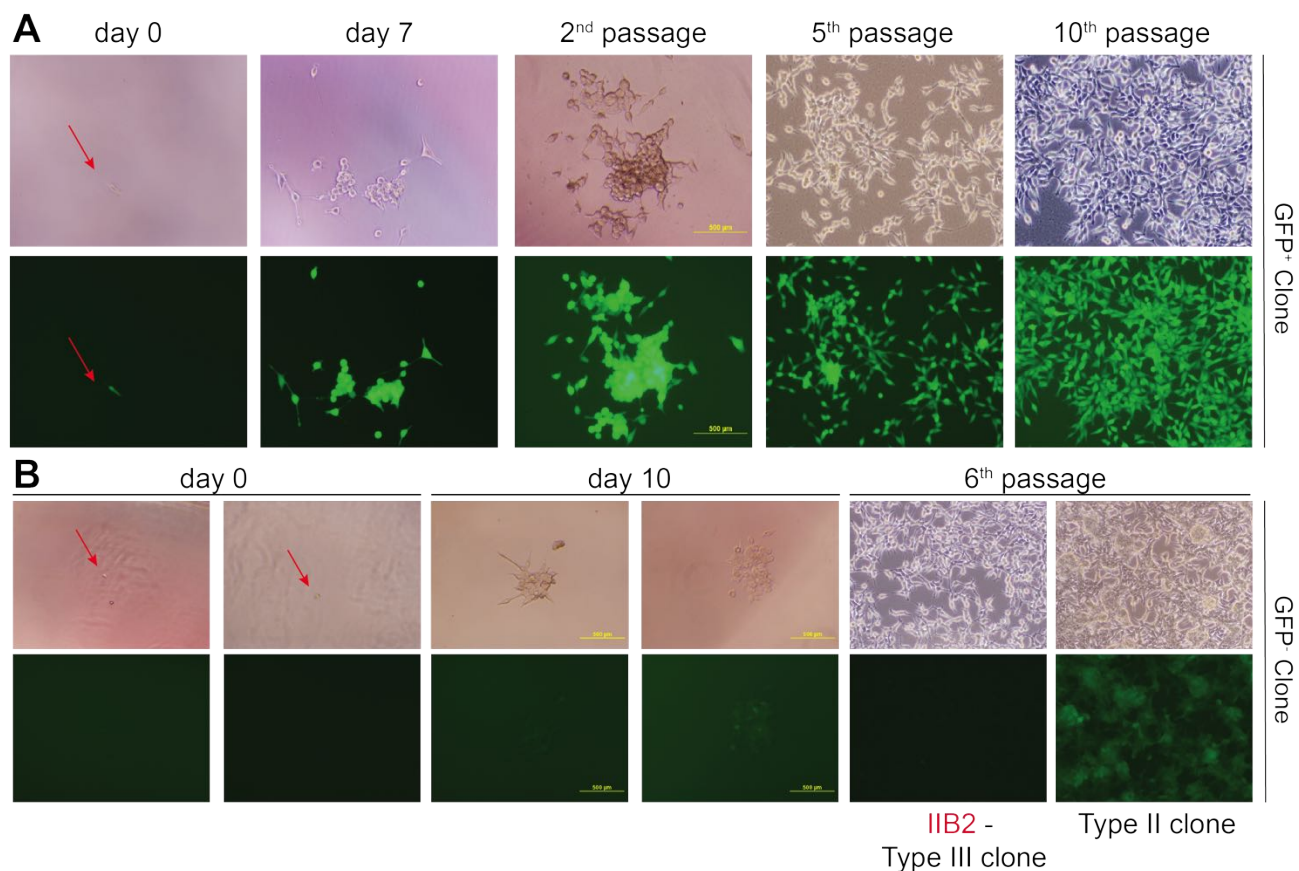


Figure 2-3 Single cell cloning of the GFP⁺ and GFP^{-/lo} LNCaP cells

Shown are representative GFP⁺ (A) and GFP^{-/lo} (B) clonal cell images (scale bar, 500 µm)

A. Shown is one GFP⁺ cell that developed into a homogenous GFP⁺ culture (Type I clones) in four weeks.

B. Shown are two representative GFP⁻ clones: type II clones were a mixture of GFP⁺ and GFP⁻ cells, and type III clones were homogenous GFP⁻ cells. [7]

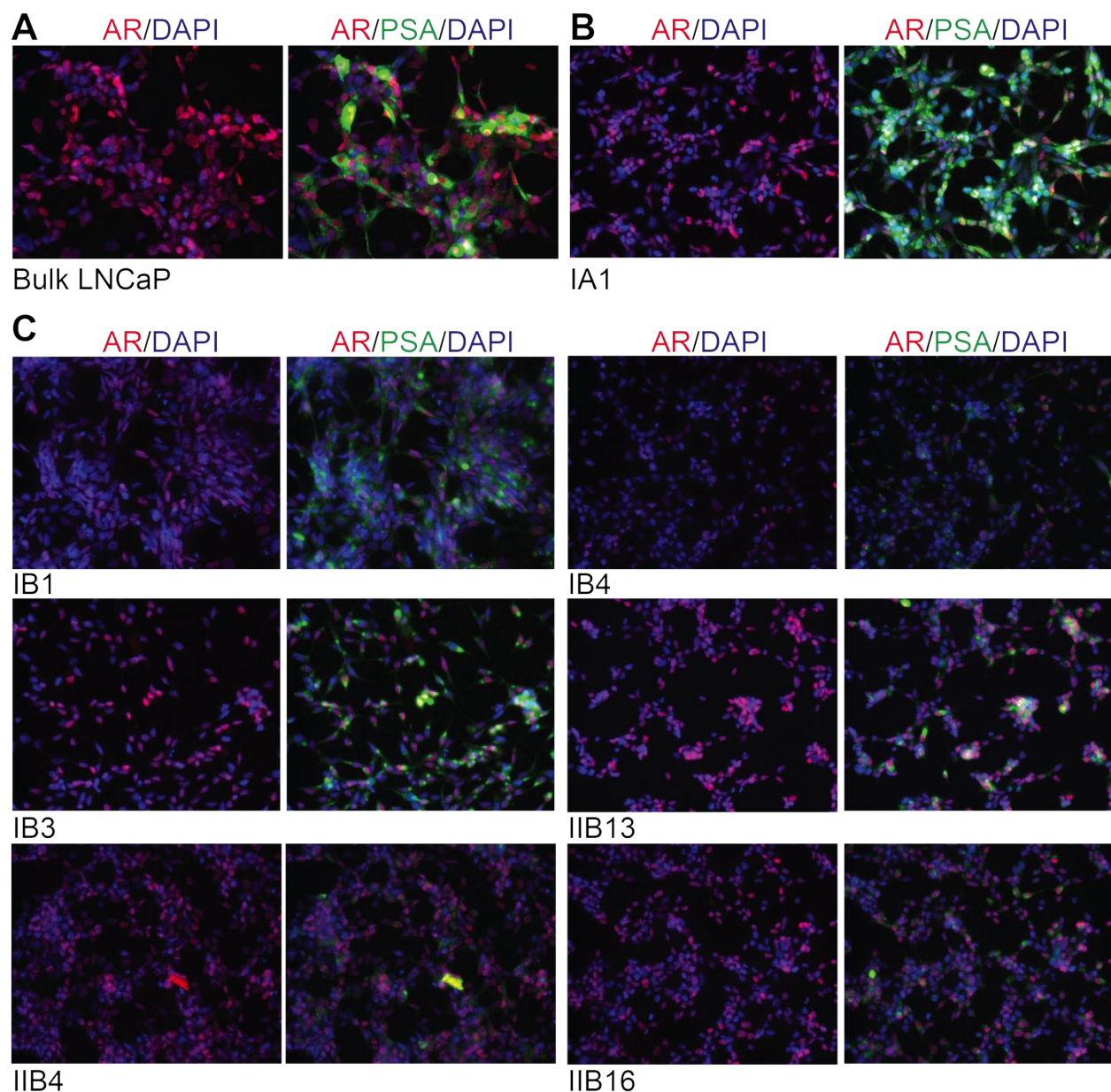


Figure 2-4 AR and PSA expression in the clones

Shown are images of the AR and PSA double IF staining.

A. AR and PSA double IF staining in bulk LNCaP cells.

B. IA1 was the PSA-GFP⁺ clone, in which both AR and PSA staining was strong.

C. IB1, IB3, IB4, IIB4, IIB13 and IIB16 were GFP^{-lo} clones, in which presented weaker PSA staining compared to the IA1 clone and bulk LNCaP cells, but AR expression varied between and within clones.

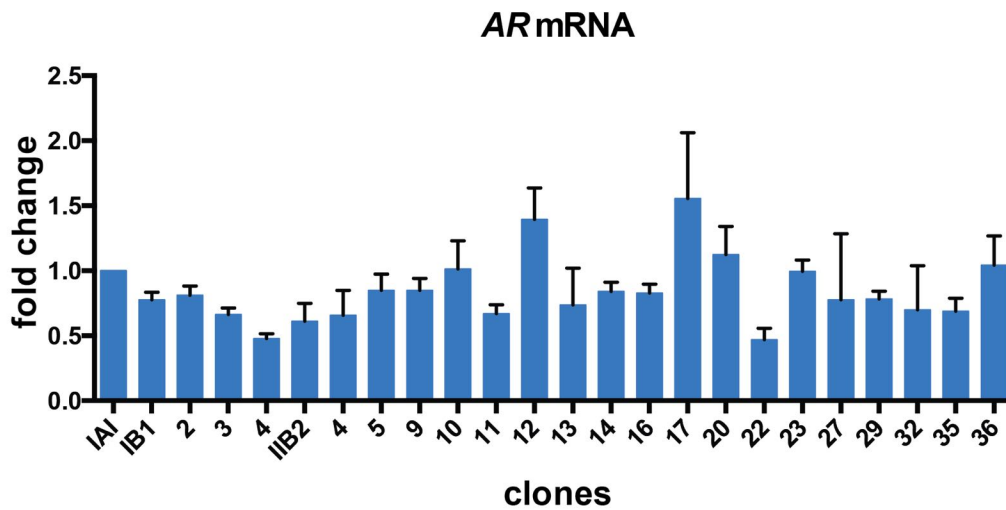
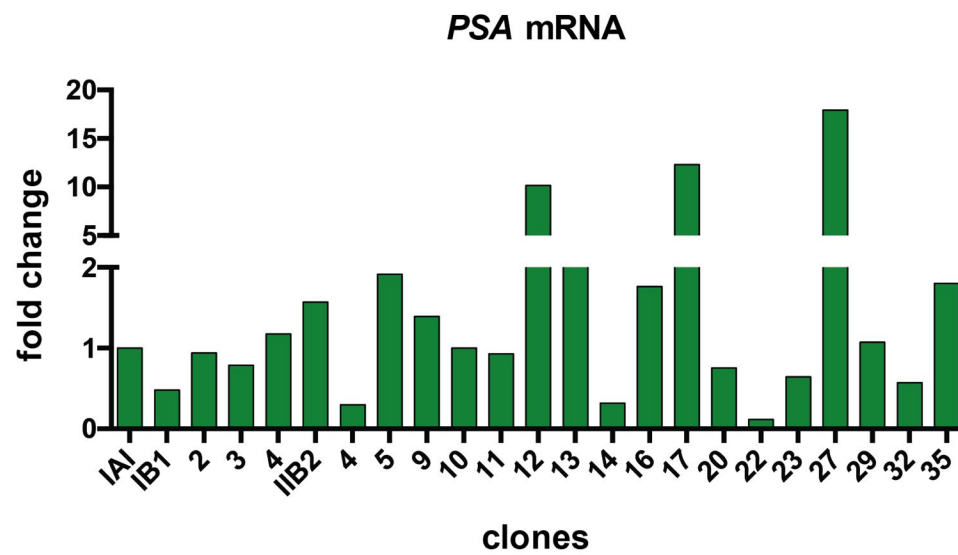
A**B**

Figure 2-5 AR and PSA mRNA expression levels in the clones

Shown are relative mRNA levels of *AR* (**A**) and *PSA* (**B**) of the GFP^{-lo} LNCaP cell clones compared to the IA1 GFP⁺PSA⁺ clone.

2.3.2. Establish ARP-RFP reporters to separate AR⁺ and AR^{-lo} PCa cells

Simultaneously, in order to report the endogenous AR expression in PCa cells, we attempted to build a different lentivector reporter in which an AR promoter (ARP) drives red fluorescence protein (RFP). We identified four potential ARP fragments based on research from Takane *et.al.* and McPhaul *et.al.* [94]. The Full AR promoter was defined as the 3.5 kb fragment, from -2423 bp to +1024 bp. Takane and McPhaul identified three regions within the full AR promoter as active ARPs in T47D, DU145 and other PCa cell lines: the 1.7 kb fragment, from -748 bp to +1024 bp; the 588 bp fragment, from -276 bp to +304 bp, and the 155bp, from -76bp to +87bp (Figure 2-6, A). We cloned the ARP fragments from LNCaP genomic DNA, inserted the fragments into PGL4.11 luciferase reporter vector (Figure 2-6, B), and confirmed that the four ARPs were active in LNCaP cells with luciferase reporter assays (Figure 2-6, C). To test the specificity of the ARPs for AR expression, we treated cells with 10 nM dihydrotestosterone (DHT) for 72 hrs [95]. As predicted, two of the four ARPs displayed a reduction in ARP luciferase activity, with specifically the 3.5 kb ($P = 0.0357$) and 588 bp ($P = 0.0134$) fragments showing significant reductions. Despite confirming the activity and specificity of all four ARPs in LNCaP cells, we opted to use only three ARPs for further experiments, due to the short length of the 155 bp APR.

To make the ARP-DsRed reporter system, we inserted the 588 bp, 1.7 kb and 3.5 kb ARPs into the pDS-Red express-DR plasmid (Figure 2-7, A). Unfortunately, we could only detect ~ 1% DsRed positive cells (Figure 2-7, B). To improve the lentiviral infection delivery efficiency, we inserted the ARPs into the pLVX-DD-tdTomato lentivector in order to make lentivirus with 293FT cells (Figure 2-8, A). By infecting LNCaP cells at an MOI of 5, we successfully achieved an 80% insertion rate, confirmed via puromycin selection

(Figure 2-8, B). Despite this, the RFP positive cells were still too scarce for us to do further characterization (Figure 2-8, B).

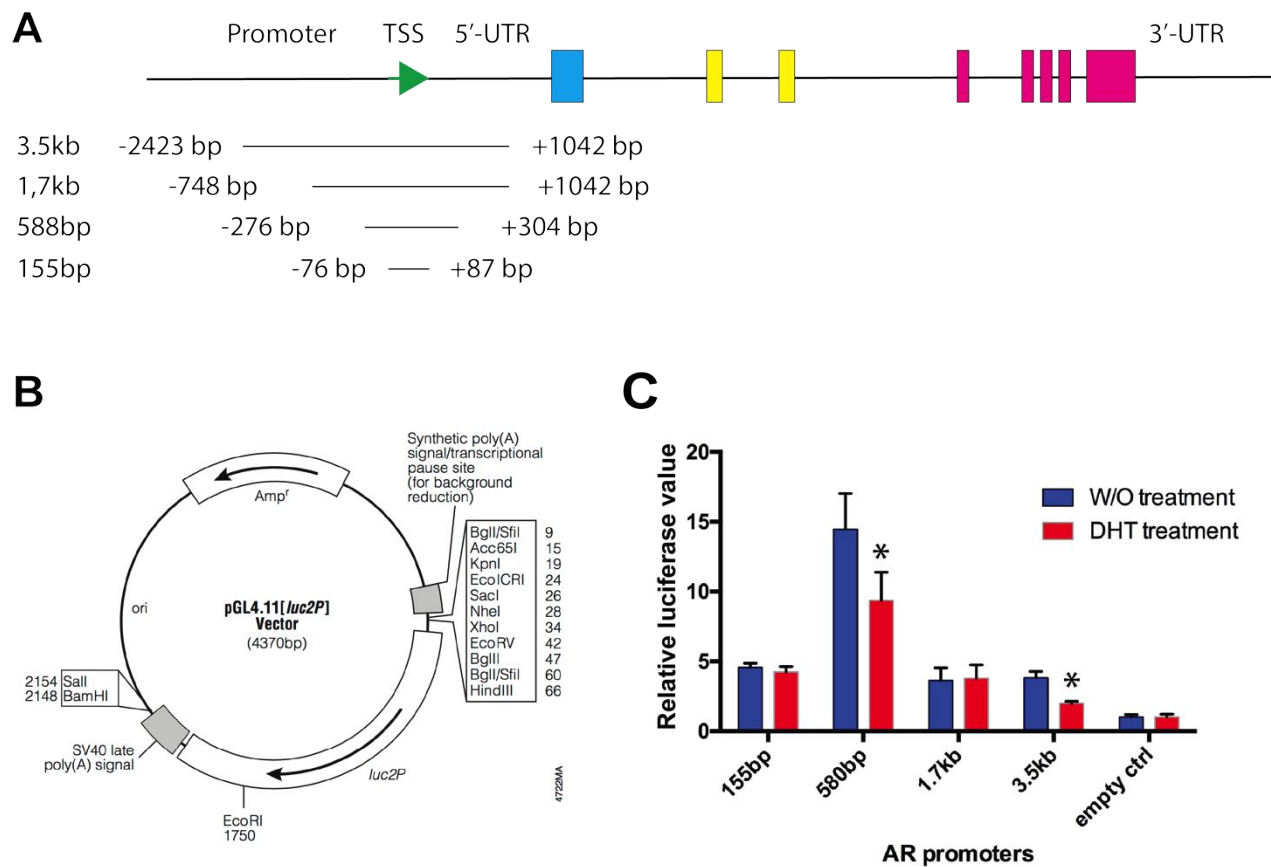


Figure 2-6 AR promoter fragments and luciferase report assays

A. Shown is the gene structure of AR and the relative positions of the four ARP fragments.

B. The vector map of the pGL4.11 luciferase reporter plasmid. Enzyme sites XhoI and HindIII were used to insert the ARP fragments.

C. ARP luciferase report assay in LNCaP cells with or without 10 nM dihydrotestosterone (DHT) treatment. * $P < 0.05$

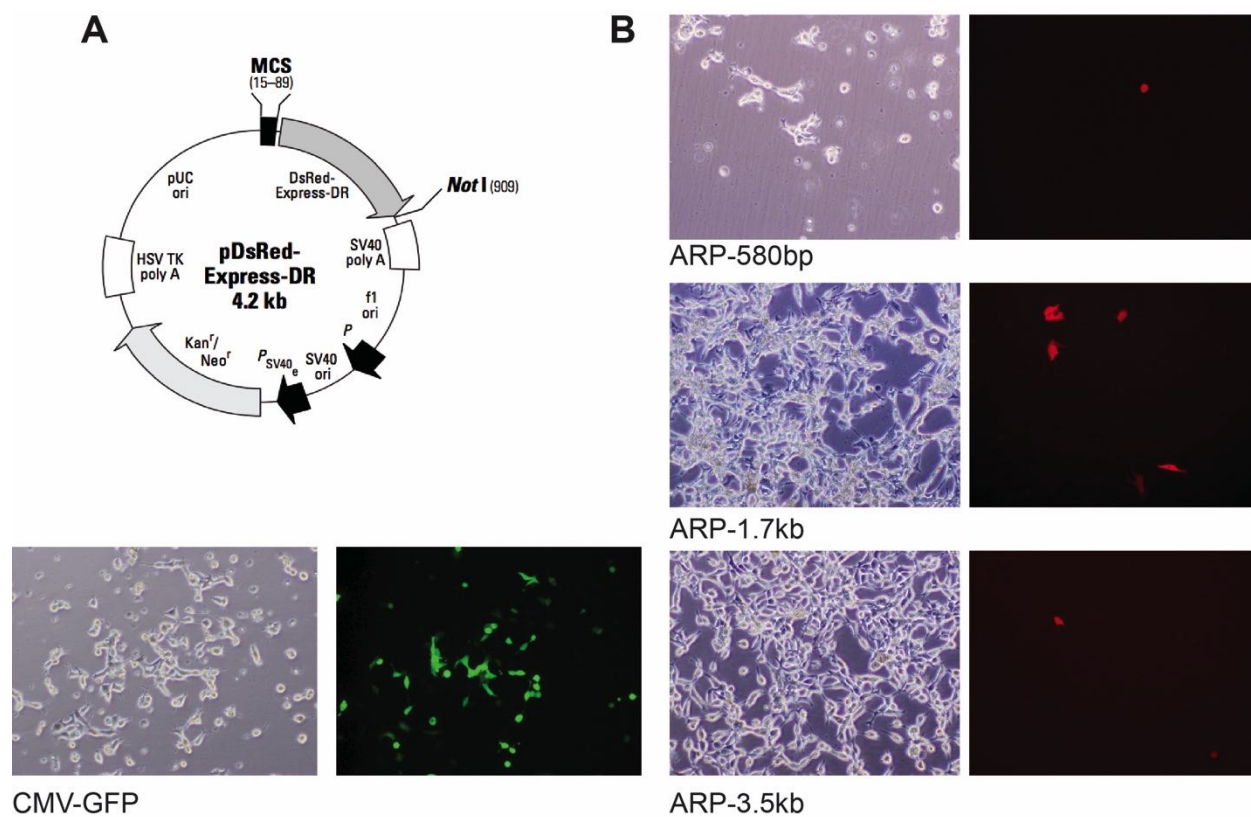


Figure 2-7 ARP-DsRed reporter studies in LNCaP cells.

A. The pDsRed-Express-DR vector map. XhoI and AgeI were used to insert the APRs.

B. Representative images of LNCaP cells 72 hrs after transfection with ARP-DsRed reporters. The cmv-GFP vector transfection was used to show transfection efficiency.

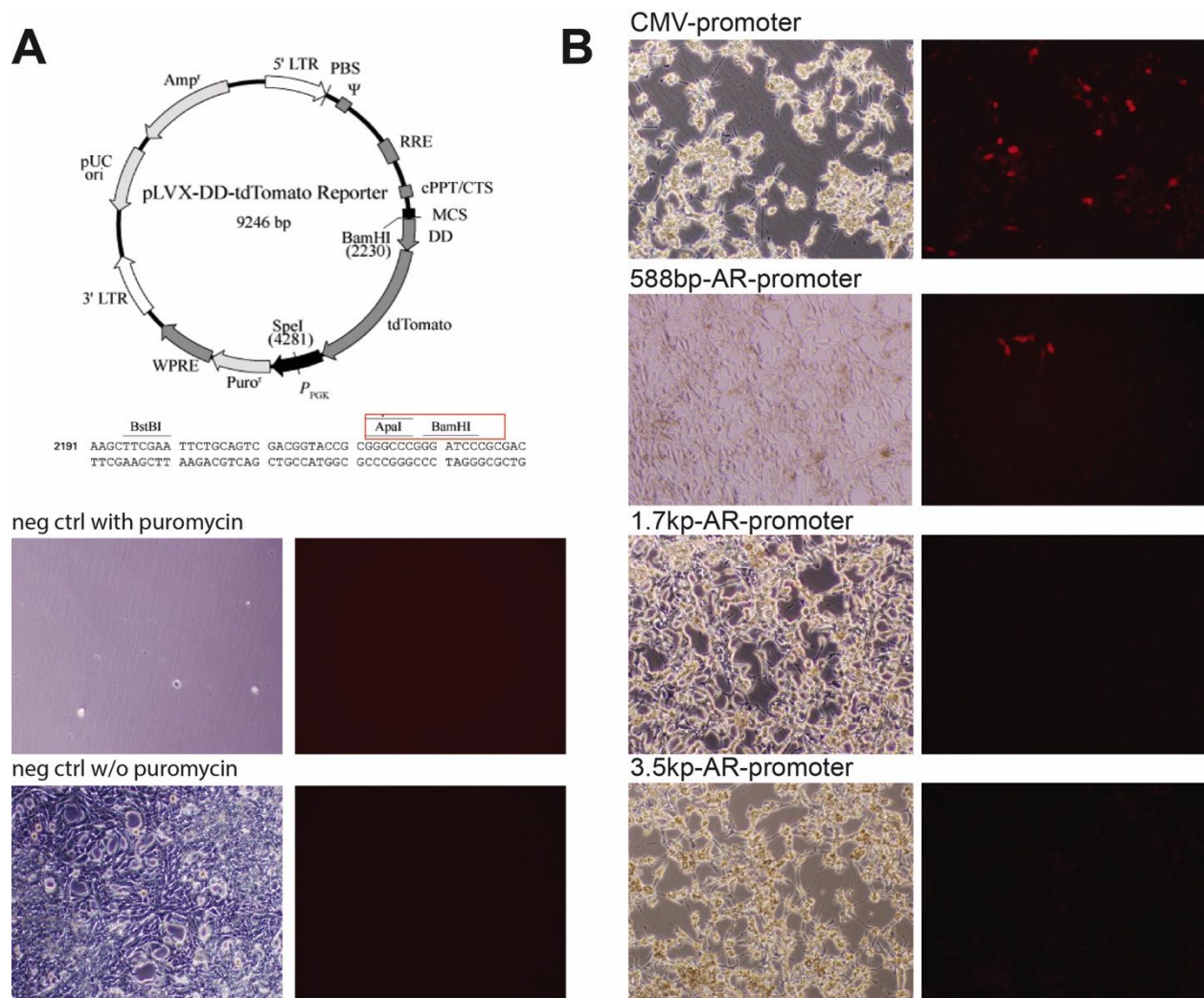


Figure 2-8 ARPs in pLVX-DD-tdTomato lentiviral reporter system.

A. The pLVX-DD-tdTomato construct. Apal and BamH1 were used to insert the ARPs.

B. Representative images of LNCaP cells 72 hrs after the lentivirus infection. Cells were infected (MOI 5) and puromycin (1 μ g/ml) was used to select cells with the lentiviral insertion. The pLVX-CMV promoter-DD-tdTomato was used as a positive infection control. Cells without lentiviral infection served as a control (Left lower panels).

2.4. Discussion

In this part of study, our goal was to employ the AR or PSA promoter-reporter system in order to conduct functional and molecular studies on highly purified homogeneous AR⁺ versus AR⁻ PCa cells. We selected LNCaP cells as our primary experimental model based on their well-documented variable expression of AR (i.e., 60% of LNCaP cells express high levels of AR, 20% low AR and 20% AR-negative [2]).

A previous study demonstrated that AR⁻ cells were enriched in the PSA⁻ cell population [2]. Therefore, we first utilized the PSAP-eGFP tools to select for the AR⁻ cells. Despite low PSA expression in GFP⁻ LNCaP clones, they displayed heterogeneous AR expression (Figure 2-4). This suggests that PSA expression is not fully concordant with that of AR expression in PCa cells; there are AR⁺/PSA⁻ and AR⁻/PSA⁻ PCa cells, as we previously observed in primary prostate tumor samples (Figure 1-4) [2]. Hence, we were unable to establish pure AR⁺ or AR⁻ clones with the PSAP-eGFP system.

We then proceeded to the AR promoter system. Compared to the PSAP, we predicted that the ARP will theoretically be more specific for AR expression. The 4 ARP fragments included the 3.5 kb full AR promoter and three shorter fragments. They were active and specific in LNCaP cells based on the luciferase assays (Figure 2-6, C). However, when ARPs were used to drive RFP in LNCaP cells, the labeling efficiency was so limited that very few cells were RFP⁺. Considering that the majority of LNCaP cells are AR⁺, the low RFP expression in the transfected or infected cultures suggested low efficiency of the ARP activity. These results may be due to the fact that AR expression may not depend solely on the 3.5 kb or the shorter promoter region, but also on the presence of additional enhancers or post-transcriptional factors, which regulate

AR expression in LNCaP cells. We concluded that the two non-genomic strategies we adopted here do not seem to be sufficient to select for AR⁺ versus AR^{-/^{lo}} subpopulations. Consequently, our next efforts focused on the generation of novel genetic models featuring zinc finger nucleases (ZFNs) mediated integration and CRISPR-Cas9 system mediated AR knockout.

Chapter 3. Build AR-tagging clones with Zinc Finger Nucleases (ZFNs)

3.1. Introduction

Conventional gene editing technology relies on homologous recombination (HR) in embryonic stem (ES) cells to edit specific gene loci and generate animal models [96]. Unfortunately, targeting of specific genes and regulatory elements by virtue of HR generally results in an extremely low number of desired recombination events, thus presenting a huge challenge for routine use in of gene targeting. Studies have demonstrated that DSBs (double-strand breaks) are potent inducers of recombination in mammalian cells, and a DSB at the target locus can stimulate gene targeting by 1,000 fold [97]. Due to the limited availability of sequence-specific endonuclease in mammalian cells, DSB-induced HR did not contribute significantly to gene targeting until recently. Fast developing programmable nucleases, including ZFNs, transcription activator-like effector nucleases (TALENs), and the *Streptococcus pyogenes*-derived CRISPR–Cas9 (clustered regularly interspaced short palindromic repeats-CRISPR-associated 9) comprise a group of powerful gene-editing tools in human cells [98, 99]. The above three types of nucleases operate via the same mechanisms of action: cleavage of chromosomal DNA in a site-specific fashion triggering endogenous DNA repair systems resulting in targeted genome modification. DSBs in the chromosome are then repaired by nonhomologous end joining (NHEJ), which is an error-prone process that can lead to disruption of the targeted gene. On the other hand, DSBs can be repaired by homology-directed repair (HDR), a form of HR that faithfully copies the genetic information from a given sequence, allowing for the integration of an expression cassette into certain genomic harbor or for the insertion of a functional copy of a disease-causing mutated gene downstream of its own promoter [100] (Figure 3-1, C).

The specificity of these programmable nucleases is determined by different factors. In ZFNs, zinc-finger binding domains are engineered to recognize a DNA sequence of interest and each zinc-finger recognizes three to four nucleotide bases (Figure 3-1, A and B). The zinc-fingers are then fused to the nuclease domain of *FokI* endonuclease to yield a highly specific ZFN. Because *FokI* must form a dimer to induce a DSB, two ZFNs were needed to successfully introduce a DSB (Figure 3-1, A). In contrast, the CRISPR–Cas9 RNA-guided DNA endonuclease is localized to a specific DNA sequence via a single guide RNA (sgRNA) sequence. The guide RNA base pairs with a specific targeting sequence that is adjacent to a protospacer adjacent motif (PAM) sequence in the form of NGG or NAG. The flexibility and modularity of these gene-editing tools has led to the development of numerous genome-engineering applications, greatly facilitating cancer research [101].

To study AR heterogeneity and select for homogeneous AR positive PCa cells, we constructed a novel AR-tagging model with ZFNs. To do this, we inserted a tag gene, tagRFP, in frame into the C terminus of the endogenous *AR* locus to report AR expression in LNCaP cells, and established multiple stable RFP⁺/AR⁺ LNCaP clones.

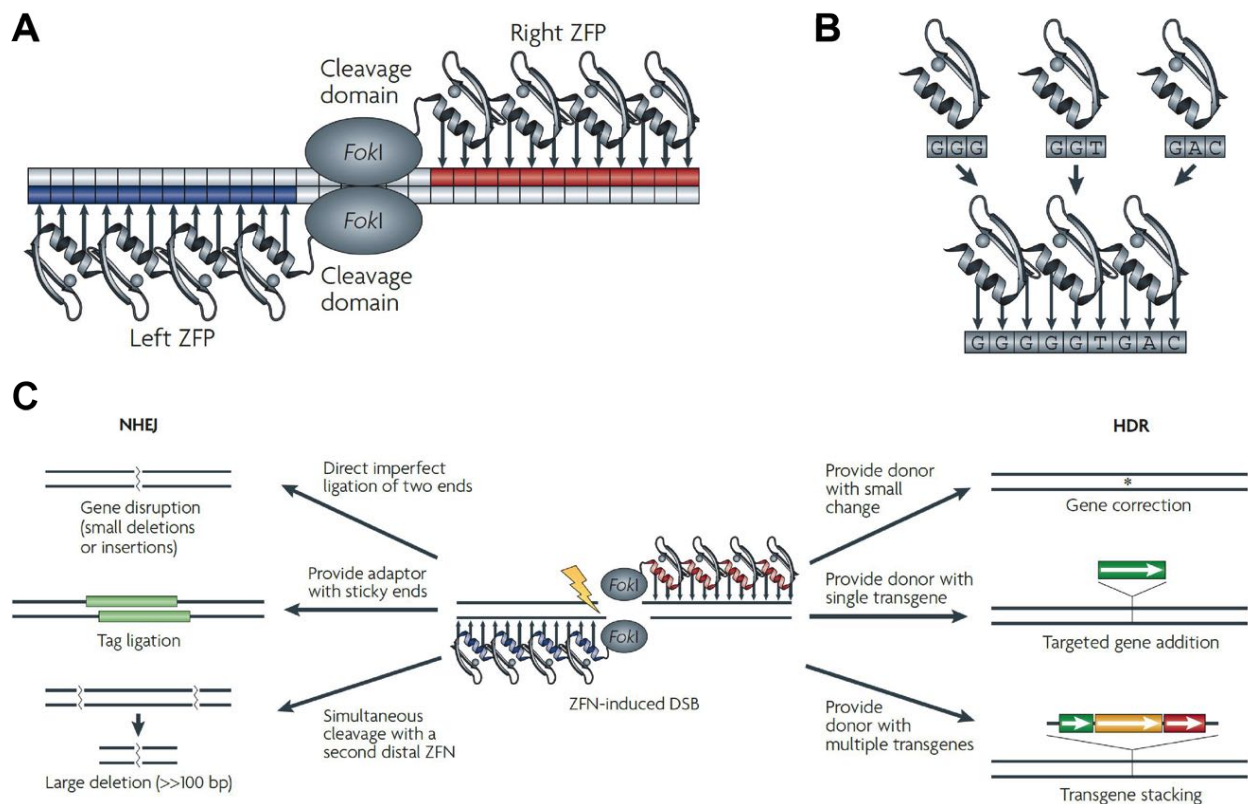


Figure 3-1 Structure and design of ZFNs, and the outcome of genome editing using programmable nucleases

This figure is adapted from Urnov, F.D., Rebar, E.J., Holmes, M.C., Zhang, H.S., and Gregory, P.D., Genome editing with engineered zinc finger nucleases. *Nature reviews. Genetics*, 2010. 11(9): p. 636-46, [102] with the permission License number: 4033781145018

A. Sketch of a ZFN dimer bound to its target. Each ZFN contains the cleavage domain of FokI linked to an array of three to six zinc fingers (four are shown here) that have been designed to specifically recognize sequences (blue and red boxes) that flank the cleavage site. A small number of bases (typically five or six) separate the ZFN targets.

B. Modular assembly of a three-finger protein from individual fingers. To generate a zinc finger protein (ZFP) with specificity for the sequence GGGGGTAC, three fingers are identified that each bind a component triplet.

C. A diagram depicting various outcomes that can potentially result from the introduction of a site-specific DNA break. A ZFN pair is shown bound to a genomic target site (the two different DNA binding domains are shown in red and blue). The DSB generated by ZFN cleavage induces DNA repair processes that may be influenced by the addition of an investigator-designed donor DNA. As shown on the left, if the break is resolved via non-homologous end joining (NHEJ) (which will occur in the absence of donor DNA), this can lead to the following outcomes (from top to bottom): gene disruption — the two ends can be ligated back together, frequently with loss or gain of genetic information at the

site of the break, resulting in small insertions or deletions; tag ligation — if a double-stranded oligonucleotide is provided with overhangs complementary to those left by the ZFNs (an adaptor), it will be ligated into the chromosome, thus producing, for example, a tagged allele; large deletion — two simultaneous DSBs made on the same chromosome can lead to a deletion of the entire intervening stretch. As shown in the right panels, if the break is resolved via homology-directed repair (HDR) (which will occur in the presence of donor DNA), this can result in (from top to bottom): gene correction — if the donor specifies solely a single-base-pair change (for example, a restriction fragment length polymorphism encoding a novel allele), this will result in 'gene correction' that subtly edits the endogenous allele; targeted gene addition — if a donor is provided that carries a transgene or multiple linked transgenes at the position corresponding to the site of the break, the sequence will be transferred to the chromosome via the synthesis-dependent strand annealing pathway. [102]

3.2. Materials and methods

3.2.1. Zinc finger nuclease design

Three customized ZFN pairs were designed to target the C terminus of AR right before the stop codon TGA: ZFN1 (GCCCATCTATTTCCACACCCnGTGAAGCA TTGGAA), ZFN3 (CAAGCCCATCTATTnnnACACCCAGTGAAGCATTGGAA) and ZFN14 (ACCTGCTAATTAATCAAGTCACnnATGGTGAGCGTGGACTTTCCG) (Sigma, St. Louis, MO). The vector map is shown in Figure 3-2, A.

3.2.2. Construction of donor plasmid

Donor vector contains the sequences of furin binding peptide, spacer, P2A peptide and tagRFP cDNA. This backbone was flanked with homologous arms, which are the sequences immediately upstream and downstream *AR* stop codon (Figure 3-2, B). The original donor plasmid has two 800 bp HR arms, which were synthesized by GeneScript (Piscataway, NJ). We synthesized two more donor plasmids with different HR arm lengths, 300 bp and 156 bp and both 2 kb at 5' and 3' ends. In order to report the activity of the donor transgene, we inserted the transgene into a pEGFP-C1 (Clontech) vector via XhoI and BamHI sites.

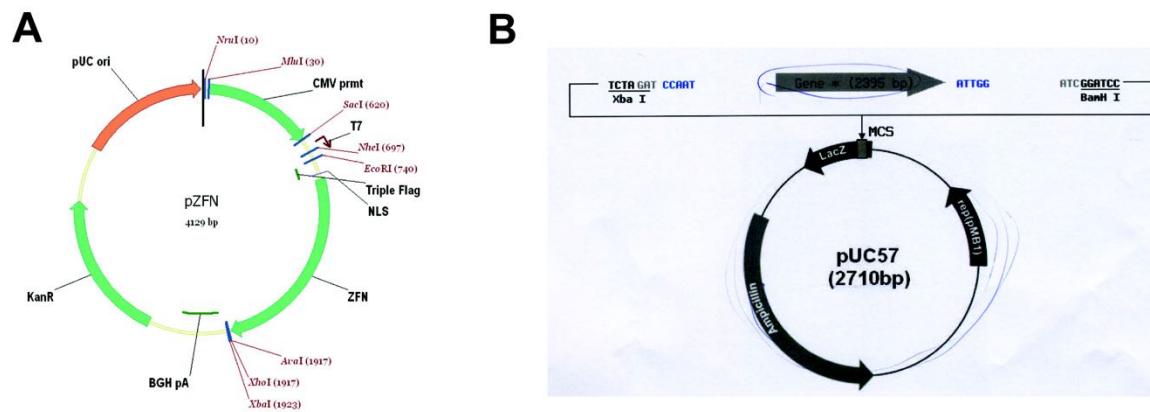


Figure 3-2 ZFNs and the donor structure map

A. The ZFN vector map. CMV promoter drives the ZFN expression. Total construct size is 4129 bp.

B. The donor plasmid map. 2395 bp of transgenes were inserted into pUC57 backbone between XbaI and BamHI sites.

3.2.3. Cell culture and transfections

K562, LNCaP, and PC3 cells were obtained from ATCC (Manassas, VA), and were maintained in RPMI 1640 supplemented with 10% FBS. The first round of ZFN and donor plasmid transfection was performed with Lipofectamine 2000. Four groups of 150,000 cells were plated in a 6-well plate one day before transfection. A mixture of 10 μ L Lipofectamine 2000 carefully added to 90 μ L Opi-MEM, was incubated at room temperature (RT) for 5 min. Four separate tubes, containing 5 μ g of pmaxGFP-only, 5 μ g of donor-only, 5 μ g of ZFNs-only or 10 μ g of ZFNs+donor, were prepared and mixed with Opi-MEM to a total volume of 100 μ L. The DNA mixtures were then carefully added, in a drop-wise manner, to the Lipofectamine 2000 mix and incubated at RT for 20 min. After changing the cell medium to 800 μ L OpiMEM, the four DNA and lipofectamine 2000 mixtures (200 μ L total) were added into separate wells, and after 8 hours, 100 μ L FBS was added to each well. A second round of ZFN and donor plasmid transfection was done with Electroporation (Bio-rad, CA). In this experiment, $4\text{-}5 \times 10^6$ cells were harvested, pelleted, washed once with 1xPBS, and suspended in Gene Pulser® Electroporation Buffer (Bio-rad, CA) at a density of 5×10^6 cells/400 μ L. Each 400 μ L single cell suspension was then combined with the four groups of DNAs including 5 μ g of pmaxGFP, 5 μ g of donor-only, 5 μ g of ZFNs-only, 10 μ g of ZFNs+donor, transferred to a 0.4 cm Gene Pulser® cuvette (Bio-Rad, CA) and electroporated at 200v/~mA. A third round of ZFN and donor plasmid transfection was performed with Nucleofector™ (Lonza, NY). In this experiment, $4\text{-}5 \times 10^6$ cells were harvested, washed with 10 ml HBSS twice, and resuspended in 100 μ L solution R. We then combined 100 μ L containing 5×10^6 single cell suspensions with four groups of DNAs including 5 μ g of pmaxGFP, 5 μ g of donor-only, 5 μ g of ZFNs-only, or 10 μ g of ZFNs+donor. The cell/DNA mixtures were then

transferred into a nucleofector cuvette. Program T-016 was specifically used for K562 cells, T-013 for PC3 cells, and program T-009 for LNCaP and other cell lines.

3.2.4. Cel-1 assays

Genomic DNA from ZFNs-only and pmaxGFP-only cells was extracted via the QiAamp DNA Mini Kit at 48 and 72 hrs post transfection. For PCR, 200 ng of genomic DNA for each sample was used to amplify the genomic region around the ZFN target sites using 5'-GGGGAGAAGTCACGCTATGA and 3'-CAAGACTTGCTCGTTCCTCC primers. PCR products were purified with the QIAquick PCR purification kit per the manufacturer's instructions. PCR product from each sample (400 ng total), was eluted in 20 μ l 1xGoTaq buffer, and subjected to a re-annealing process to enable heteroduplex formation (95°C for 10 min, 95°C to 85°C ramping at -2°C/s, 85°C to 25°C at -0.1°C/s, and 25°C hold for 1 min). After re-annealing, products were treated with 1 μ L SURVEYOR nuclease and 2 μ L SURVEYOR enhancer at 42°C for one hr. Products were then analyzed on a Novex 10% TBE gel (Life Technologies) at 240 v for 20 min. Gels were stained with ethidium bromide (Life Technologies) for 5 min at RT and imaged with Image Quant LAS 4000 (GE) (Figure 3-3, A).

3.2.5. Targeted integration analysis

Genomic DNA was isolated from ZFNs+donor and donor-only cells using the QiAamp DNA Mini Kit 48 and 72 hrs post transfection. For PCR, 200 ng of genomic DNA from each sample was used to amplify the region flanking both the 5' and 3' homologous arms (Figure 3-3, B), using FWD 5'-GTGCAGCCTGTAAGCAAAC-3' REV 5'-CTTAATCAGCTCTTCGCCCTTA-3' or FWD 5'-CAAAGAGACCTACGTGAGC-3' and REV 5'-TTTGGGGGTGAGGCATTAAC-3' primers. The PCR cycling program was as

follows: 95°C 5 min, 95°C 30 sec (decrease 0.5°C every cycle) and 68°C 1.5 min for 15 cycles, 95°C 30s 58°C 30s and 72°C 1.5 min for 20 cycles, last extension for 5 min at 72°C. PCR products were run on a 1% TAE agarose gel at 100 v for 40 min, and imaged with Image Quant LAS 4000 (GE) (Figure 3-3, B).

3.2.6. Fluorescence-activated cell sorting (FACS)

PCa cells, 72 hrs post transfection with ZFNs+donor and donor-only, were trypsinized and dissociated into 5×10^5 cells/ml in 1xPBS. Generally, $1 \sim 2 \times 10^6$ cells were used for FACS. To eliminate dead cells, we stained the single-cell suspension with eFluor506 viability dye (eBioscience, 65086614) for 30 min at 4°C per manufacture's instructions. The tagRFP was excited with the 555 nm laser and analyzed at 584 nm. The viability fluorescence eFluor506 was excited at 405 nm laser and analyzed at 506 nm.

3.2.7. LNCaP conditioned media collection

LNCaP cells were cultured in RPMI supplemented with 10%FBS. Once at 70% confluence, media was aspirated and cells were rinsed three times with sterile 1xPBS, and three times with serum-free RPMI. After cells were incubated in 50 ml serum-free RPMI for 48 hrs, the conditioned media was removed and filtered with a 0.45-micron filter. A 1:1 ratio of conditioned media to normal growth media was then subsequently used to culture single LNCaP cells.

3.2.8. LNCaP single-cell clonal culture

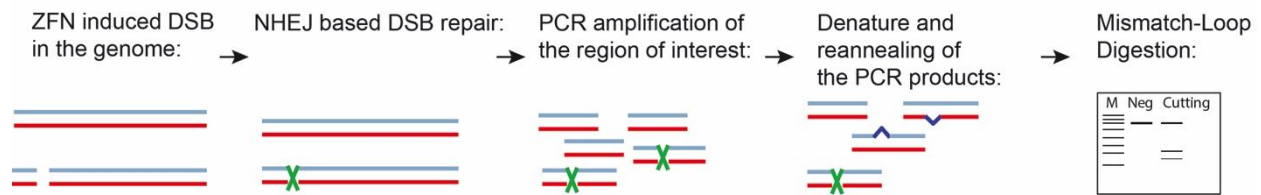
The RFP⁺ LNCaP cells sorted from the ZFN and donor co-transfected group, were cultured for one week, and then trypsinized and seeded into 96-well plates at a ratio of 1 cell per 200 μ L of media per well. After 5 hrs, fluorescence microscope was used to scan

all wells, and wells containing a single RFP⁺ cell were marked. Single LNCaP clones were identified after three weeks, and were passed into 24-well plates. Approximately half of the cells at the 24-well stage were stored in liquid nitrogen.

3.2.9. Genotyping

Genomic DNA was isolated from RFP clonal cells using the QiAamp DNA Mini Kit. Two sets of primers were used for genotyping these clones including: P1 flanking the ZFN cutting site FWD: 5'-GAAGGGGGAGGAAACAAAAG-3' and REV: 5'-TAGAGGAAATTCCCCAAGGC-3', and P2, which were designed inside the transgene tagRFP, FWD: 5'-ACTTCAAGTGCACATCCGAGG-3' and REV: 5'-AGTTTGCTAGGGAGGTCGC-3'.

A Cel-1 Assay:



B Junction PCR:

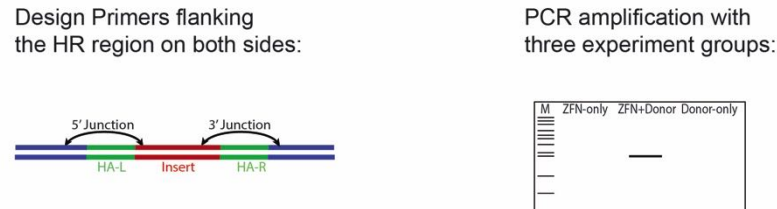


Figure 3-3 Cel-1 assay and junction PCR

A. The Cel-1 assay was used to estimate the cutting efficiency of ZFNs in targeted region. The region of interest was amplified, denatured and then the PCR products were re-annealed. The alleles with mismatches can be annealed with wild-type alleles, and form mismatch loops. Using the SURVEYOR enzyme, which can recognize and digest the mismatch loops, appearance of the two lower bands on gel compared to the negative control indicates DSBs and ZFN cutting efficiency.

B. Junction PCR was used to predict the possibility of integration using genomic DNA. We designed primers flanking 5' and 3' HRs, and only the genomic DNA containing integrated region should show a positive band. Donor-plasmid-only transfected cells were used as negative control.

3.3. Results

3.3.1. Design an AR tracking model in PCa cells with ZFNs

In this section, our goal was to generate AR-tagged PCa cell line models, in which a reporter gene was knocked into the C-terminus of AR under the control of endogenous promoter. The workflow and overall strategy are shown in Figure 3-4 and Figure 3-5. First, among the four commonly used human PCa cell lines, LAPC9, LAPC4, PC3 and LNCaP, we discovered a ~100 bp consensus region upstream of the *AR* stop codon (Figure 3-6). In this region, sixteen ZFN candidates were identified and three of them were selected for further studies including ZFN14, which displayed the highest cutting efficiency, and ZFN1 and ZFN3, which were closer to the stop codon (Figure 3-7). Meanwhile, donor constructs containing the reporter tagRFP were designed for the HDR (Figure 3-8). The 2A peptide was used to link AR and tagRFP, based on the observation that not only can 2A peptide divide the two proteins during translation, but their expression levels were highly coordinated as well [103]. The P2A peptide (ATNFSLLKQAGDVEENPGP) was used in the final donor construct, which produces the highest cleavage rates in multiple human cancer cell lines [104]. Further, the P2A peptides have been optimized for transgene expression by adding furin cleavage site (RAKR) and spacer (SV-SGSG) peptides [105]. Furin is a ubiquitously expressed endoprotease and cleaves many precursor proteins at specific internal peptide bonds in the trans-Golgi network. This design allows furin to cut off the 2A residues, leaving a minimum attachment (RAKR) to AR. To test the reporting efficiency of the transgene in PCa cells, the transgene was inserted into the C terminal of pEGFP-C2 (Clontech, CA) (Figure 3-8, upper panels). At 72 hours post transfection (5 μ g), we observed a highly coordinated expression of eGFP and tagRFP in LNCaP cells (Figure 3-8, lower).

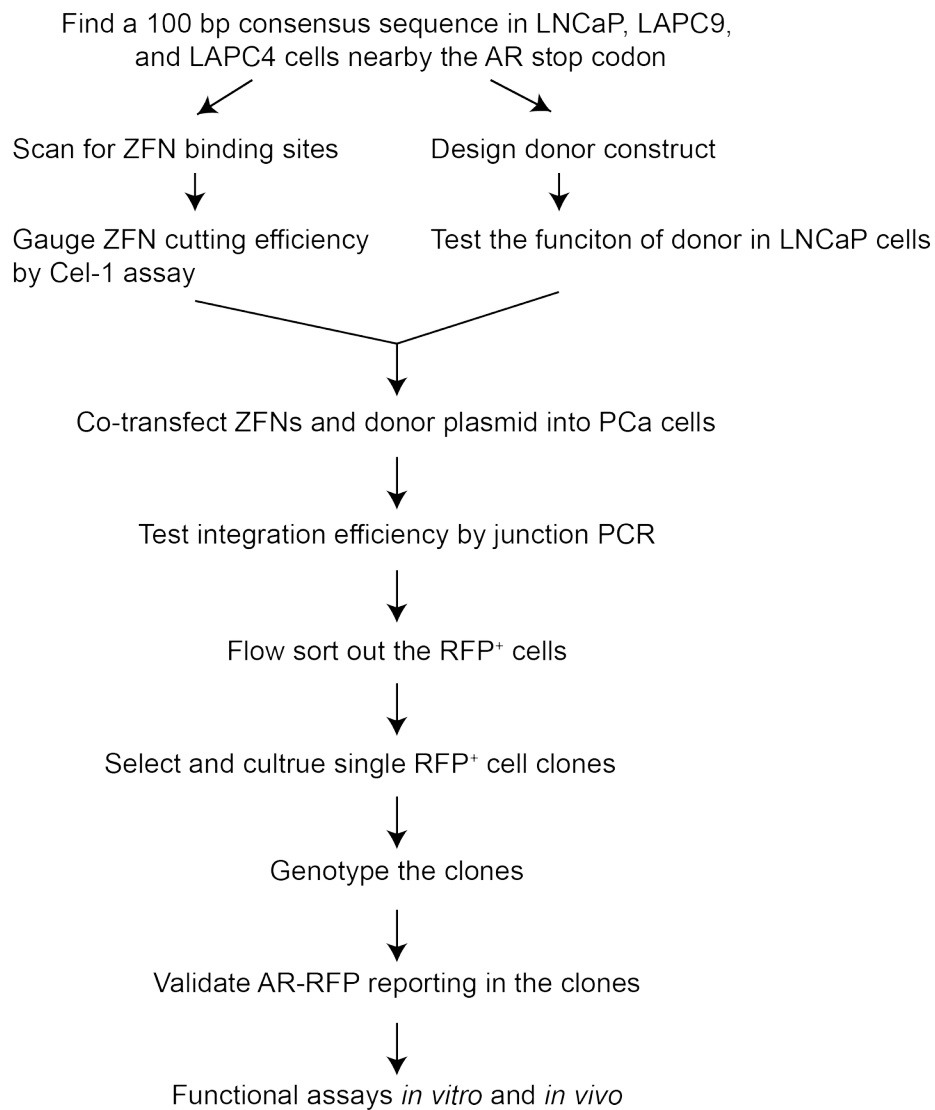


Figure 3-4 workflow of generating AR-tagging clones with ZFNs.

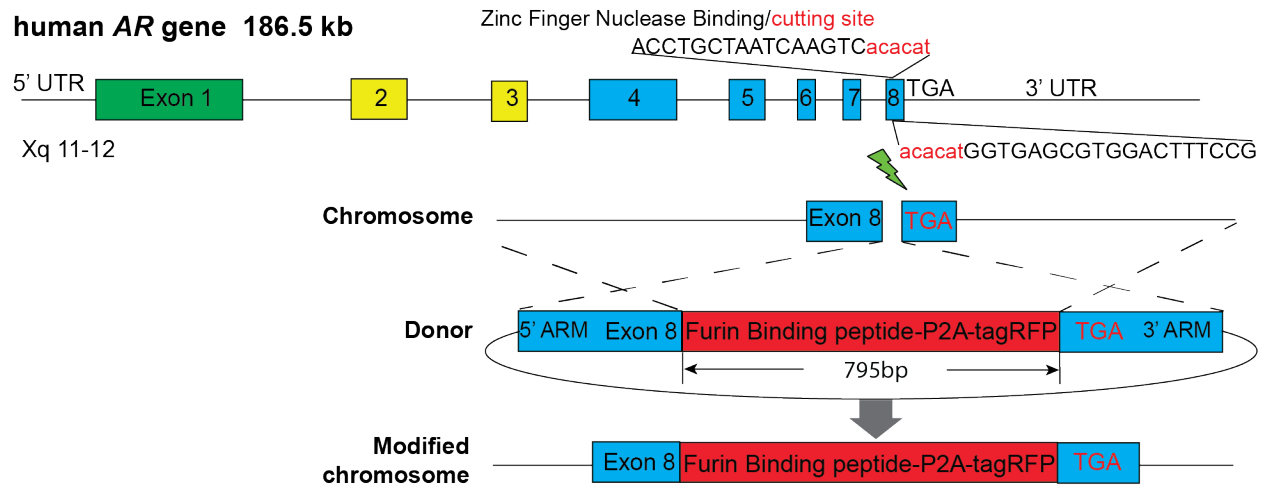


Figure 3-5 AR tagging strategy

ZFN14 pair (ACCTGCTAATTAATCAAGTCACnnATGGTGAGCGTGGACTTTCCG) was designed to induce DSB at the 3' of AR gene before the stop codon TGA. Donor vector contains the sequences of furin binding peptide, P2A peptide and tagRFP cDNA. This backbone was flanked with 800 bp homologous arms on each side, which are the sequences immediately upstream and downstream of AR stop codon. With HDR, the transgenes were inserted into AR gene before TGA.

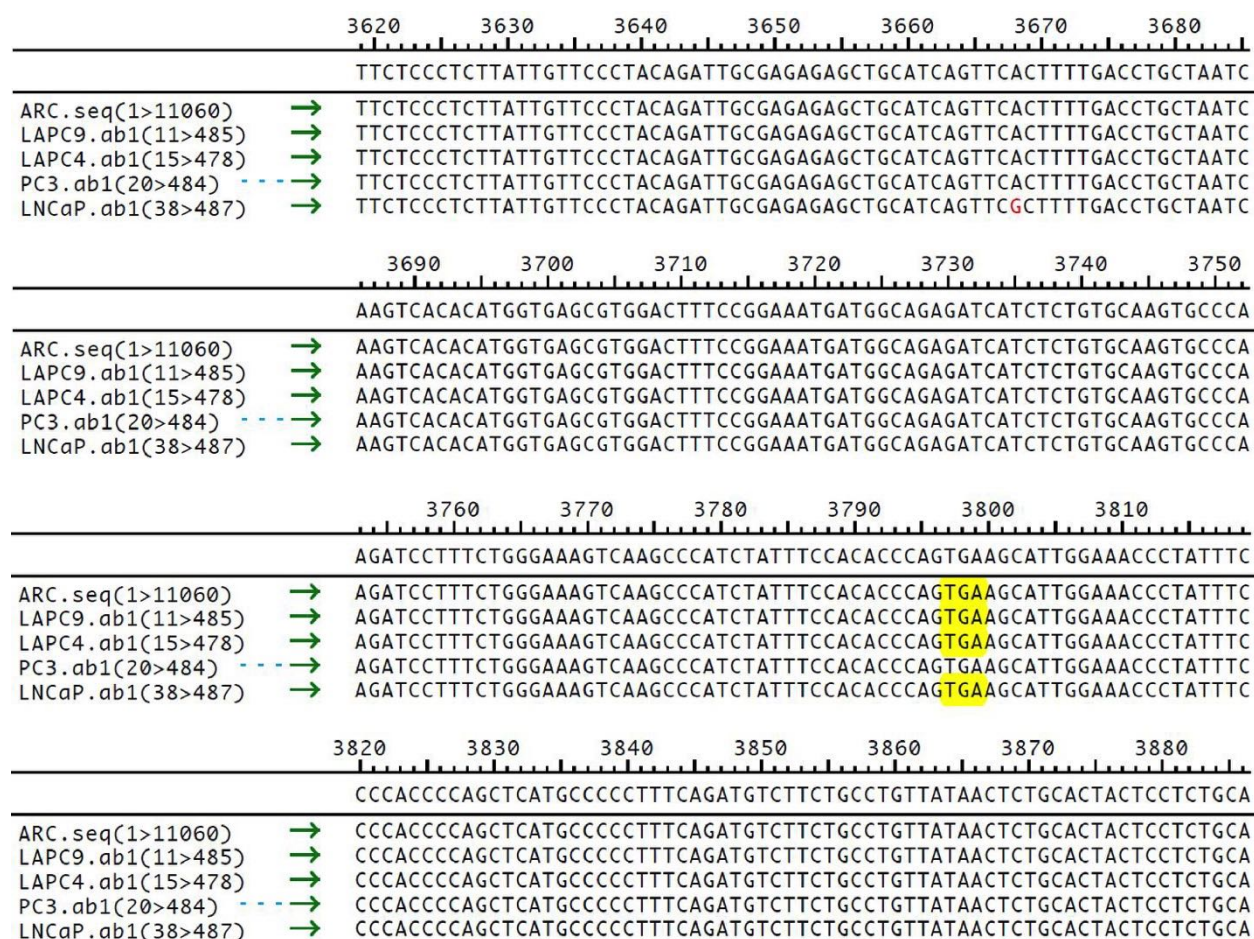


Figure 3-6 Consensus sequence at the AR C terminal region in 4 human PCa cell lines.

Alignment of the AR C-terminal sequence in cultured LAPC9, LAPC4, PC3 and LNCaP cells with the hAR sequence (NC_000023.11) at GeneBank. The sequence between the T877A mutation (red) in LNCaP cells and the stop codon (TGA; highlighted in yellow) was conserved among the four PCa cell lines.

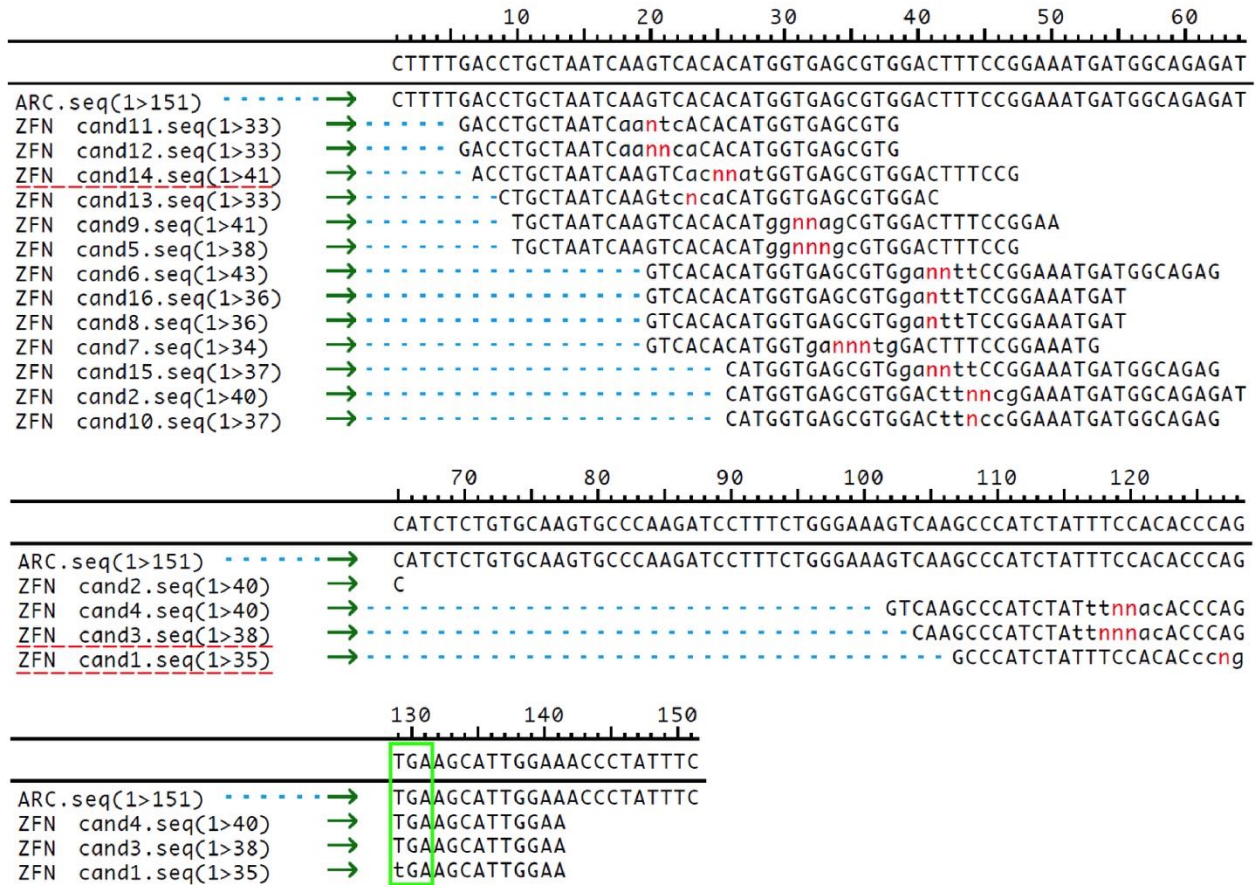


Figure 3-7 ZFN candidates for AR targeting

Shown are the 16 ZFN candidates (cand 1- cand 16) located about 130 bp upstream of the AR C-terminal stop codon (TGA; boxed). ZFN candidate 14, 3 and 1 were synthesized and used in this study.

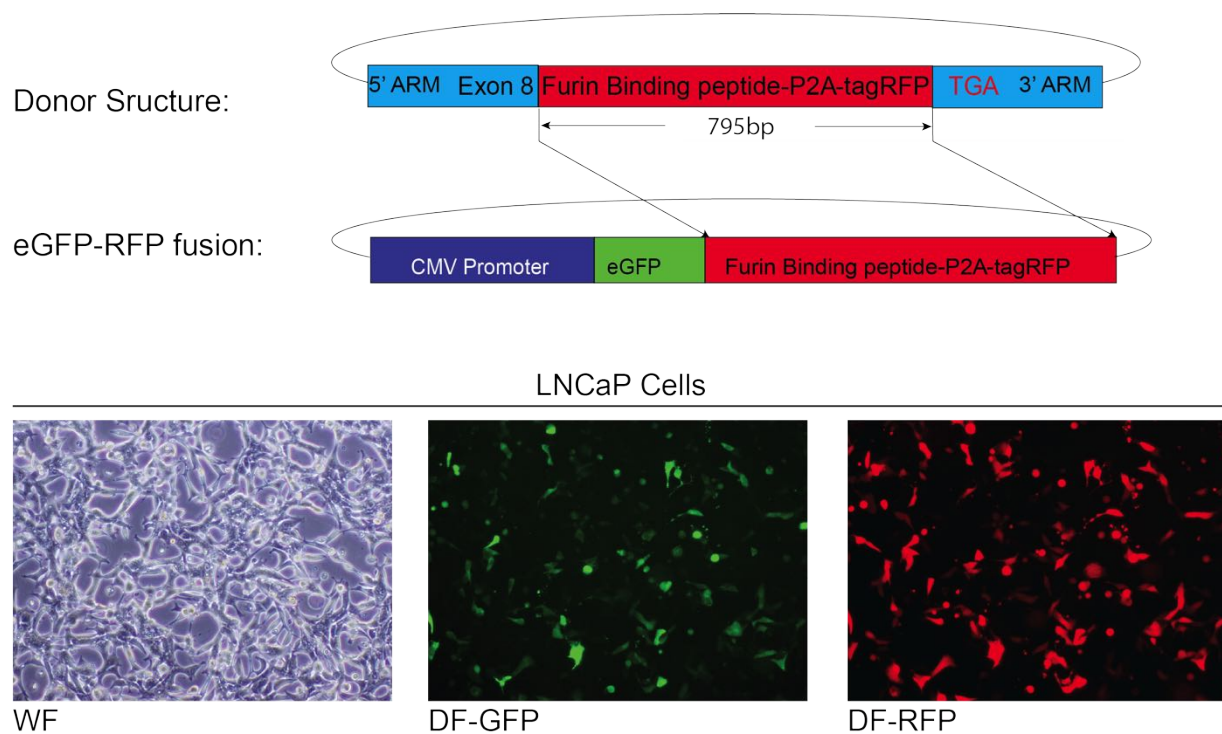


Figure 3-8 Donor plasmid verification

The transgenes in the donor construct were inserted into pEGFP-C2 (Clontech, CA) following eGFP (upper panel). Representative images of LNCaP cells 72 hrs post transfection with the GFP-RFP fusion protein (lower panel).

3.3.2. ZFN14-mediated AR tagging in K562 cells

We initially utilized K562 cells for optimizing the experimental setting. The K562 cell line is a human erythromyeloblastoid leukemia cell line, derived from a 53-year-old female chronic myeloid leukemia patient in blast crisis [106]. In comparison to the majority of PCa cell lines, K562 cells have a higher proliferation rate and are easier to manipulate. Importantly, K562 cells express low levels of AR. In an effort to identify the most efficient method to deliver ZFN pairs, lipid-based transfection, Nucleofection™, and electroporation at different voltage (v) and capacitance (μF) (i.e., 200 v/125 μF, 200 v/150 μF, 250 v/150 μF and 300 v/125 μF), were tested and compared. Results showed that Nucleofection™ with ZFN14 yielded the highest cutting efficiency, as 51% of the tested cells were cut (Figure 3-9). Co-transfection of ZFN14 and the donor construct with Nucleofection™ in K562 cells generated ~14% RFP⁺ cells (Figure 3-10, A and C). The positive junction PCR band confirmed integration in the co-transfected group (Figure 3-10, B). These results suggest that this system works well in cancer cells.

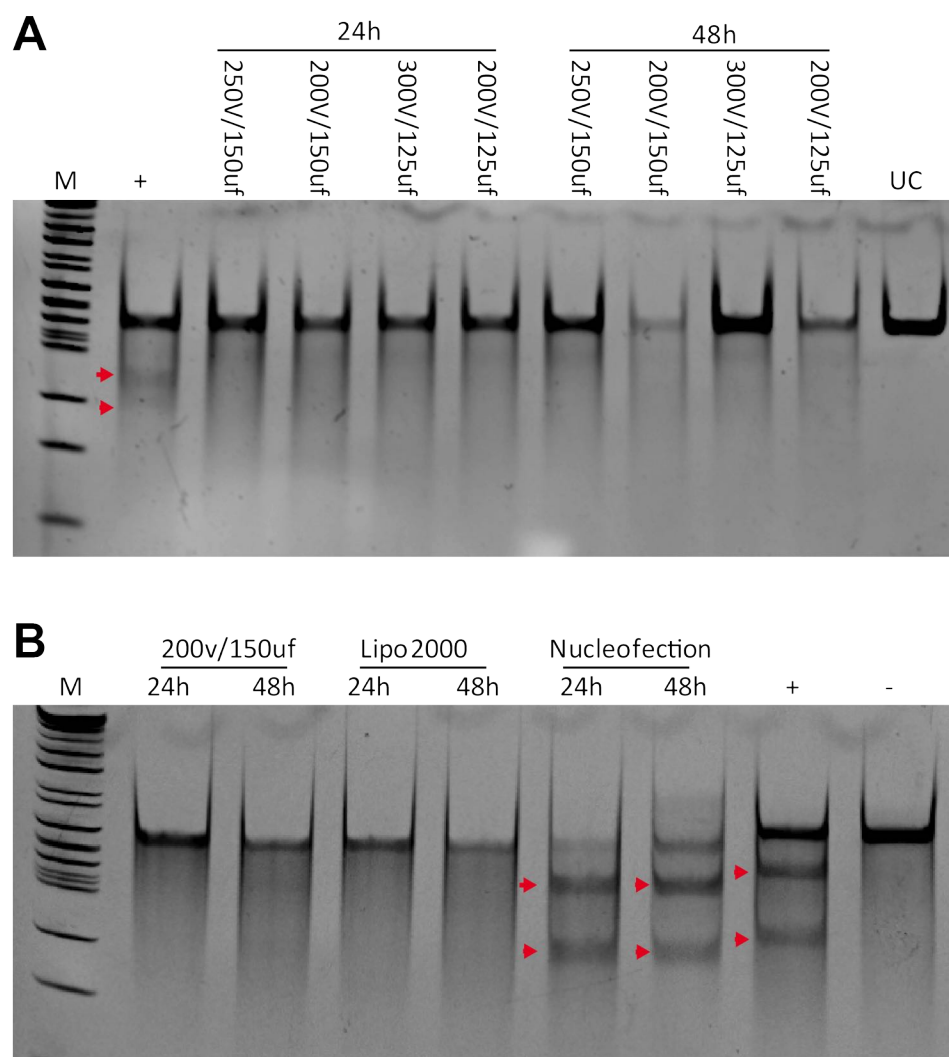


Figure 3-9 Cutting efficiency of ZFN14 in K562 cells

A. Results from the K562 Cel-1 assay. Cells were transfected with 5 ug ZFN14 pairs using the following electroporation conditions: 200 v/125 μ F, 200 v/150 μ F, 250 v/150 μ F and 300 v/125 μ F. Red arrows indicate DSBs induced cut bands.

B. Cel-1 assay results in K562 cells transfected with ZFN14 using three transfection methods: electroporation (200 v/150 μ F), Lipofectamine 2000, and Nucleofection (T-016). Red arrows indicate DSBs induced cut bands.

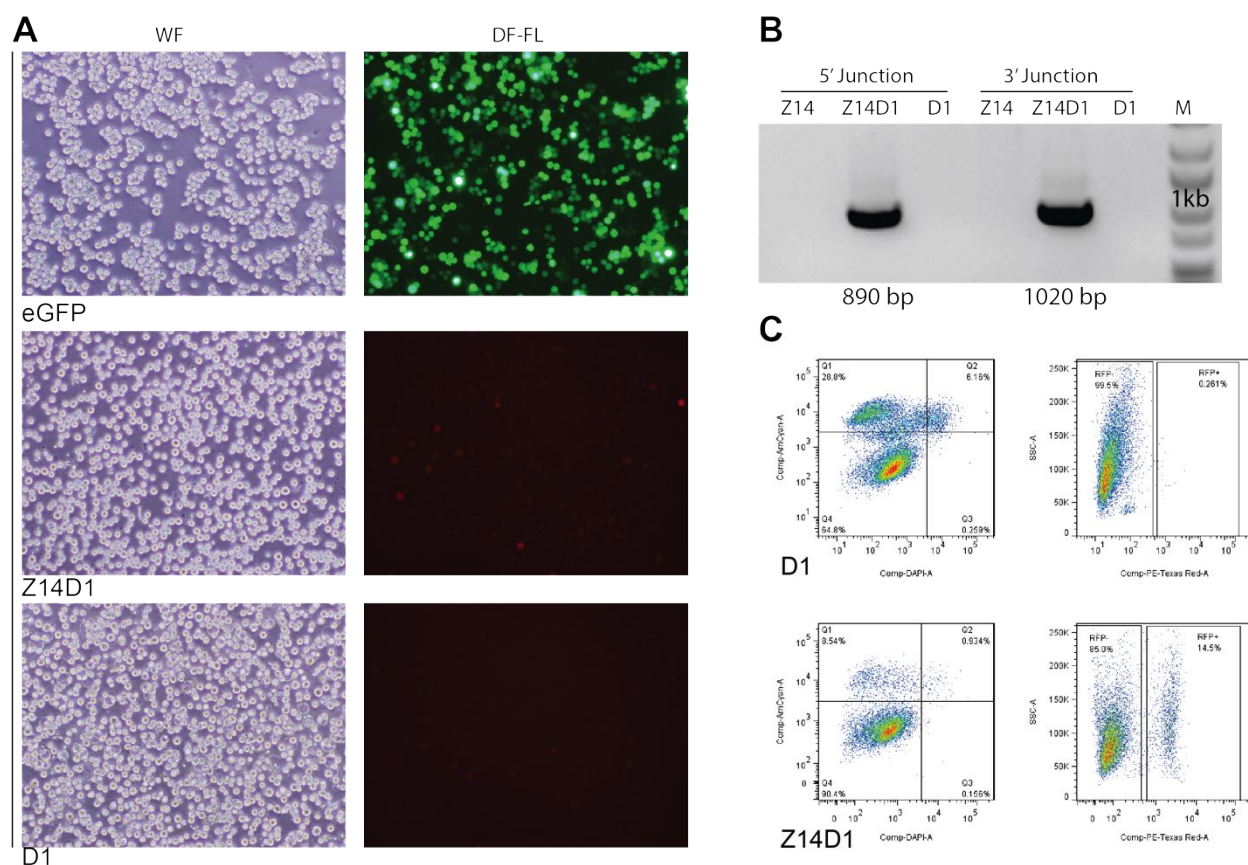


Figure 3-10 AR tagging system in K562 cells

A. Representative images of K562 cells transfected via three different transfection methods: 5 μ g pEGFP (upper row), ZFN14 and Donor1 (D1) plasmid (middle row), Donor1 only (lower row). Shown on the left are phase images, and on the right are dark-field fluorescence images.

B. Gel image of the 5' and 3' junction PCR results. Z14: ZFN14-only transfection, Z14D1: ZFN14 and donor 1 co-transfection, and D1: Donor1-only transfection. Expected PCR product of 5' junction is 890 bp and of 3' junction is 1020 bp.

C. FACS plots of K562 cells. Annexin V and eFluor506 were used to screen for live cells. RFP⁺ cells represent 14% of the total in the co-transfected group, compared to the D1 only group.

3.3.3. ZFN14-mediated AR tagging in LNCaP cells

As LNCaP cells displayed heterogeneous AR expression, our next goal was to select for clonal AR-positive LNCaP cells using the ZFN-KI system.

To deliver ZFN pairs to LNCaP cells, we found that the Nucleofection™ method was again the most efficient, introducing DSBs in approximately 62.5% of the cells (Figure 3-11). In this protocol, Lipofectamine 2000® was used for the ZFN and donor cotransfection, which increased cell survival. Two additional ZFN pairs, ZFN1 and ZFN3 (Figure 3-12, A), were also tested based on their closer proximity to the integration site and the propensity of such ZFNs to yield higher homologous recombination rates [107]. Meanwhile, two additional donor plasmids with differing lengths in the homologous arms were also made providing more options. Donor2 (D2) contains two shorter HRs (300 bp and 136 bp) and Donor3 (D3) contains longer 5' and 3' HRs that are 2 kb each (Figure 3-12, B).

Among the three ZFN pairs tested, ZFN14 was the most efficient yielding 38% of the total DSBs in LNCaP cells, whereas ZFN1 and ZFN3 pairs introduced DSBs in approximately 10% cells (Figure 3-13, A). We didn't observe a significant increase in efficiency when cells were cultured at 30°C (Figure 3-13, A). Additionally, the ZFN plasmid was more efficient than the ZFN14 mRNA (Figure 3-13, C).

Comparing all different combinations of ZFNs and donors, only the group cotransfected with ZFN14 and the original donor (Donor1) produced positive bands in both 5' and 3' junction PCRs (Figure 3-13, B and C), suggesting possible integration at the target site with the ZFN14/D1 combination. Approximately 1% of the RFP⁺ cells with this combination could be identified and sorted out for single cell expansion (Figure 3-13, D). Culturing these LNCaP cells in different conditions (i.e., RPMI + 15% FBS; 10%

Matrigel + RPMI + 15% FBS; RPMI + 15% FBS + 10 nM DHT; or RPMI + 15% FBS + EGF/FGF) proved extremely difficult due to their fragile nature. However, culturing single sorted cells in LNCaP-conditioned media [108] allowed us to successfully establish 46 RFP⁺ LNCaP clones. Two sets of primers, P1 flanking the sequences around the ZFN cutting sites and P2 inside the tagRFP gene (Figure 3-14, A), were used for genotyping. All of the 46 clones harbored one larger allele and one short wild type allele (Figure 3-14, B). All six clones we tested (including Clone 19, 30 and 31) also had positive RFP bands with P2 amplification (Figure 3-14, B). Sequencing of the upper bands indicated successful integration of the transgenes (Figure 3-14, C). We name the tagged clones as AR-clone number, such as AR-30.

We characterized two AR-tagged clones AR-30 and AR-31 first by AR IF staining. We observed homogeneous AR⁺ expression in both clones, compared to 60-70% of AR^{+/hi} cells in bulk LNCaP cell culture (Figure 3-15, A). And the AR-tagged clones were highly RFP⁺ under the fluorescent microscope (Figure 3-15, B). Further, by western blotting with AR and tagRFP antibodies, we demonstrated that AR protein in the tagged clones has the same molecular weight 110 kDa as that in the wild type LNCaP cells (Figure 3-15, C). Using tagRFP antibody, we did not detect any AR signal in the tagged clones AR-30 and AR-31 (Figure 3-15, D). The data suggests that tagRFP was fully cleaved from AR protein in the tagged clones by P2A peptide and furin binding site.

We also verified the correlation between RFP expression and endogenous AR protein level. We observed a loss in RFP⁺ cells 72 hrs post AR siRNA treatment (Figure 3-16, A). FACS analysis confirmed this by revealing that the RFP⁺ population decreased from 60.1% to 30.2% (Figure 3-16, B). This experiment suggested that the RFP faithfully reported endogenous AR expression in LNCaP cells. Four RFP-tagged AR⁺ LNCaP

clones: AR-12, AR-19, AR-30 and AR-31 were utilized in the further studies, which were discussed in Chapter 5.

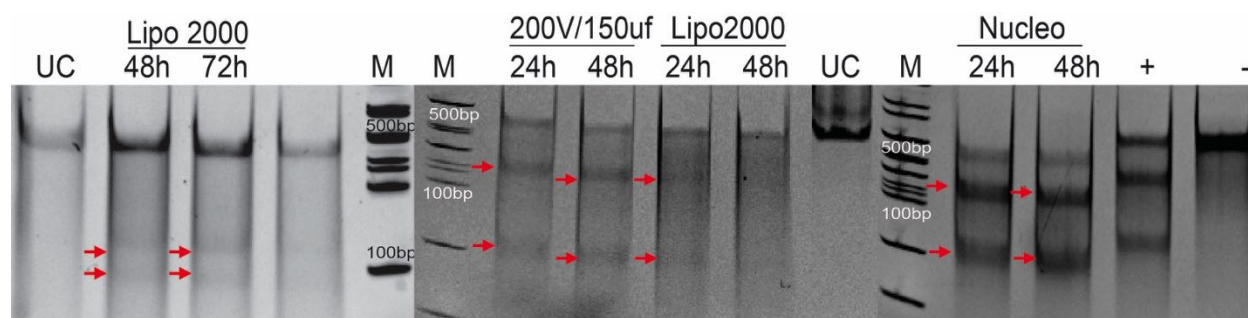
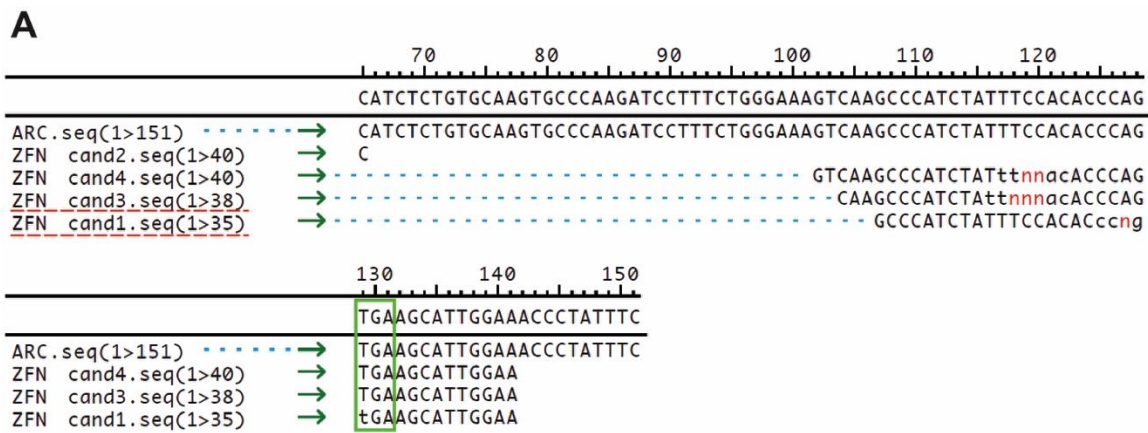


Figure 3-11 Cutting efficiency of ZFN14 in LNCaP cells

Cel-1 assay results of LNCaP cells transfected with 5 μ g ZFN14 pairs using three methods: Lipofectamine 2000[®], electroporation (200 v/150 μ f) and Nucleofection (T-009). Red arrows indicate lower bands cut by ZFNs. The highest cutting efficiency (62.5%) was yielded 48 hrs post Nucleofection.



B Alternative donor Plasmid

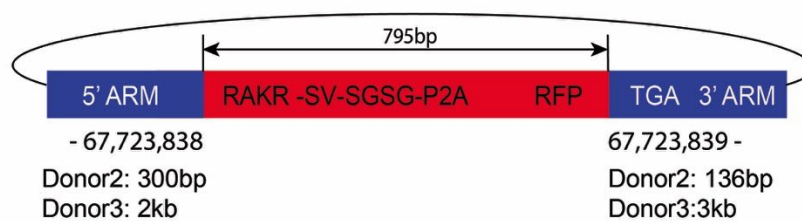


Figure 3-12 Alternative ZFNs and donor plasmid modifications

A. Additional ZFNs. ZFN1 cuts at one nucleotide before the *AR* stop codon TGA. ZFN3 cuts at eight nucleotides before the *AR* stop codon. A red “n” indicates cutting sites.

B. Two modifications were made to the original donor plasmid (Donor1) including: two shorter HRs, 300bp and 136bp (Donor 2), and longer 5' and 3' HRs that are each 2kb (Donor 3).

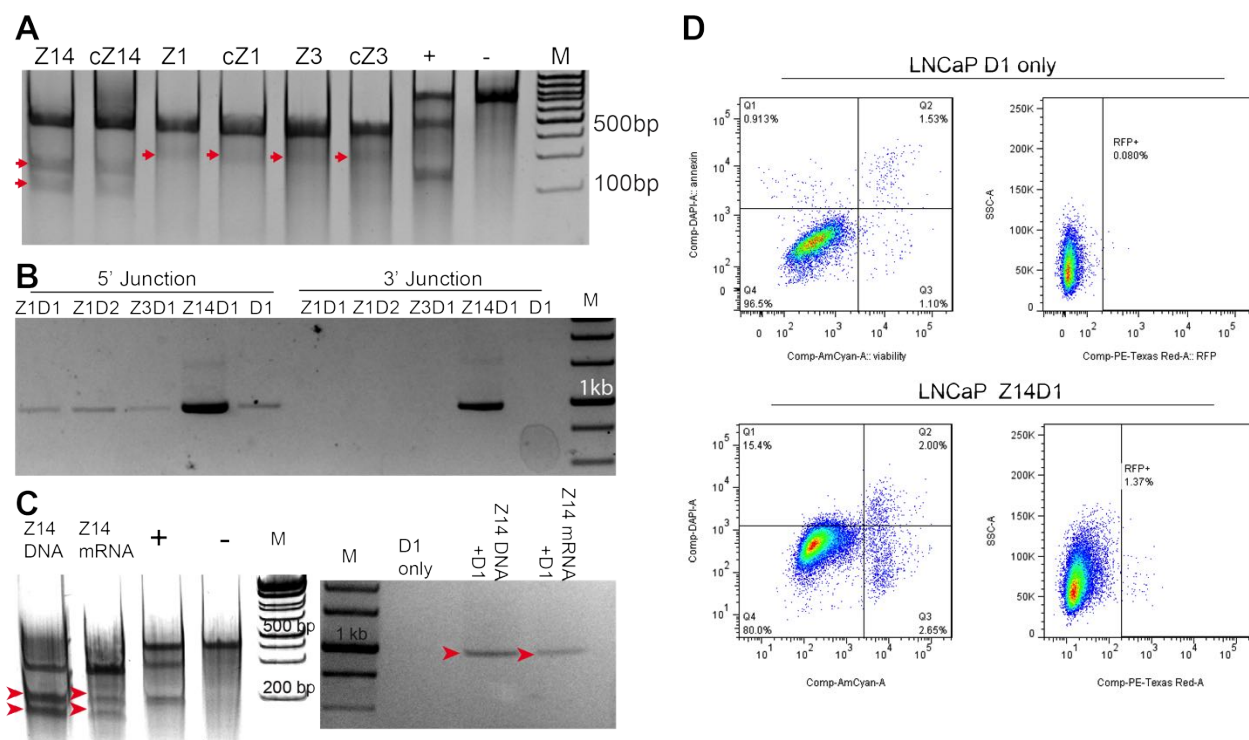


Figure 3-13 The AR tagging system in LNCaP cells

A. Cel-1 assay results. Nucleofection (T-009) was used to deliver 5 μ g of ZFN pairs 1, 3, or 14 d into LNCaP cells. One group of cells was cultured at 30°C to induce a cold shock after the transfection and is indicated as cZ14, cZ1 and cZ3. Red arrows indicate bands cut by ZFNs. +/-: Cel-1 assay positive and negative control.

B. The 5' and 3' junction PCR results of co-transfected cells. Donor1-only (D1) was used as the negative control. Z1D1, Z1D2, Z3D1 and Z14D1 are different combinations of ZFN1, ZFN3, ZFN14 and Donor plasmids Donor 1 and donor 2. Expected PCR product of 5' junction is 890 bp and of 3' junction is 1020 bp.

C. Cel-1 assay and junction PCR results using mRNA and DNA from ZFN14. ZFN14 mRNA was shown to be less efficient in inducing DSBs (red arrows) with Cel-1 assay (Left panel) and homologous integration (red arrows) by junction PCR (Right panel) compared to ZFN14 plasmid.

D. Gating strategy and FACS analysis of tagRFP in LNCaP cells 72hrs post co-transfection of ZFN14 and Donor1. LNCaP cells were stained with Annexin V and eFluor506 to select for live cells. In the examples shown, the RFP⁺ population in the co-transfected group represented 1.37% of the total population, and in the donor-only group RFP⁺ cells represented 0.08%.

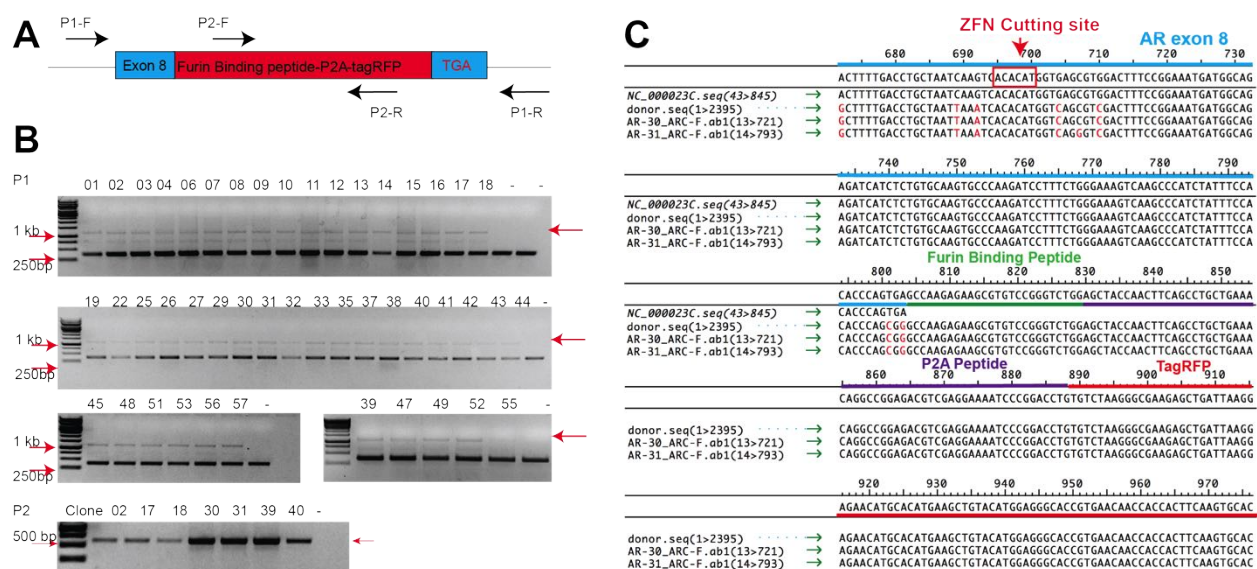


Figure 3-14 Genotyping of the RFP clones

A. Primers used in the RFP⁺ clones genotyping (left panel). P1 and P2 represent the 2 pairs of primers. F, forward; R, reverse.

B. Representative gel images of PCR data utilizing primer 1 (P1) and primer 2 (P2) (right panel). With P1, the upper bands 1174 bp represent the integrated allele and the 400 bp bands the wild type band. With P2, the positive 614 bp bands represent the tagRFP sequences.

C. BLAST results of the RFP clones and wild type AR. The first line represents the wild type AR C-terminus sequence. The second line represents the donor plasmid sequence. The remaining sequences are from clones 30 and 31. The green bar indicates the furin binding peptides, the yellow bar indicates 2A peptides, and the red bar indicates the tagRFP sequences.

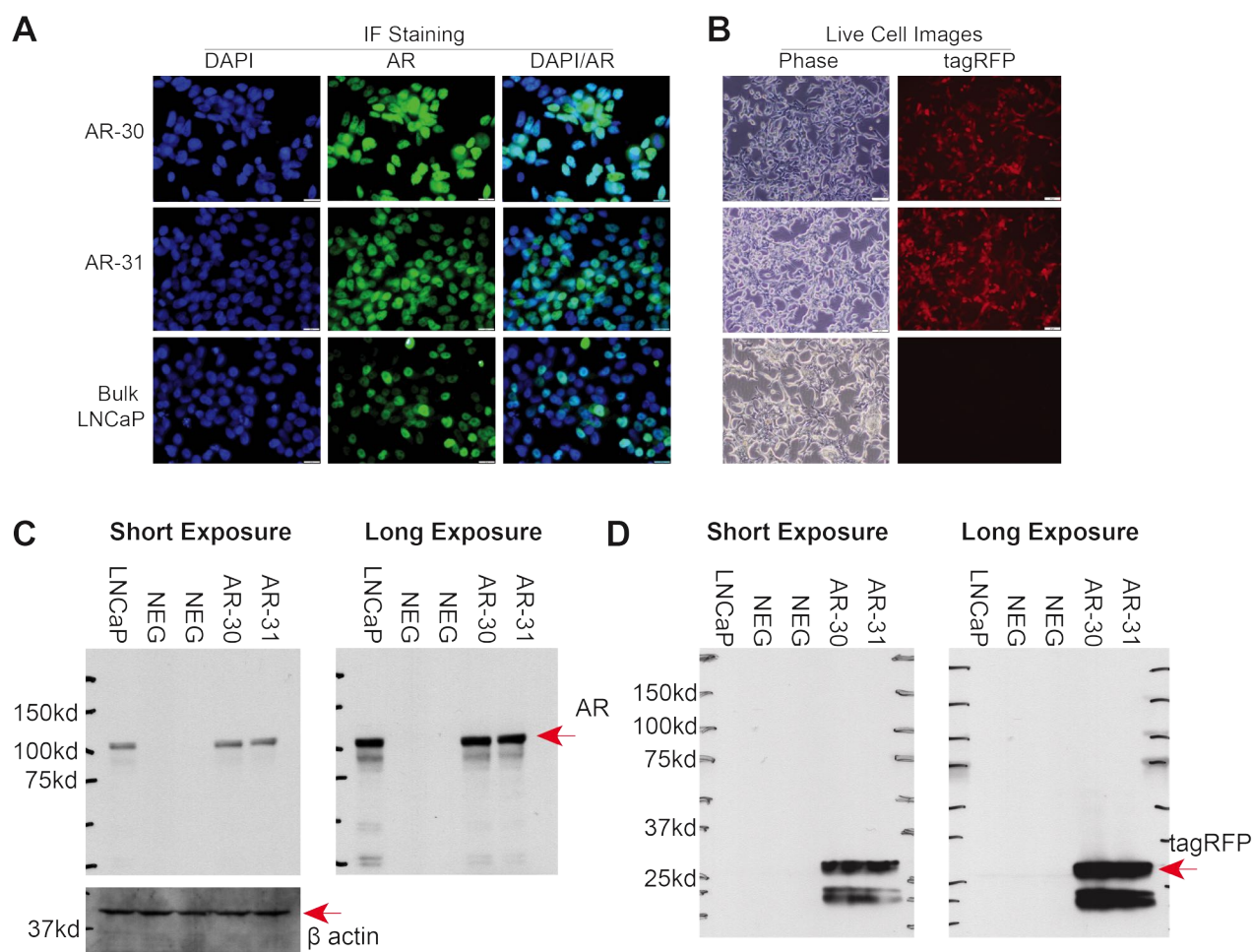


Figure 3-15 Characterizations of the AR-tagged clones

A. AR-tagged clones are homogeneously AR⁺. Representative images of AR IF staining in two AR-tagged clonal cells (AR-30 and AR-31), and in bulk LNCaP cell cultures, in which AR expression is apparently heterogeneous. Scale bar: 20 μm

B. AR-tagged clones are RFP⁺. Live cell images of both phase and dark field of AR-tagging cells and bulk LNCaP cells. Scale bar: 200 μm

C-D. tagRFP was fully cleaved from AR at the protein level. Western blot analysis of AR (**C**) and tagRFP (**D**) protein levels in AR-30, AR-31 and bulk LNCaP cells. Short time exposure films are on the left sides, and longer time exposure films are on the right sides. β actin was probed as an internal loading control.

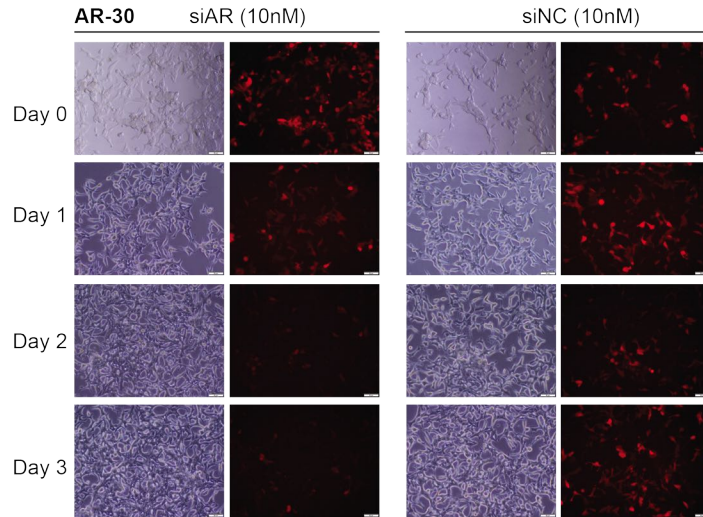
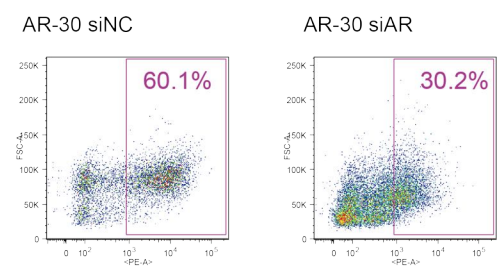
A**B**

Figure 3-16 AR siRNA knockdown in RFP⁺ clones

A. Representative images of two groups of AR-30 cells treated with AR siRNA or negative control (NC) siRNA. The RFP signal is lost in cells treated from day 1 to day 3 with AR siRNA. (Scale bar 20 μ m)

B. FACS analysis showing the knockdown effect of AR siAR on RFP expression

3.3.4. ZFN14-mediated AR tagging in PC3 cells

The AR-negative PC3 cell line model was used as the negative control. Among the three transfection methods, Nucleofection™ was again the most efficient resulting in DSBs in 37% of PC3 cells (Fig 3-17, A). Junction PCR results suggested positive integration at the target site (Fig 3-17, C). However, no RFP⁺ cells were observed upon ZFN14 and D1 cotransfection, supporting the specificity of the tagRFP reporting system. (Fig 3-17, B and D)

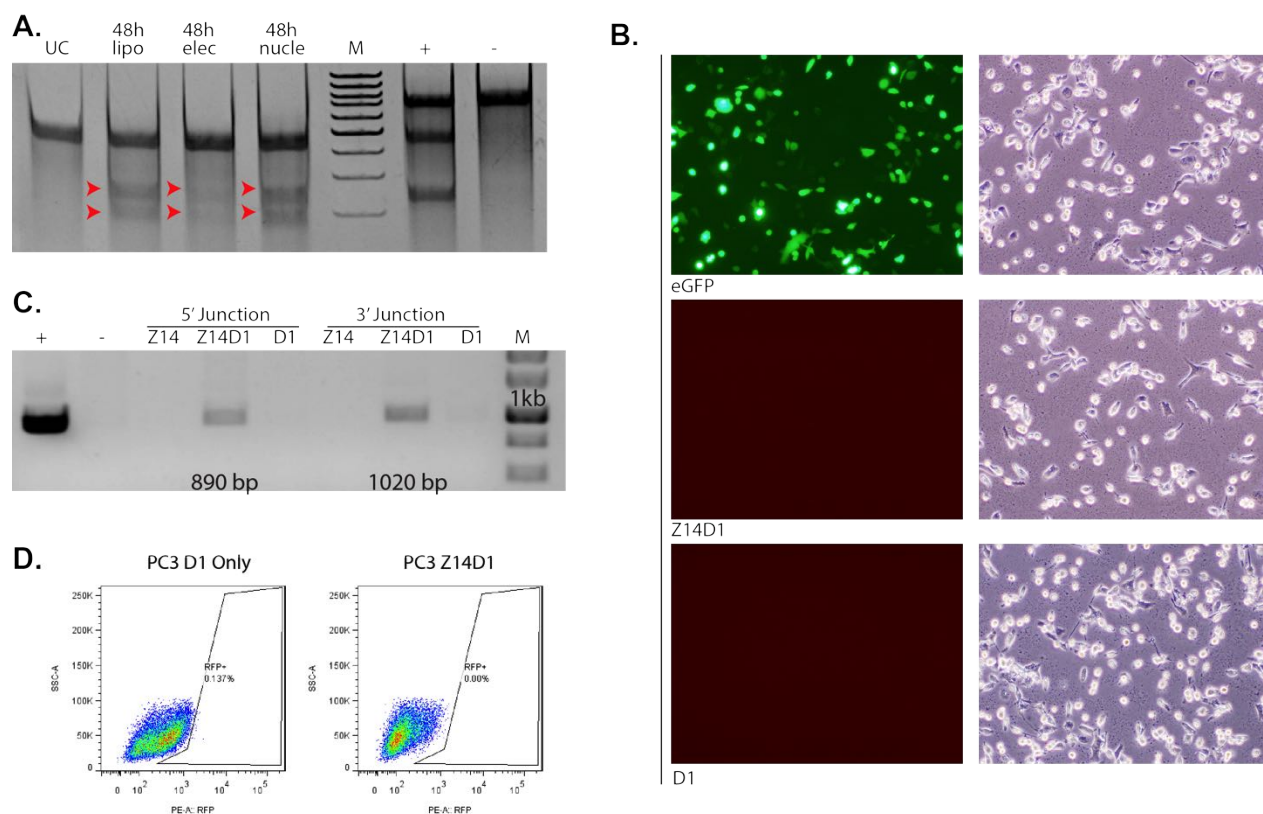


Figure 3-17 The AR tagging system in PC3 cells

A. Cel-1 assay results for PC3 cells. Three groups of PC3 cells 48 hrs post the transfection with 5 μ g ZFN14 by Lipofectamine 2000[®] (lipo), electroporation (elec) and Nucleofection (nucle) are reported. UC represents PC3 cells transfected with 5 μ g GFP.

B. Representative images of cells infected with the indicated plasmids.

C. The 5' and 3' junction PCR results. Expected PCR product of 5' junction is 890 bp and of 3' junction is 1020 bp.

D. FACS analysis plots of PC3 cells subjected to either Donor1 only or ZFN14 and Donor1 co-transfection.

3.4. Discussion

In this part of the project, we have successfully designed a genetic strategy to knock in a fluorescent reporter into the endogenous *AR* locus using ZFN-induced DNA DSBs and a donor plasmid template (Figure 3-5). In brief, we inserted tagRFP in-frame with the endogenous *AR* gene and selected individual LNCaP clonal cell lines, which were verified by sequencing. Although the applications of ZFNs, TALENs and CRISPR/Cas9 technologies have been shown to improve the HDR efficiency, knock-in of large DNAs with HDR-mediated integrations in cancer cells has proven to be extremely difficult. Many of the experimental parameters influencing the efficiency of genome editing need to be finely tuned to achieve a decent integration rate. In our case, we tested three ZFN pairs with various distances to the insertion site, to induce DSBs (Figure 3-7), and we delivered both DNA and mRNA forms of ZFN pairs using three different methods (Figure 3-9, 3-11 and 3-13). Further, we flanked the transgene with three versions of HR arms (~200 bp, 800 bp and 2 kb) (Figure 3-12). With multiple combinations, the ZFN14 in combination with the donor that is flanked with 800 bp HR arm on each side is identified as the most efficient method for AR-tagging integration in LNCaP cells (Figure 3-13). In an effort to avoid the negative effects induced by antibiotic screening on LNCaP cells, we designed the donor structure in the way that the fluorescent reporter gene can be used as a positive integration-screening marker. This allowed rapid assessment of both an accurate knockin rate and quantification of AR⁺ LNCaP cells via FACS analysis. To evaluate false-positive effects, such as RFP expression from the donor without integration, all of our experiments include a donor-only transfection. Also, to minimize potential side effects induced by the AR-RFP fusion protein, we inserted both furin cleavage site and P2A peptide before the reporter gene.

This model was first tested in pEGFP-C2 vector, which revealed that both GFP and RFP were expressed simultaneously (Fig 3-8).

On the other hand, due to the fragile and slow growing nature of LNCaP cells, after multiple steps of manipulation, very few single LNCaP cells survived the selection process. This LNCaP cell attribute has prevented many scientists in the PCa field from generating isogenic LNCaP clonal cell lines. In this study, however, after designing and modifying multiple culture media, we successfully identified an LNCaP conditioned media ideal for culturing and expanding LNCaP clones.

In conclusion, we have successfully developed a genetic protocol to precisely tag the endogenous AR in cancer cells, which includes ZFN binding site selection, DNA donor design, transfection optimization, time point assessment, single cell culturing, and detection of successful integration. This research not only has allowed the establishment of novel AR-tagged LNCaP clonal models, but has also provided great potential in developing similar tagging models in other PCa cell lines (LAPC9, LAPC4, etc) as well as in primary human PCa cells. Further, the strategies described here should be applicable to other HDR-mediated insertion of large DNA fragments into different genomic locations in PCa cells.

Chapter 4. Generate AR Knockout (KO) PCa cell clones using CRISPR-cas9 technique

4.1. Introduction

The RNA-guided CRISPR-Cas9 gene-editing tool relies on the cas9 nuclease guided by small RNA through Watson-Crick base pairing with target DNA, and has proven to be efficacious in virtually all cell types [109, 110] (Figure 4-1). In an effort to establish roles for AR in a defined context, we employed the CRISPR-cas9 system to selectively knock out full-length AR in LNCaP cells. Two independent sgRNAs that target the 5' of AR gene produced null deletions in six single cell clones. These AR-KO (AR knock-out) clonal LNCaP cells did not express AR at both mRNA and protein levels, exhibited reduced to undetectable expression of AR downstream target genes such as PSA, TMPRSS2 and NKX3.1, and showed significantly lower responses to androgens compared to the AR-tagging clones. Collectively, our data supports the use of this powerful and accessible gene-editing technology in successfully establishing isogenic knockouts in PCa cells allowing elucidation of specific gene functions.

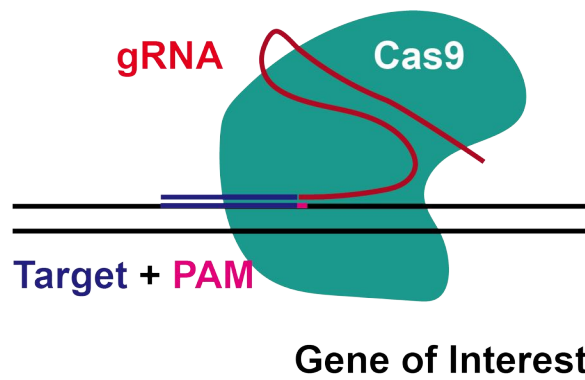


Figure 4-1 Schematic of the RNA-guided Cas9 nuclease

The cas9 nuclease from *S. pyogenes* is targeted to 'Gene of Interest' by a gRNA consisting of a 20-nt guide sequence (blue bar) and a scaffold (red). The guide sequence pairs with the DNA target (blue bar) upstream of a 5'-NGG adjacent PAM motif (pink). Cas9 then introduces a DSB ~3 bp upstream of the PAM.

4.2. Materials and methods

4.2.1. sgRNA design and CRISPR nuclease assembly

Two gRNAs, gRNA1 and gRNA2 (Figure 4-2, B) were designed targeting the AR exon 1 using the following website: <http://crispr.mit.edu>. The gRNAs scores (59 and 97, respectively) were decent and predicted limited cleavage potential at off-target sites. We designed single-stranded DNA oligonucleotides, annealed into double-stranded DNA oligonucleotides and cloned them into the CRISPR nuclease vector (A21174, ThermoFisher) (Figure 4-3, A). In the CRISPR nuclease vector, human U6 promoter drives the gRNA expression, and the CMV promoter drives the cas9 nuclease expression (Figure 4-3, A). The reporter gene, OFP (orange fluorescence protein) (Figure 4-3, A) following the cas9 nuclease was used to screen for the transfected cells via FACS analysis.

4.2.2. Fluorescence-activated cell sorting (FACS)

LNCaP cells were trypsinized and resuspended at a 5×10^5 /ml single cell concentration in 1xPBS, 72 hrs post CRISPR plasmid transfection. Approximately $1\sim 2 \times 10^6$ cells were utilized for FACS analysis. Propidium iodide was used to eliminate dead cells. OFP was excited with a 555 nm laser and analyzed at 584 nm. In order to enrich for cells that received high levels of the CRISPR-cas9 plasmid, we focused only on the top ~2% OFP-positive cells.

4.2.3. IF Microscopy

Single clonal cells were placed on poly-lysine-coated glass coverslips and incubated with mouse monoclonal anti-AR (N20, SC-816, Santa Cruz Technology; 1:200) diluted in 1xPBS containing 0.1% Triton and 5% goat serum for 2 hrs at RT. After

thorough washing, the coverslips were incubated for 60 min with Alexa Fluor 488-conjugated goat anti-Rabbit IgG secondary antibody (Invitrogen) (1:1000) in 1xPBS plus 0.1% Triton and 5% serum. After thorough washing, cells were stained with DAPI (H-1200; Vector Laboratories, Burlingame, CA) for 10 min at RT and the coverslips were mounted with 6 μ L ProLong® Gold anti-fade reagent (Invitrogen). Images were acquired within 30 min on an Olympus microscope.

4.2.4. Genotyping

Genomic DNA was isolated from AR-KO clonal cells using the QiAamp DNA Mini Kit. Primers used for sequencing included ARN FWD: 5'-GAGACAGACTGTGAGCCTAGC-3' and ARN REV: 5'-GCTGTGAAGGTTGCTGTTCC-3'.

4.2.5. Western blotting antibodies

Antibodies used in Western blotting included: anti-AR (N20, SC-816, Santa Cruz, 1:1000), anti-AR (ab74272, abcam, 1:1000, aa180-320), anti-PSA (C-19 SC-7638, Santa Cruz, 1:1000), anti-NKX3.1 (SAB2101603, Sigma, 1:1000), anti-TMPRSS2 (ST1676, Calbiochem, 1:500), anti- β actin (ab8227, Abcam, 1:2000)

4.2.6. qRT-PCR primers

Total RNA was extracted using RNeasy Mini Kit (Qiagen) according to the manufacturer's instructions. qRT-PCR was performed using an CFX Connect Real-Time PCR Detection System (Bio-Rad). qPCR data were normalized to 18S. Primer information was listed as follows. 18S: FWD: 5'-AAGTCCCTGCCCTTTGTACACA-3' REV: 5'-GATCCGAGGGCCTCACTAAAC-3' AR: FWD: 5'-

TAGGGCTGGGAAGGGTCTAC-3' REV: 5'-GGGAGGTGCTGCGCTC-3'. PSA FWD: 5'-GATGAAACAGGCTGTGCCG-3' REV: 5'-CCTCACAGCTACCCACTGCA-3'.

4.2.7. Luciferase assay

LNCaP clonal cells were seeded in 24-well plates (3×10^4 cells/well) and were co-transfected with 1 μ g ARE or PSA reporters together with the Renilla luciferase internal normalization plasmid (phRL-CMV). As a control, one group was treated with 10 nM DHT, 12 hrs before measuring luciferase activities. The ratio of firefly to Renilla luciferase activity was determined with a dual luciferase assay (Promega) 48 hrs later. Unpaired two-tailed Student's t-test was used to compare differences between groups, and $P < 0.05$ was considered statistically significant.

4.3. Results

4.3.1. Design efficient gRNAs to target human AR in LNCaP cells

The workflow depicting the generation of CRISPR-cas9 knockout cell lines is shown in Figure 4-2 A. The specificity of the cas9 nuclease is determined by the 20-nt within the sgRNA and the target sequence must be 5' to a NGG PAM sequence. Based on these specifications, it was imperative to identify 5'-NGG and to minimize the off-target effects when selecting guide sequences for gene targeting. We also had to keep in mind that DSBs at the 5' end of the gene tend to have a greater possibility of inducing frame shift mutations that may disrupt the whole gene. Additionally, it has been demonstrated that targeting functional protein domains substantially increases the efficiency of generating null mutations [111]. The NTD of AR is a critical domain that governs the transcriptional function [1], thus making the 5' end an ideal locus to target. Complying with these basic principles, we submitted the -20 bp to +150 bp sequence of *AR* gene to the <http://crispr.mit.edu> website for gRNA scanning. The two gRNAs used in this study, gRNA1 and gRNA2, are predicted to target the AR gene a short distance from the start codon (Figure 4-2, B). We cloned the 2 gRNAs into a vector containing both gRNA insertion sites and the cas9 expression cassette (Figure 4-3, A). The OFP in the vector enabled screening of cas9 expressing cells (Figure 4-3, B). Both plasmids with gRNA1 and gRNA2 were transfected into LNCaP cells with Lipofectamine 2000. The top 2% OFP⁺ cells were FACS sorted 72 hrs post transfection (Figure 4-3, B). We observed mutually exclusive expression patterns between AR and OFP via IF staining (Figure 4-3, C), indicating efficient elimination of AR by transient transfection of cas9 protein and the gRNAs.

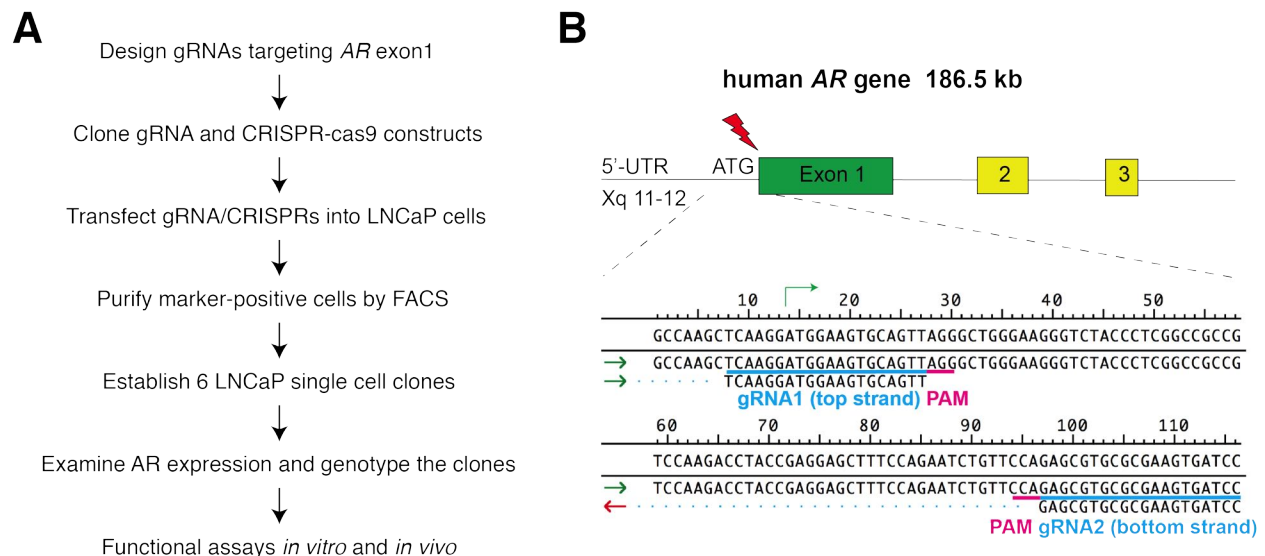


Figure 4-2 General strategies to generate AR-KO LNCaP clones using the CRISPR-cas9 system

A. Workflow of the experiments

B. Schematic depicting the two sgRNAs targeting at the 5' of human AR gene. gRNA1 (blue bar) targeted 11 bp downstream from the start codon ATG (green arrowhead) whereas gRNA2 (blue bar) targeted 86 bp away from the ATG (green arrow head). Note the gRNA2 is reverse complementary to the target sequence.

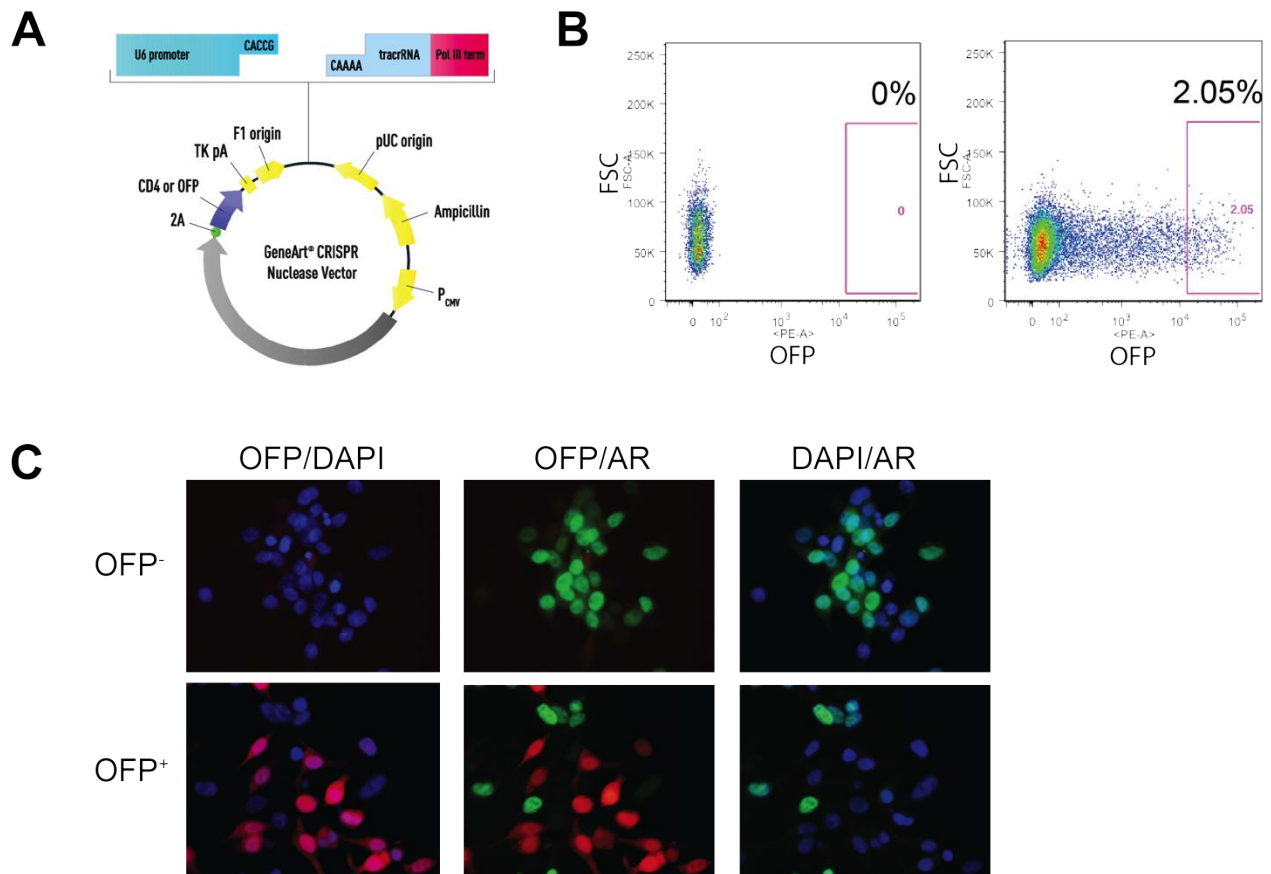


Figure 4-3 AR-KO with CRISPR-cas9 in bulk LNCaP cells

A. The GeneArt® CRISPR Nuclease Vector map. The vector (Life technologies) contains human U6 promoter that drives gRNA expression, CMV promoter that drive cas9 expression, and 2A peptide that mediates GFP/CD4 expression as cas9 reporter. The GFP vector is linearized at nucleotides 6732 and 6752 with 5 base pair 3' overhangs on each strand as indicated.

B. LNCaP cells transfected with CRISPR-cas9 plasmids containing gRNA1 and gRNA2 were FACS sorted 72 hrs post transfection. Cells of the top 2% were collected for single cell cloning.

C. GFP⁺ cells of the top 2% displayed mutually exclusive expression patterns of AR and GFP as revealed by IF staining. GFP⁻ cells showed similar AR expression patterns compared to bulk LNCaP cells (top row). The majority of GFP⁺ cells did not express AR (bottom row).

4.3.2. Establish AR-KO LNCaP cell clones

Use of the CRISPR-cas9 knockout system enabled the successful generation of AR knockout LNCaP cell lines. Next, single OFP^{hi} LNCaP cells were resuspended in LNCaP conditioned media and seeded into 96-well plates in an effort to support clonal growth. After six weeks, 35 clones were collected and six were identified as homogeneous AR⁻ clones, we name the clones as KO-01, KO-03, KO-14, KO-16, KO-21 and KO-41 (Figure 4-4, A). CTRL-12 was selected as a negative control, which originated from an OFP⁺ cell but displayed AR positive expression. These six clones were further probed with two additional AR antibodies producing similar results to IF staining (Figure 4-4, B).

To identify specific modifications induced by the DSBs in the six clones, we amplified the 5' region of the *AR* gene (Figure, 4-5, A) with the six clones. Based on the gel image (Figure 4-5, B), we proposed that KO-14 and KO-41 possessed two different modifications on the two alleles, one with large insertions, and the other may have harbored minor changes undetectable on the gel. The other AR-KO clones may also have had minor deletions or indels in the genome, which produced the AR null phenotype. By sequencing the PCR products, the mutations in the clones were identified: KO-01 had +3 bp and -75 bp mutations, KO-03 had -90 bp and -75 bp mutations, KO-14 had -75 bp and +284 bp mutations, KO-16 was homozygous with -75 bp deletions in both alleles, KO-21 had -5 bp and -75 bp deletions, and clone 41 had -75 bp and + 520 bp mutations around the two sgRNA directed sites (Figure 4-5, C).

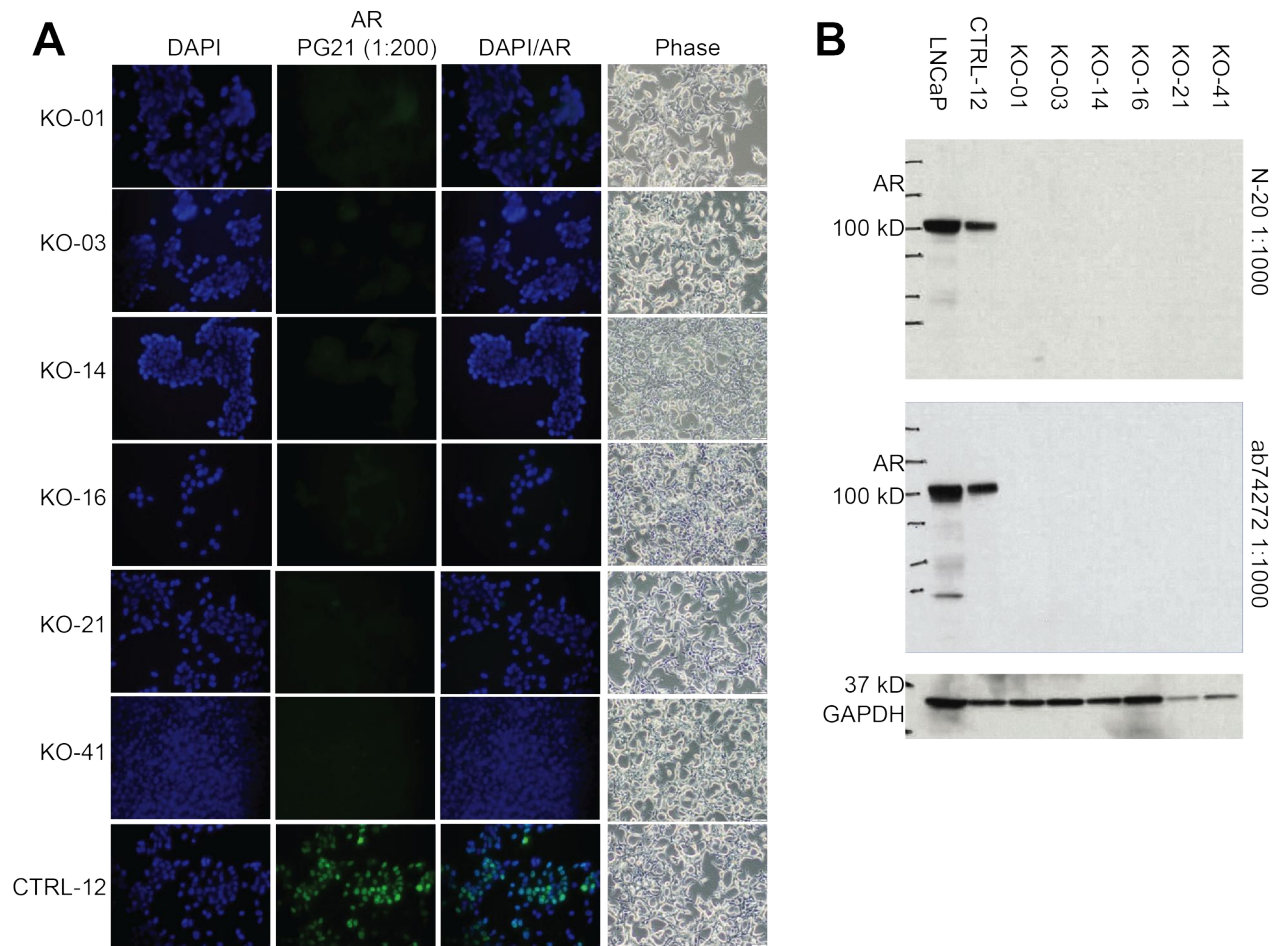


Figure 4-4 Screening of AR-KO clones

A. Clones (35 total) derived from the OFP^+ LNCaP cells were screened based on AR expression (PG-21, 1:200) via IF staining. KO-01, KO-03, KO-14, KO-16, KO-21 and KO-41 clones displayed the AR-knockout phenotype. In contrast, other clones such as CTRL-12, originally also derived from OFP^+ cells, were heterogeneously AR^+ .

B. The lack of AR protein in the six clones was further confirmed via Western blotting using two additional AR antibodies: N-20 (1:1000) and ab74272 (1:1000).

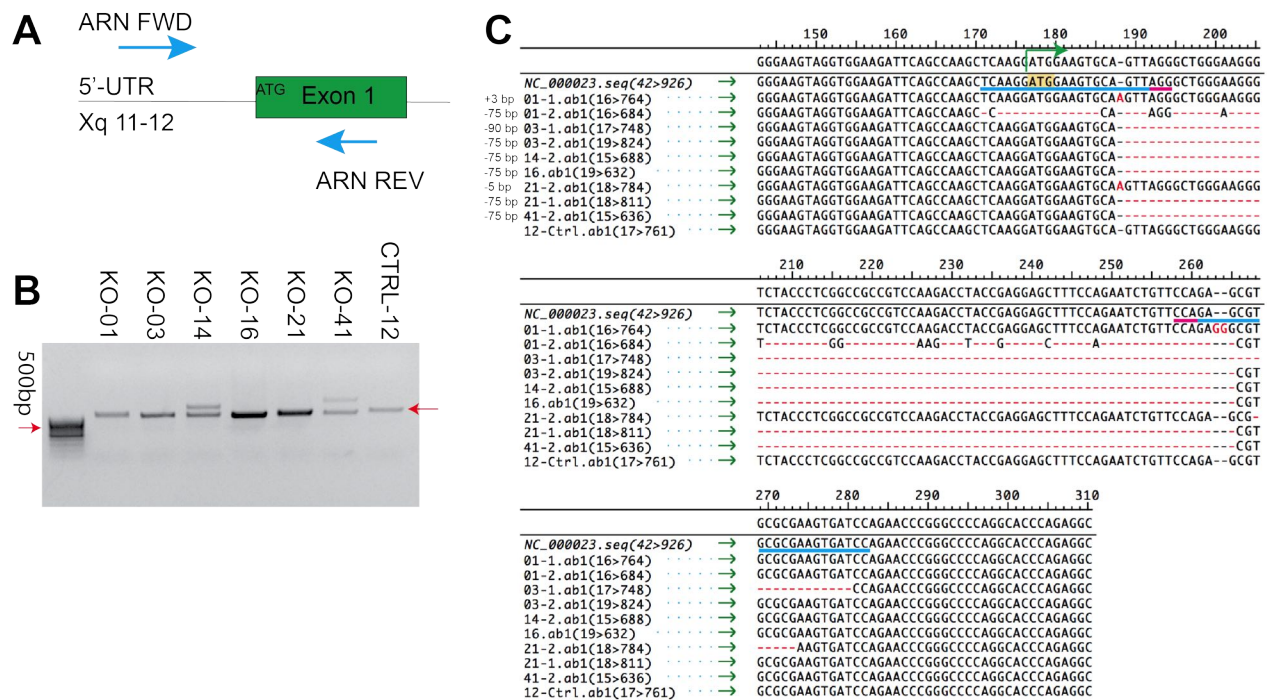


Figure 4-5 Genotype of the AR-KO clones

A. Primers used to amplify the targeted region (ARN FWD and REV).

B. Genotyping of the AR-KO clones. Genomic DNA extracted from the indicated clones was amplified with ARN primers. KO-01, KO-03, KO-16 and KO-21 clones showed minor changes in the genome that cannot be deciphered on a gel. One allele of KO-14 and KO-41 harbored large insertions (284 bp and 520 bp, respectively), and the other allele may have small modifications. KO-12 was used as negative (non-targeted) control.

C. BLAST results of the six AR-KO clones. Mutations are shown in red. gRNAs and PAM sequences were indicated as blue and pink bars. The 2 alleles in the six clones contained different mutations, indicated on the left. Clone 16 had the same deletions in both alleles.

4.3.3. Characterize AR functions in the AR-KO clones

AR is paramount for the prostate lineage-specific differentiation, and it maintains the differentiated state of prostate epithelium via regulation of prostate-specific genes such as *PSA*, *TMPRSS2* [112] and *NKX3.1* [113]. To test AR activity in the AR-tagging and AR-KO LNCaP cells, downstream target genes were analyzed via Western blot and qRT-PCR analysis comparing to two RFP-tagged AR⁺ LNCaP clones. PSA was undetectable in KO-03 and KO-16 cells at both the mRNA and protein levels (Figure, 4-6). *TMPRSS2* and *NKX3.1* expression were significantly reduced in the KO clones compared to AR⁺ clones (Figure 4-6, A). To test the canonical ligand-induced AR activity, *ARE* and *PSA* luciferase assays were performed in AR-KO and AR⁺ cells with and without 10 nM DHT treatment. A significantly lower baseline activity and extremely low response to androgen stimulation were observed in the AR-KO cells compared to AR⁺ cells. Collectively, our data demonstrated undetectable AR mRNA and protein expression, low canonical AR signaling, and blunted androgen responses in AR-KO cells.

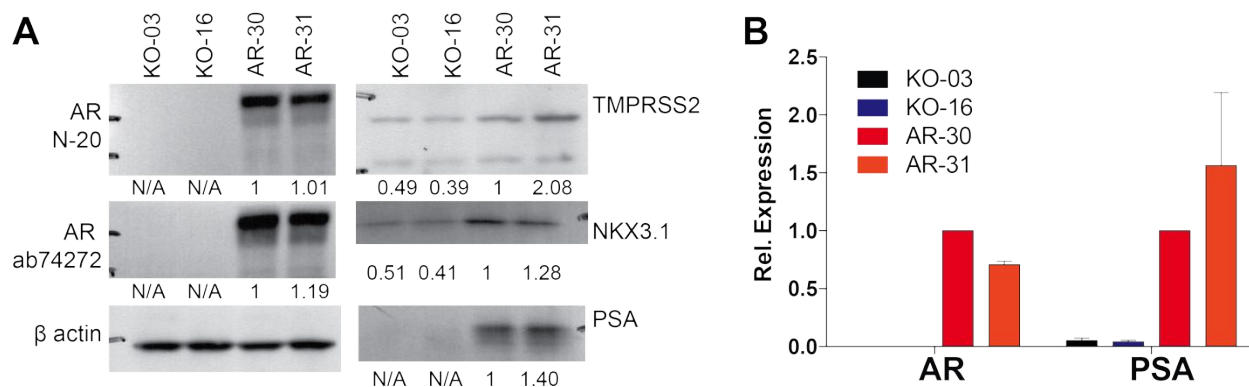


Figure 4-6 Attenuated AR signaling in AR-KO clones

A. Western blot analysis of AR, TMPRSS2, NKX3.1 and PSA protein expression in AR-30, AR-31, KO-03 and KO-16 clones. Indicated below are relative expression levels as determined by densitometric scanning of the individual bands and normalized to respective β actin and compared to the protein levels in AR-30.

B. qPCR analysis of *AR* and *PSA* mRNA levels in AR-30, AR-31, KO-03 and KO-16 clones. Values represent mean \pm s.e.m. of triplicates from three independent experiments, and were normalized to the levels in clone AR-30.

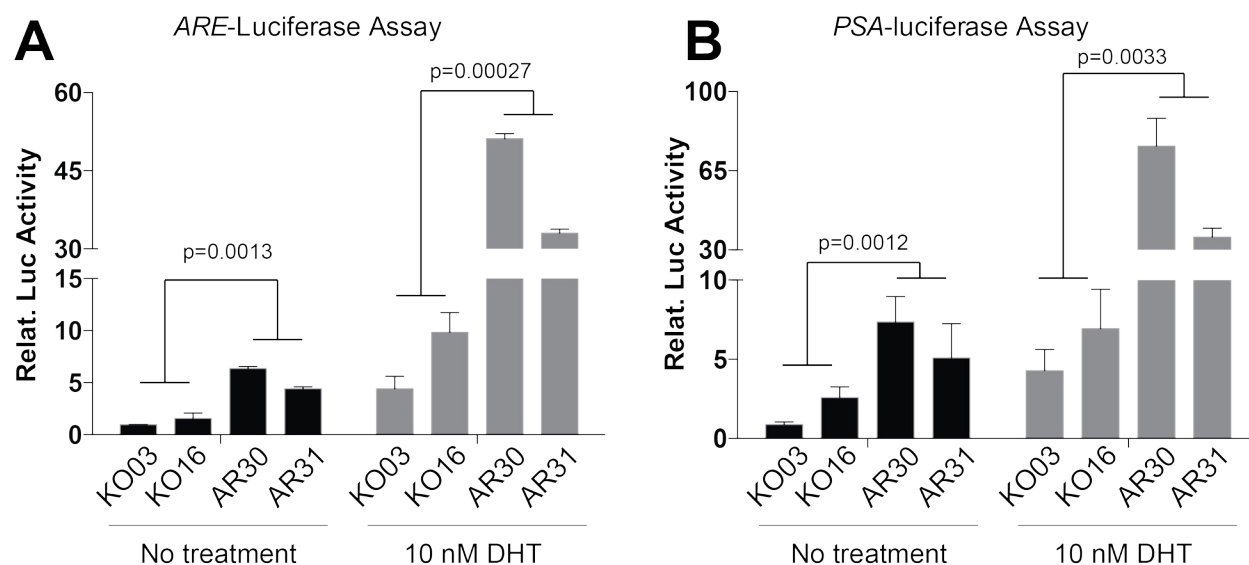


Figure 4-7 Lower AR activity and blunted DHT responses in AR-KO cells.

Presented are results of ARE (**A**) and PSA (**B**) Luciferase reporter assays in AR-30, AR-31, KO-03 and KO-16 clonal cells with and without 10 nM dihydrotestosterone (DHT) treatment. Values represent mean \pm s.e.m. of triplicates from three to five independent experiments. *P* values were determined using unpaired student's *t*-test.

4.4. Discussion

Prostate-specific deletions of *AR* in mice resulted in increased proliferation and less differentiated epithelium [28, 29]. However, silencing *AR* with small-interfering RNA [114] or short-haripin RNA [72] in human PCa cell lines (LNCaP and C4-2 cells) suggested an oncogenic role for AR. The major concern with the study [71, 72] is the heterogeneous AR knockdown effect on AR⁺ and AR^{-lo} cells that co-exist in LNCaP and C4-2 cells. The effects from dominant subpopulation may provide misleading results. In order to overcome this issue and establish accurate roles for AR in human PCa cells, establishment of a defined context is fundamental.

Herein, we have outlined our approach to selectively knock out full-length AR in LNCaP cells using the CRISPR-cas9 system and the subsequent successful derivation of isogenic AR-KO clones. We chose a CRISPR-Cas9 construct that harbors an OFP expression cassette in order to observe transfection efficiency and to enable cell sorting for enrichment of deletion alleles. Two adjacent but independent sgRNAs were designed to help control for inefficient sgRNA and maximize clones with biallelic deletions. The commonly observed outcomes included small deletions at the cas9 cleavage sites and bulk deletions between the two sgRNA sites. Two large insertions in KO-14 and KO-41, and between the two cutting sites were mapped to the CRISPR-cas9 vector sequence. Notably, clones with both in-frame and frameshift mutations displayed indistinguishable AR negativity, suggesting that both mutational classes were genetic nulls. These results could be ascribed to the critical role of the AR NTD. Similar functionally defective in-frame mutations have been observed in other genes. For example, Shi *et. al.* [111] showed, via deep sequencing, that in-frame deletion in BD1 domain of *Brd4* gene, ATPase domain in *Smaraca4* gene, methyltransferase domain in *Ezh2* and *Dot1l* genes

all contribute to null mutations. In our studies, to further minimize the CRISPR-Cas9 off-target effects [115], six AR-KO clones were generated and three (KO-01, KO-03 and KO-16) were utilized in subsequent functional studies.

In summary, we have successfully generated novel isogenic AR-KO LNCaP cell clones utilizing CRISPR-Cas9 system. These AR-KO clones do not express AR at both the mRNA and protein levels (Figure, 4-6). Also, the AR activity in these clones is significantly dampened as evidenced by reduced responses to androgen stimulation (Figure 4-7) and much reduced expression of downstream target genes including PSA, TMPRSS2 and NKX3.1, compared to the RFP-tagged AR⁺ clones (Figure, 4-6, A). Importantly, this study has provided practical guidelines for harnessing CRISPR-Cas9 system in PCa cells, a technique that can be shared potentiating collective advances in the PCa field.

Chapter 5. Functional and molecular studies in isogenic AR⁺ and AR-KO LNCaP cells

5.1. Introduction

The current mainstay clinical treatment for advanced PCa includes ADT compounds such as traditional antiandrogens and second generation AR antagonists such as enzalutamide and abiraterone. Unfortunately, the inevitable failure of ADT results in the progression to CRPC. The exact mechanisms underlying the switch from androgen-dependent PCa to CRPC are incompletely understood and thus, metastatic CRPC remains incurable. Identification and characterization of PCa cell targets may potentially lead to new multi-pronged therapeutic approaches to successfully eliminate CRPC cells. In previous studies, we reported that PSA^{-/lo} PCa cells possess long-term tumor propagating properties, and can initiate robust tumor regeneration in fully castrated hosts [7]. Further, we showed discordant mRNA and protein expression patterns between AR and PSA in all stages of PCa (Figure 1-4 and 1-5). In addition, different patterns of AR expression were shown in CRPCs: AR^{-/lo}, AR^{+hi} and cytoplasmic AR (Figure 1-6). These results suggest that AR signaling as well as AR-independent signaling pathways are involved in CRPC progression. The goal of this study is to elucidate how this AR heterogeneity may impact PCa biology and response to clinical treatments.

Using our isogenic AR⁺ and AR⁻ LNCaP cells, we performed systematic analysis to compare the intrinsic biological properties and tumor regenerating capabilities of the two subpopulations in both androgen dependent (AD) and androgen independent (AI) environments. Our data showed highly distinct and context dependent tumor regenerating abilities in both subpopulations. In terms of therapeutic resistance, AR⁻ cells demonstrated higher resistance to enzalutamide treatment compared to AR⁺ cells. Taken together, these studies link AR heterogeneity to distinct androgen environment and

castration/enzalutamide responses, and provided evidence for a more efficacious therapeutic strategy that targets AR^{-lo} PCa cells/clones, in addition to AR⁺ cells.

5.2. Materials and methods

5.2.1. Animals and reagents

All AR⁺ and AR-KO LNCaP cell lines were regularly authenticated in our institutional CCSG Cell Line Characterization Core and examined to be free of mycoplasma contamination. Immunodeficient mice, NOD/SCID (non-obese diabetic/severe combined immunodeficiency) and NOD/SCID-IL2R γ ^{-/-} (NSG), were obtained from the Jackson Laboratory, and breeding colonies were maintained in standard conditions in our animal core. All animal-related studies have been approved by our Institutional Animal Care and Use Committee (IACUC) at the M.D. Anderson Cancer Center (ACUF#00000923-RN00) and the Roswell Park Cancer Institute (animal protocol# 1331M). Therapeutic reagents used in this study included Enzalutamide/MDV3100 (Selleck Chemicals, Cat# S1250).

5.2.2. Clonal and clonogenic assays

For clonal assays, 5,000 AR-KO or AR⁺ cells were seeded in 6-well plates. After two weeks, cells were stained with 1:20 giemsa and plates were scanned using an HP® scanner. Cell clones were quantified using ImageJ software. For clonogenic assays, 500 AR-KO or AR⁺ cells were suspended in 100 μ L of a 50% matrigel, 50% normal media mixture, supplemented with 0.1 nM DHT or 2 μ M enzalutamide, and spread carefully into 24-well plates. Fresh media with DHT and enzalutamide were changed every other day. After two weeks, sphere numbers were enumerated under a phase-contrast microscope and images were taken using an Olympus inverted epifluorescence microscope.

5.2.3. AR-KO and AR⁺ competition assays

For *in vitro* assays, AR-KO cells were labeled with GFP via infection with pGIPZ non-silencing GFP control plasmid at an MOI of 10. 5,000 AR-KO (GFP⁺) cells and 5,000 AR⁺ (RFP⁺) cells were mixed and seeded into a 6-well plate. Cell images were captured using a JuLI™ Stage Real-Time microscope at 2 hr intervals. Three focal points in each well were recorded and cell confluence data was measured using ImageJ software. For *in vivo* tumor assays, 200,000 AR-KO (RFP⁻) cells and 200,000 AR⁺ (RFP⁺) cells were mixed and injected into castrated or testosterone-implanted NSG mice. Two tumors were harvested per time point and 10,000 single cells were analyzed per tumor using a BD LSR II flow cytometer for the abundance of GFP⁺ and RFP⁺ cells.

5.2.4. BrdU incorporation assays

Cells at 50% confluence were incubated with 2 μ M 5-Bromo-2'-deoxyuridine (BrdU) for 5 hr. Cells were fixed with 4% PFA for 5 min and permeabilized with 1% Triton-X100. DNA was denatured using 3 M hydrochloric acid in 1% Triton-X100 for 20 min and then treated with 0.1 M sodium borate for 15 min. Cells were blocked with background sniper (BS996; Biocare Medical, Concord, CA) for 20 min and incubated with mouse monoclonal anti-BrdU antibody (#B2531 Sigma, MO) for 5 hr at RT, followed by incubation with goat anti-mouse IgG conjugated to Alexafluor 488. After counterstaining with DAPI, images were taken using an Olympus inverted epifluorescence microscope.

5.2.5. Tumor regeneration assays

AR-KO and AR⁺ cells were suspended in 50% Matrigel and 50% normal media and injected subcutaneously (s.c) into intact, castrated or testosterone-implanted

NOD/SCID or NSG male mice (8-10 weeks old). Tumor size was measured twice per week in two dimensions using a caliper. Tumor volume was calculated using the following equation: $1/2 \text{ (length} \times \text{width}^2)$. Animal body weight and health status were monitored and recorded. At the end of the experiments, tumors were harvested, tumor incidence, weight, and images were recorded.

5.2.6. Enzalutamide treatment

250,000 AR-KO cells were s.c-implanted into castrated NSG male mice (~6 weeks old), and 250,000 AR⁺ cells were s.c-implanted into intact NSG male mice (~6 weeks old). Once tumors were palpable, mice were randomly divided into two groups: vehicle/control treated mice (n=10) and enzalutamide treated mice (n=10). Enzalutamide was initially dissolved in DMSO at 90 mg/ml to make a stock solution, and then was diluted in corn oil (Sigma; C8267) to achieve a 2.5 mg/ml working solution. Mice were treated with 100 μ L enzalutamide working solution intraperitoneally (i.p) 3 times per week (30 mg/kg/week) in the treatment group. The mice in the control group were treated with 100 μ L corn oil (Sigma; C8267) with 2.5% DMSO 3 times per week.

5.2.7. IHC staining in FFPE (formalin fixed and paraffin-embedded) sections

Formalin fixed and paraffin-embedded (FFPE) sections (4 μ m) were deparaffinized in xylene and hydrated in gradient alcohols to water. Slides were then treated with 10 mM citrate buffer (pH 6.0) for antigen retrieval, blocked with 2.5% horse serum, incubated with primary antibodies followed by corresponding secondary antibodies, and then counterstained with hematoxylin. IHC images were captured via an Olympus microscope.

5.2.8. Statistic analysis

Unpaired two-tailed Student's *t*-test was used to compare significance in clonal assays, and to compare tumor weights and volumes obtained in *in vivo* experiments. Chi-squared test was employed to compare tumor incidence. The results were presented as mean \pm S.D with a P value < 0.05 considered statistically significant.

5.3. Results

5.3.1. AR⁺ cells are more tumorigenic in androgen-proficient environment

To compare the clonal and sphere-formation abilities between AR⁺ and AR-KO cells in an androgen-proficient environment, single cells were suspended in 2D and 3D culture media supplemented with DHT (0.1 nM). After two weeks, AR-30 and AR-31 cells gave rise to significantly more clones in the 2D culture, compared to the KO-03 or KO-16 cells (Figure 5-1, A). Additionally, AR⁺ clones formed larger and more spheres than AR-KO clones (Figure 5-1, B). Results from the BrdU incorporation assay show a larger percentage of AR⁺ cells in S-phase compared to AR-KO LNCaP cells, when cultured in DHT supplemented conditions (Figure 5-2, A-B). In addition, AR⁺ clones showed significant proliferation advantages compared to GFP-tagged AR-KO clones in a competition assay with DHT supplement at 0.1 nM under a time-lapse microscope (Figure 5-2, C-D).

In order to compare the *in vivo* tumorigenic abilities between the two isogenic cell types, 500,000 each of AR-12, AR-31 and KO-03 and KO-16 cells were s.c-implanted into intact male NOD-SCID mice. Results revealed that AR⁺ cells generated larger and a greater overall number of tumors than AR-KO LNCaP cells (Figure 5-3, A). An independent repeat experiment was conducted in intact male NSG mice s.c-implanted with AR-12, AR-31, KO-01 and KO-03 cells. Consistent with previous results, AR⁺ cells were much more tumorigenic compared to AR-KO cells (Figure 5-3, B). To eliminate inter-animal variations and control androgen levels in each animal, we supplemented NSG male mice with testosterone pellets and injected identical numbers of AR⁺ and AR-KO LNCaP cells on opposite flanks in the same animal (i.e., AR⁺ cells on the right side and AR-KO cells on the left) (Figure 5-4, A). During the *in vivo* assays, we consistently

observed significantly larger tumors on the right flanks of mice (Figure 5-4, C). On day 63, when endpoint tumors were harvested, we observed that the two AR⁺ clonal cells generated a greater overall number of tumors (27/30) (number of mice with tumors/ total number of mice injected) that were much larger (average weight: 0.65 g), when compared to AR-KO cells, which generated fewer tumors (7/30) that were smaller (0.05 g) (Figure 5-4, B-D). IHC staining for AR expression in the endpoint tumors confirmed positive AR expression in AR⁺ cell-derived xenografts, whereas AR-KO xenograft tumors were negative for AR expression (Figure 5-3, E).

Together, this study provided direct evidence that in an androgen proficient environment, AR⁺ LNCaP cells form more clones, spheres and tumors than AR-KO LNCaP cells (Figure, 5-1 to 5-4). Thus, androgen-dependent proliferation in AR⁺ LNCaP cells is critical for tumor formation.

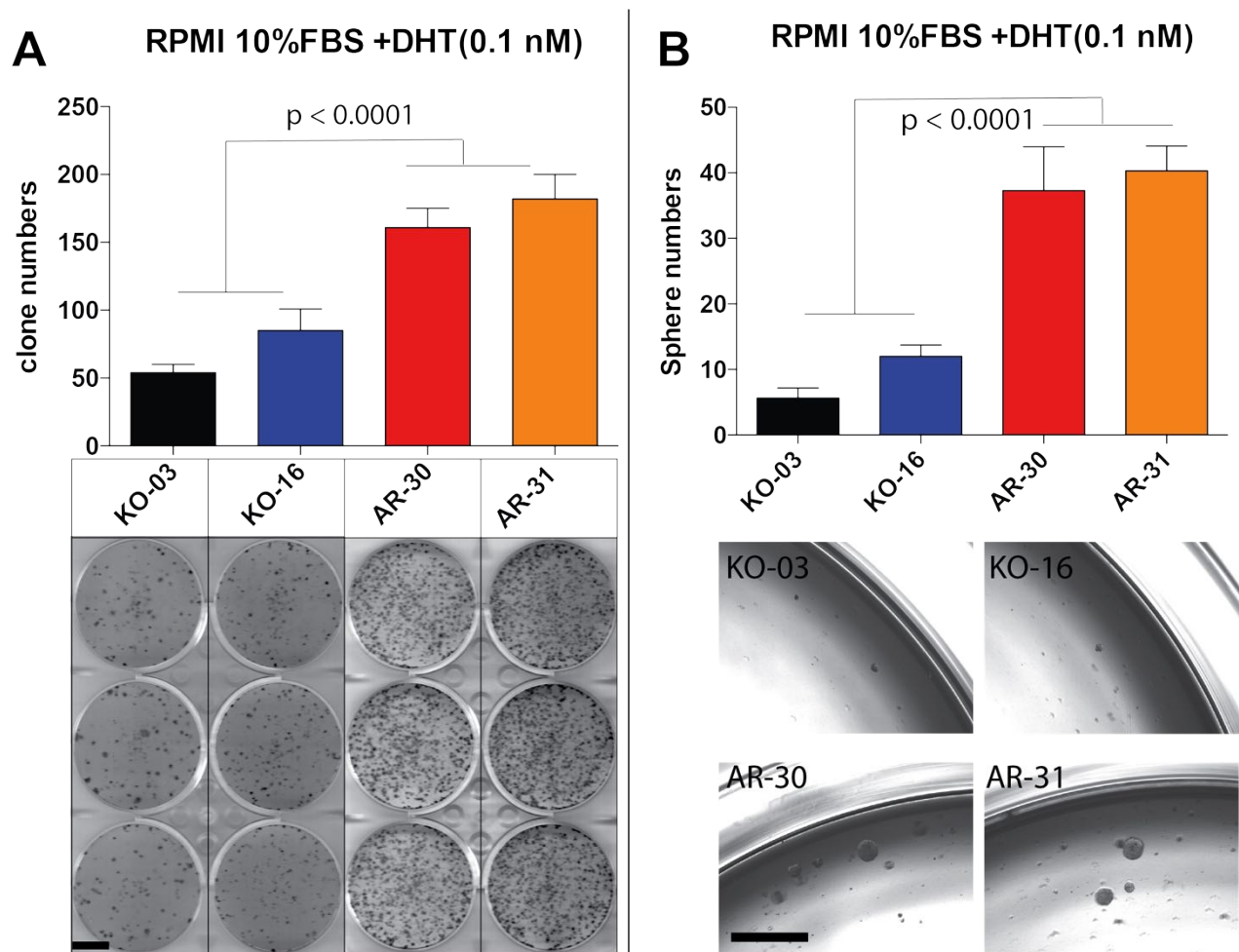


Figure 5-1 AR⁺ cells possess higher clonal and sphere-forming abilities in androgen-proficient conditions than AR-KO cells

A. Quantification of clones formed by KO-03, KO-16, AR-30 and AR-31 cells in 2D culture conditions using RPMI supplemented with 10% FBS + 0.1 nM DHT (upper panel). Representative images of giemsa stained clones generated from the four different clones are shown (lower panel). Scale bar: 1 cm.

B. Quantification of spheres formed by KO-03, KO-16, AR-30 and AR-31 cells in 3D culture conditions using RPMI supplemented with 10% FBS + 0.1 nM DHT (upper panel). Representative images of spheres generated from the four clones are shown (lower panel). Scale bar: 1 mm.

Values represent mean ± SD of triplicates of the experiment. P values were calculated using unpaired Student's *t*-test. Applies to both **A** and **B**.

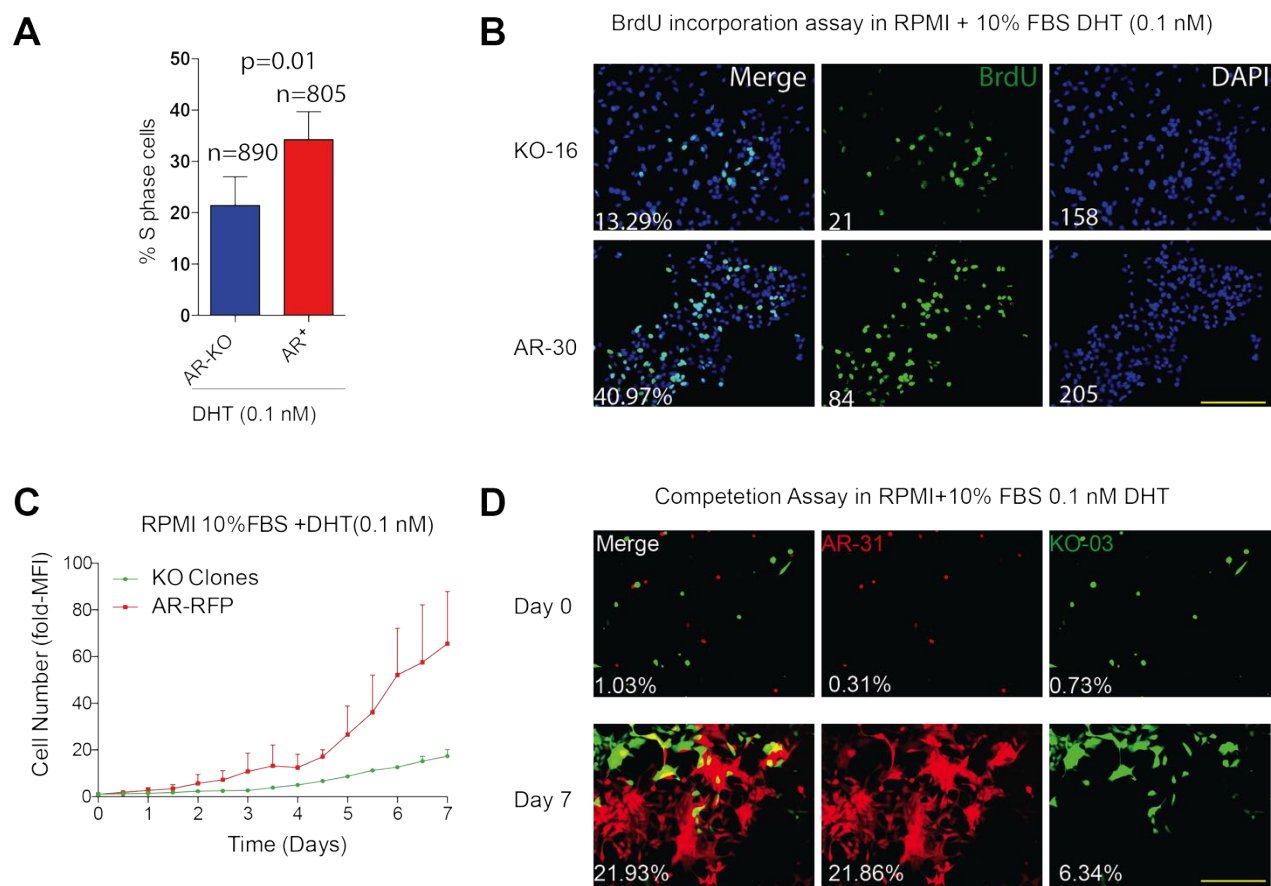


Figure 5-2 AR⁺ LNCaP cells are more proliferative than the isogenic AR-KO cells in androgen-proficient conditions.

A-B. A greater percentage of DHT treated AR⁺ LNCaP cells were in the S-phase compared to AR-KO LNCaP cells. **A.** Quantification of BrdU positive AR-KO and AR⁺ cells cultured in RPMI supplemented with 10% FBS + 0.1 nM DHT media (left panel). Values represent mean \pm SD of triplicates from three independent experiments. n indicates the total number of cells analyzed. *P* values were calculated using unpaired Student's *t*-test. **B.** Representative images of BrdU stained AR-KO and AR⁺ cells (right panel). The percentage of BrdU positive cells is indicated on "Merge" images. Cell numbers representing BrdU and DAPI positive cells are indicated. Scale bar: 250 μ m.

C-D AR⁺ LNCaP cells exhibit proliferative advantages in androgen-proficient conditions **C.** Quantification of DHT treated (0.1 nM) AR-KO (GFP) and AR⁺ (RFP) LNCaP cell confluence measured daily and presented as fold change. 5,000 AR-KO (GFP⁺) cells and 5,000 AR⁺ (RFP⁺) cells were mixed and seeded into a 6-well plate on day 0. Values represent mean \pm SD of triplicates of the experiment. **D.** Representative images of DHT treated (0.1 nM) AR-KO and AR⁺ LNCaP cells on day 0 (upper panels) and day 7 (lower panels). Percentages of fluorescent positive areas are indicated on the lower left corners of the images. Scale bar: 250 μ m.

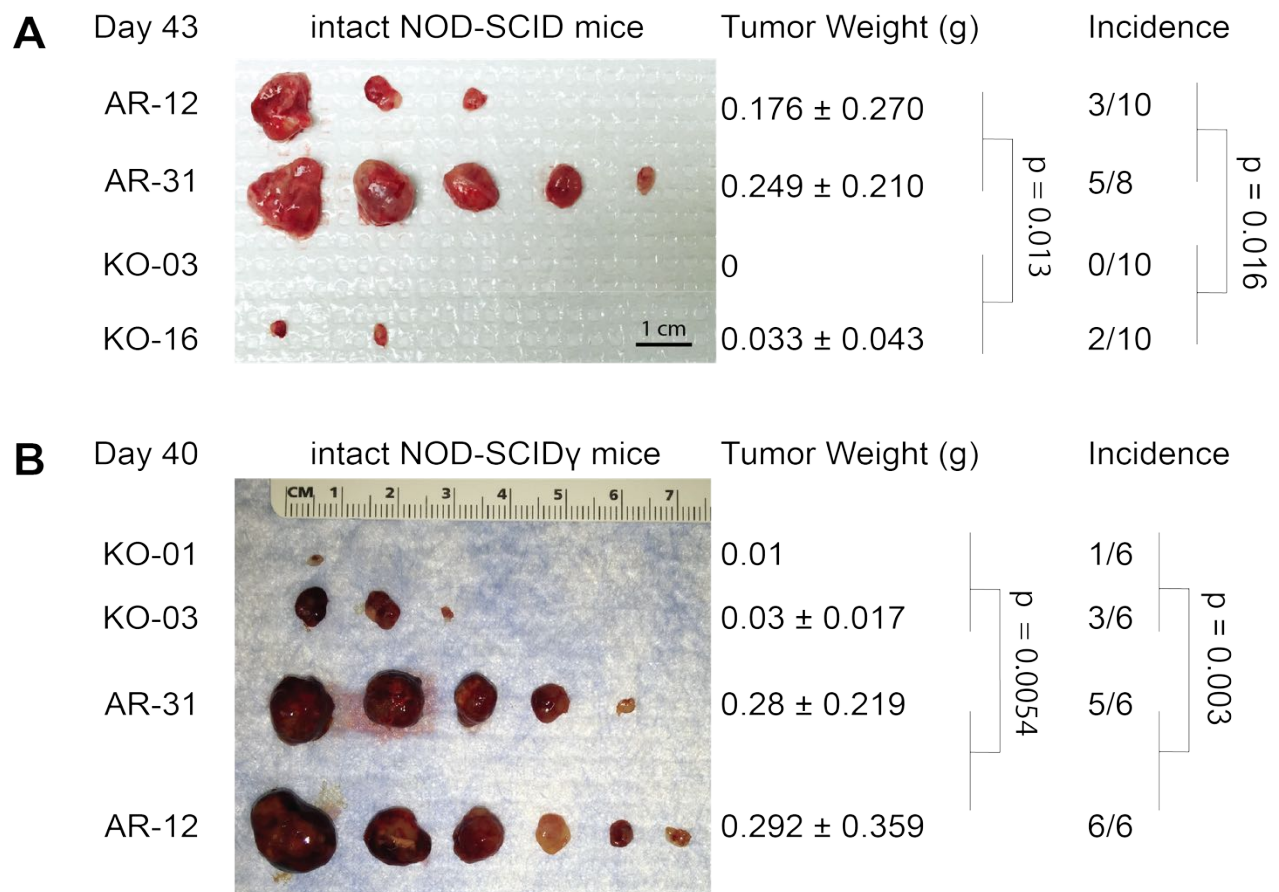


Figure 5-3 AR⁺ cells are more tumorigenic in intact NOD-SCID and NSG mice compared to isogenic AR-KO LNCaP cells.

Results from two independent tumor regenerations assays: AR-12, AR-31, KO-01, KO-03 and KO-16 cells (500,000) were subcutaneously (s.c) implanted in intact NOD-SCID male mice (**A**) intact NSG mice (**B**). Images of endpoint tumors, as well as corresponding tumor weight, tumor incidence, and *P*-values are shown. *P*-values for tumor weight and tumor incidence were calculated using unpaired student's *t*-test and Chi-squared test, respectively.

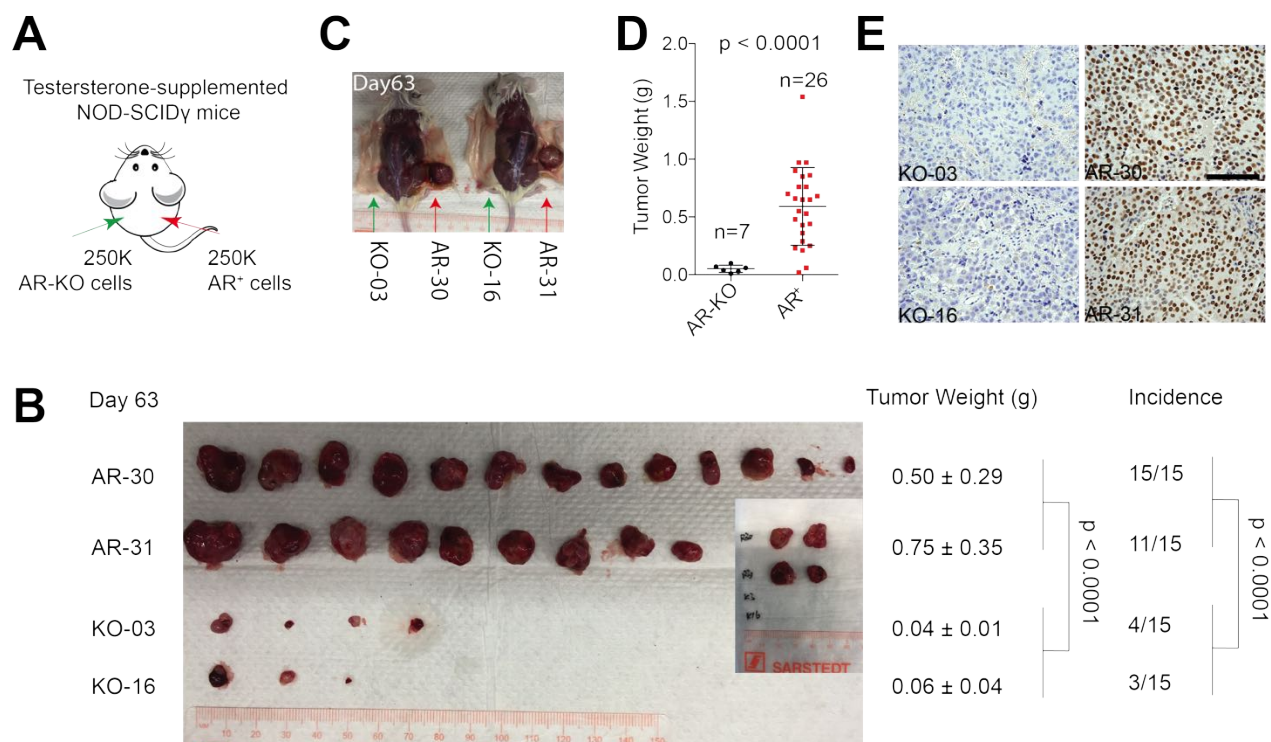


Figure 5-4 AR⁺ LNCaP cells are more tumorigenic in testosterone-supplemented NSG mice than isogenic AR-KO cells.

A. Schematic depicting cell number and type, and mouse implantation sites in tumor regeneration assays.

B. Images of endpoint tumors, with corresponding tumor weight, tumor incidence, and *P*-values. Small image shows four tumors of AR-30 and AR-31, harvested on day 56 due to large sizes. *P*-values of tumor weight and tumor incidence were calculated using unpaired Student's *t*-test and Chi-squared test, respectively.

C. Representative images of two mice each s.c.-implanted with AR⁺ LNCaP cells (right flank) and AR-KO LNCaP cells (left flank). Note that both mice bear a tumor on their right flanks (AR⁺ cells) but not on their left flanks (AR-KO cells).

D. Quantification of endpoint tumor weights in AR⁺ and AR-KO LNCaP cell experimental groups.

E. Representative images of IHC staining for AR expression in endpoint tumors. Note that tumors derived from AR⁺ LNCaP cells (AR-30 and AR-31) are positive for AR expression whereas tumors derived from AR-KO LNCaP cells (KO-03 and KO-16) are AR negative. Scale bar: 250 μm

5.3.2. AR-KO LNCaP cells are resistant to castration and highly tumorigenic in castrated mice

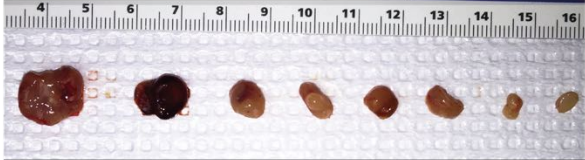



Our next aim was to determine how these observed tumorigenic abilities in isogenic AR⁺ LNCaP and AR-KO LNCaP cells in androgen proficient mice differ when assessed in castrated NSG mice. In our pilot experiments, AR-KO LNCaP clones generated 10 tumors out of 16 injections (62.5%) whereas AR⁺ LNCaP clones generated 4 tumors out of 18 injections (22.2%) during a four-month span (Figure, 5-5). Additionally, tumors derived from AR-KO LNCaP cells were four times larger than tumors derived from AR⁺ LNCaP cells (Figure, 5-5). These results suggested that AR-KO LNCaP clonal cells were resistant to castration and more tumorigenic than AR⁺ cells in androgen ablated hosts. In order to confirm these observations, we performed a comprehensive tumor regeneration assay in which identical numbers of isogenic AR-KO and AR⁺ LNCaP cells (250,000 each) were implanted in the same castrated NSG mouse on opposite flanks. Tumor size and incidence were closely monitored twice per week (Figure 5-6, A). Among the three groups of cells tested, the group consisting of KO-16 and AR-31 (Figure 5-6, E), and the group consisting of KO-01 and AR-19 (Figure 5-6, F) showed more AR-KO tumors (left flank) with significantly larger volumes (Figure 5-6, B) and endpoint tumor weights (Figure 5-6, D) when compared to the corresponding AR⁺ tumors (right flank). Additionally, the two groups KO-01 and AR-19 (Figure 5-6, F) and KO-03 and AR-30 (Figure 5-6, G) generated significantly more tumors in the left sides than in the right sides. Overall, this data suggests that AR-KO LNCaP cells possess significantly greater tumor regeneration ability in castrated hosts than AR⁺ LNCaP clones (Figure 5-6 C). IHC staining for AR expression status in tumor tissues confirmed the AR expression in the endpoint tumors from AR-KO and AR⁺ clones (Figure 5-6, H). Taken together, our

data illustrate that AR-KO LNCaP cells are intrinsically more tumorigenic in an androgen-depleted environment than isogenic AR⁺ LNCaP cells.

Next, we explored the effects of systemic androgen levels on the relative abundance of AR⁺ vs. AR⁻ cells during tumor progression. To test this, the same number of clonal AR⁺ and AR-KO LNCaP cells (250,000 each) were mixed at 50:50 and implanted into testosterone-supplemented (n=15) and castrated NSG mice (n=15). As the tumor progressed, we analyzed ratios of AR⁺ (RFP⁺) to AR-KO (RFP⁻) cells via flow analysis (Figure 5-7, A). In androgen-supplemented mice (AD), tumors at week 4 harbored an average of 91.4% RFP⁺ cells and 8.6% RFP⁻ cells (Figure 5-7, B red line). The abundance of RFP⁺ cells increased at later time points such that the two tumors at week 7 harbored 98.6% RFP⁺ and 1.14% RFP⁻ cells, respectively (Figure 5-7, B red line). The experimental AD group was terminated on week 7 due to large tumor sizes. In order to mimic the transition from an AD to AI environment, mice from the AD group (n=7) were castrated and had their testosterone pellets removed on week 4 (AD→AI group). In this AD→AI group, the RFP⁺ AR⁺ LNCaP cells remained the dominant population (97.9%) in the tumors when analyzed at week 7 (i.e. 3 weeks post castration) (Figure 5-7, B blue line). However, by week 9, tumors in the AD→AI group showed significant increases in AR-KO (RFP⁻) LNCaP cells to 69.4% and, in the meantime, AR⁺ LNCaP cells dropped to 30.6%. (Figure 5-7, B blue line).

In the castrated group (AI), two tumors analyzed at week 3 showed an average of 32.9% AR⁺ cells and 67.1% AR-KO cells (Figure 5-7, B black line), and these numbers remained stable till week 9 (Figure 5-7, B black line) with AR-KO LNCaP cells being the dominant subpopulation. Competition assays further demonstrated intrinsic differences between AR⁺ and AR-KO clonal LNCaP cells in terms of tumor initiation and progression

capabilities in different androgen contexts. In summary, AR⁺ PCa cells may be the driving force of tumor development in AD environments, while AR^{-/⁰} PCa cells may play an important role in the development of CRPC.

Day 118	Castrated NOD-SCID γ mice	Tumor Weight (g)	Incidence
KO-16		0.285 ± 0.236	8/8
KO-03		0.102 ± 0.327	2/8
AR-12		0.044 ± 0.068	4/8
AR-31		0	0/10

$p=0.005$

$p=0.0019$

Figure 5-5 AR-KO LNCaP cells are more tumorigenic than AR⁺ cells in castrated hosts.

Endpoint tumors on day 118 of KO-03, KO-16, AR-12 and AR-31 regenerated in castrated NSG mice. Images of endpoint tumors, tumor weight and tumor incidence with corresponding *P*-values. *P*-values of tumor weight were calculated using unpaired Student's *t*-test. *P*-values of tumor incidence were calculated using Chi-squared test.

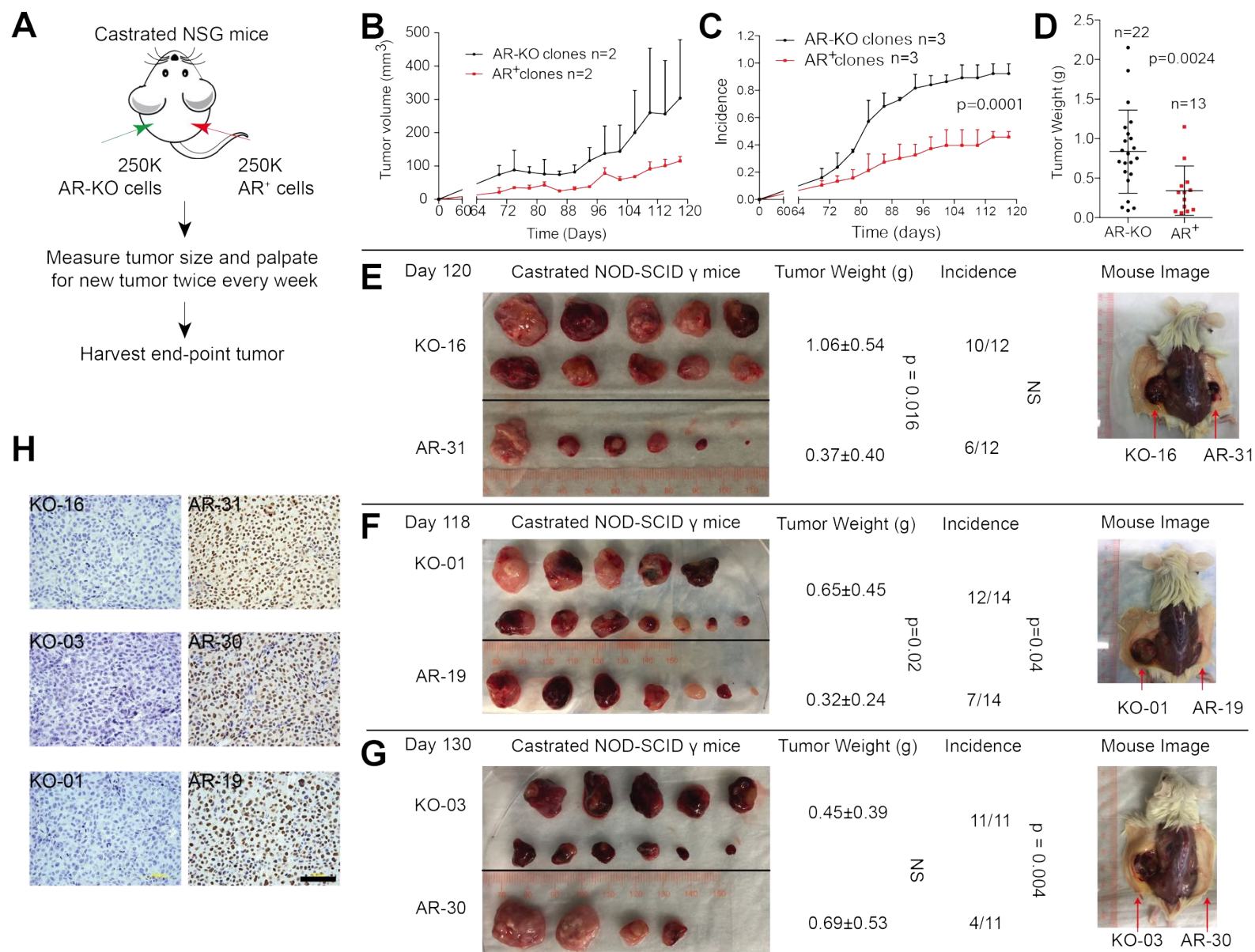


Figure 5-6 AR-KO LNCaP cells are more tumorigenic than AR⁺ LNCaP cells in the same castrated NSG mice

Figure 5-6 AR-KO LNCaP cells are more tumorigenic than AR⁺ LNCaP cells in the same castrated NSG mice

A. Schematic of the experimental design: 250 K AR-KO LNCaP cells were injected subcutaneously into the left flank of castrated NSG mice and 250 K AR⁺ LNCaP cells were injected into the same mice on the right flank. Three groups of cells were used in the experiment: KO-16 and AR-31 (n=12 mice), KO-01 and AR-19 (n=14 mice) and KO-03 and AR-30 (n=11 mice).

B. Tumor volumes measured twice every week in animals with AR-KO (KO-16 and KO01) and AR⁺ (AR-31 and AR-19) LNCaP cells injections starting from day 64 post implantation (mean \pm SD).

C. Tumor incidence observed twice every week in all three groups of animals starting from day 64 post implantation (mean \pm SD).

D. Graphical presentation of endpoint tumor weights in **E** and **F**.

E-G: Images of endpoint tumors, tumor weight and tumor incidence with corresponding *P*-values. *P*-values of tumor weight were calculated using unpaired Student's *t*-test. *P*-values of tumor incidence were calculated using Chi-squared test. Representative mice images (right panels) bearing tumors only on the left flanks (AR-KO cells) but not on the right flanks (AR⁺ cells).

H. Representative AR IHC staining images of the endpoint tumors. Scale bar: 250 μ m

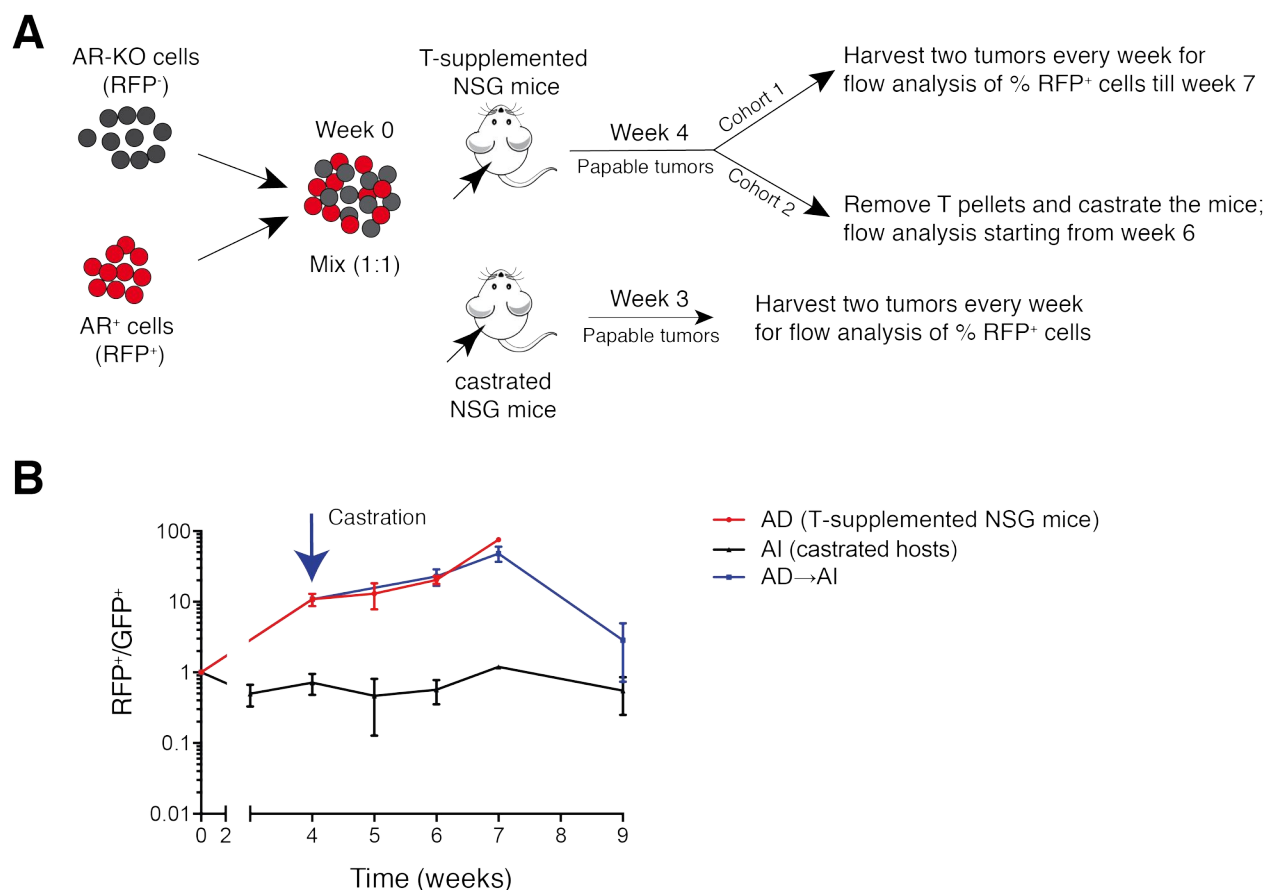


Figure 5-7 The dynamics of AR-KO and AR⁺ LNCaP cells in animals with different systemic androgen levels

A. Schematic of the experimental design depicting cell type, implantation in mice, and subsequent experiments.

B. Normalized RFP⁺/RFP⁻ ratios in the three groups at various time points. Two tumors were analyzed at each condition and time point and data is shown as mean \pm SD. The red line represents ratios in tumors from T-supplemented mice (AD group). The blue represents ratios in tumors from T-supplemented mice castrated on week 4 (AD→AI group). The black line represents ratios in tumors from castrated mice analyzed starting from week 3 (AI group).

5.3.3. AR-KO LNCaP cells are resistant to Enzalutamide

In order to compare clonal and sphere-formation capacities between AR-KO and AR⁺ LNCaP cells in response to AR antagonists, we seeded single cells in both 2D and 3D culture conditions supplemented with 2 μ M Enzalutamide. AR-KO LNCaP cells formed a significantly larger number of clones and spheres that were also larger in size than AR⁺ LNCaP cells (Figure 5-8). Further, we assessed proliferation rates of the two populations treated with enzalutamide via BrdU incorporation assays, single cell tracking and *in vitro* competition assay (Figure 5-9). After pulsing enzalutamide treated (2 μ M) clonal cells with BrdU for 5 hr, an average of 22.45% AR-KO cells showed positive BrdU⁺ staining compared to 10.04% AR⁺ cells ($p=0.0005$) (Figure 5-9, A-B). Simultaneously, we employed time lapse-based single-cell tracking to determine cell-cycle transit times in AR⁺ and AR-KO LNCaP cells. In the 34 AR-KO and 32 AR⁺ cells analyzed, AR-KO cells showed a shorter average cell-cycle transit time (20-hr) than isogenic AR⁺ cells (48-hr) (Figure 5-9, C-D). Consistent with the single-cell analysis, competition assays, wherein AR-KO (GFP⁺) clonal cells were mixed with AR⁺ (RFP⁺) clonal cells at a 1:1 ratio and treated with 2 μ M enzalutamide, revealed that AR-KO cells showed a significant growth advantage compared to AR⁺ cells (Figure 5-9, E-F). AR-KO cells gained a 9.26-fold cell number increase in 10 days compared to a 2.99-fold increases in AR⁺ cells (Figure 5-9, E). Collectively, these data (Figure 5-8 and 5-9) provide evidence that AR-KO clonal cells are resistant to enzalutamide treatment *in vitro*.

Lastly, we assessed resistance to enzalutamide in AR⁺ and AR-KO LNCaP cells *in vivo* (Figure 5-10, A). In this experiment, 250,000 AR-KO clonal cells and 250,000 AR⁺ cells were implanted into castrated hosts (n=27) and into intact mice (n=15), respectively.

When tumors emerged, mice were randomly divided into two groups. One group of mice was treated with enzalutamide at 10 mg/kg three times a week (t.i.w.) dosage and the other group was treated with 2.5% DMSO in corn oil. Tumors generated from AR⁺ LNCaP cells (4/8 tumors on day 0) were extremely sensitive to enzalutamide treatment (Figure 5-10, B-C), as evidenced by the complete regression of tumors by the end of the 30-day enzalutamide treatment. However, AR-KO cells showed no significant differences in terms of tumor initiation or tumor growth capability during enzalutamide treatment (Figure 5-10, D-E).

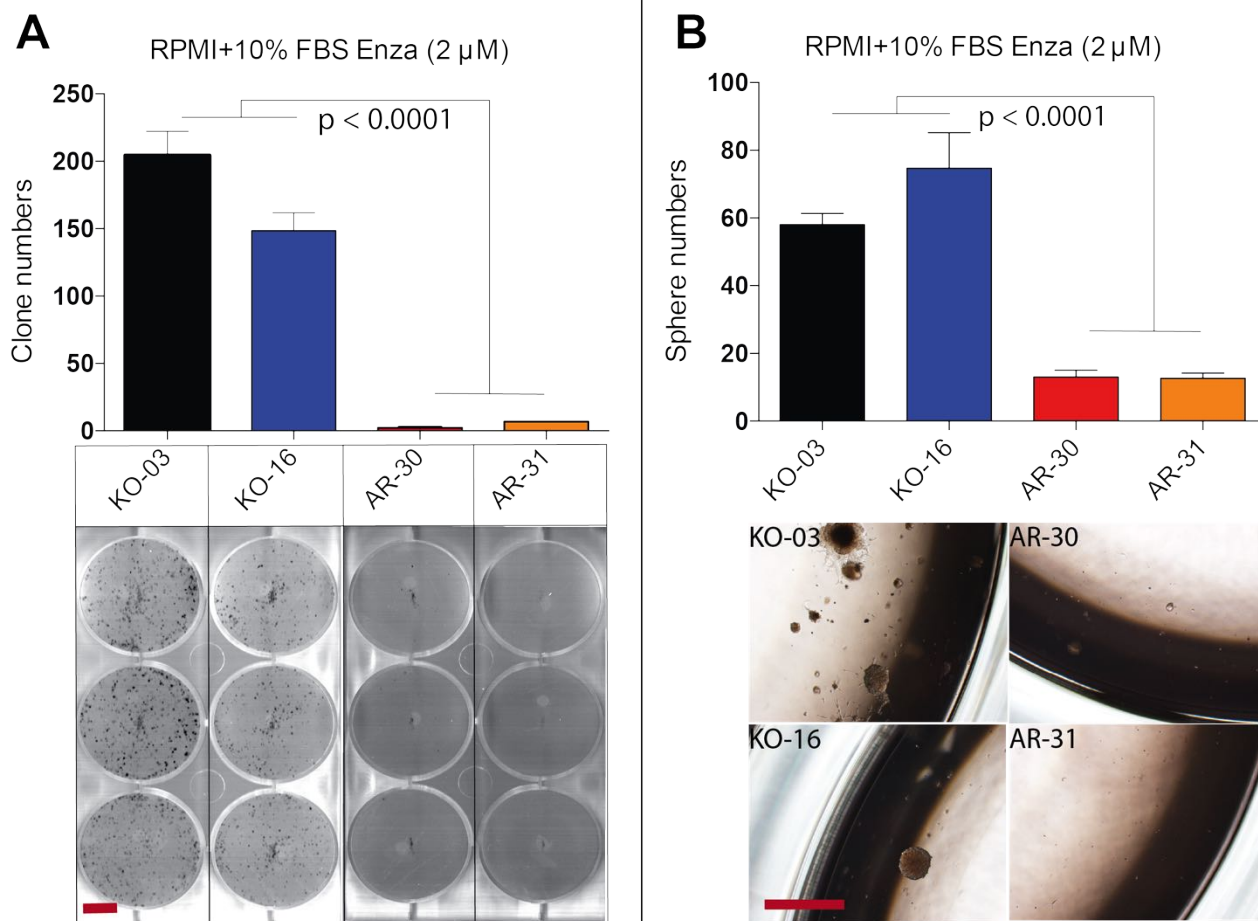


Figure 5-8 AR-KO LNCaP clonal cells form more clones and spheres than the clonally derived AR⁺ LNCaP cells under Enzalutamide treatment.

A. Quantification of clones formed by KO-03, KO-16, AR-30 and AR-31 cells in 2D culture conditions with RPMI supplemented with 10% FBS + 2 μ M enzalutamide (upper panel), and representative images (lower panel). Scale bar: 1 cm.

B. Quantification of spheres formed by KO-03, KO-16, AR-30 and AR-31 cells in 3D culture conditions with RPMI supplemented with 10% FBS + 2 μ M enzalutamide (upper panel), and representative images (lower panel). Scale bar: 1 mm.

Values represent mean \pm SD of triplicates of the experiment. P values were calculated using unpaired Student's *t*-test. Applies to both **A** and **B**.

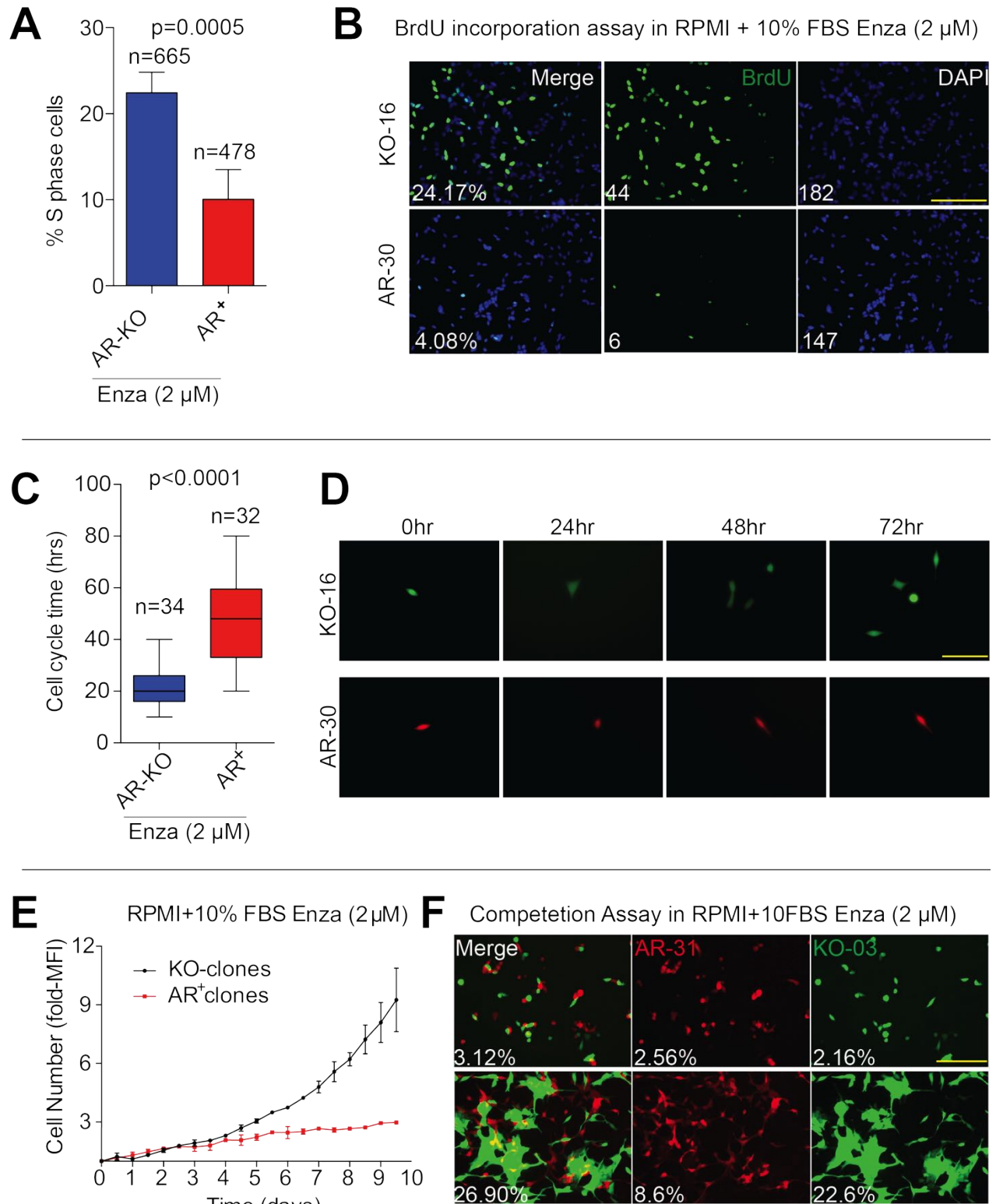


Figure 5-9 AR-KO LNCaP clonal cells are resistant to Enzalutamide treatment *in vitro*

Figure 5-9 AR-KO LNCaP clonal cells are resistant to Enzalutamide treatment *in vitro*

A-B: A greater percentage of enzalutamide treated AR-KO cells were in the S-phase compared to AR⁺ cells. **A.** Quantification of BrdU positive AR-KO and AR⁺ cells. Values represent mean \pm SD of three independent experiments. n indicates total number of cells analyzed. **B.** Representative images of BrdU staining in clonal AR-KO and AR⁺ cells. Cell number and percentage of BrdU⁺ cells are displayed in lower left corners. Scale bar: 250 μ m.

C-D: Enzalutamide treated (2 μ M) AR-KO LNCaP cells display shorter cell-cycle transit times than AR⁺ LNCaP cells as determined by time-lapse videomicroscopy. **C.** Quantification of average cell-cycle transition times in AR-KO and AR⁺ LNCaP cells based on the time-lapse tracking. **D.** Representative images of a single dividing AR-KO cell (upper panels) and a quiescent AR⁺ cell (lower panels) at different time-points. Scale bar: 250 μ m.

E-F: Enzalutamide treated AR-KO LNCaP cells are more proliferative than AR⁺ LNCaP cells. **E.** Quantification of enzalutamide treated (2 μ M) AR-KO (GFP) and AR⁺ (RFP) LNCaP cell numbers measured daily and presented as fold change. Values represent mean \pm SD of triplicates of the experiment. **F.** Representative images of enzalutamide treated (2 μ M) AR-KO and AR⁺ LNCaP cells on day 0 (upper panels) and day 10 (lower panels). Scale bar: 250 μ m.

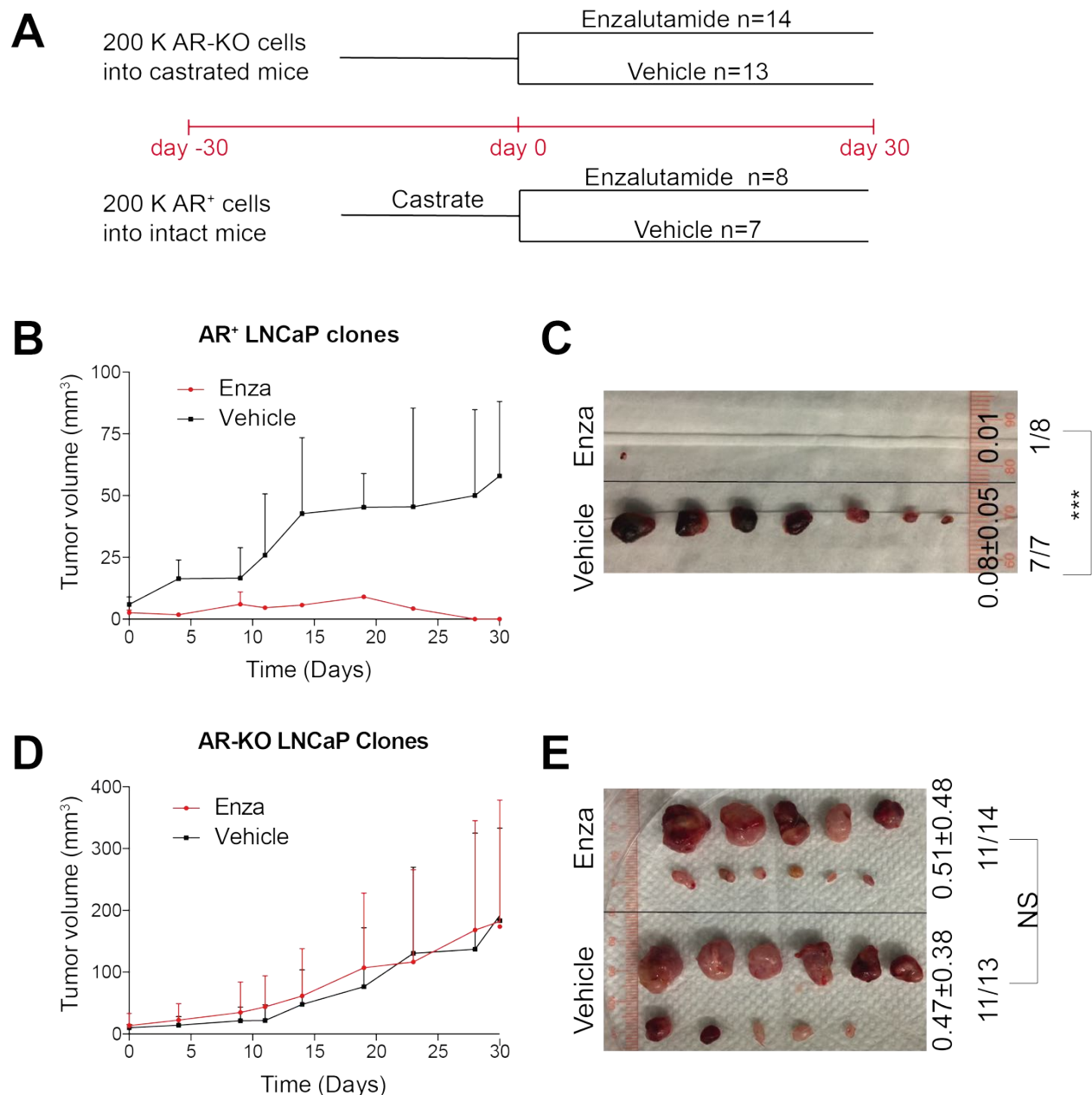


Figure 5-10 AR-KO LNCaP cells are resistant to Enzalutamide treatment *in vivo*

A. Schematic of the experiment. AR-KO and AR⁺ cells were injected into castrated mice (n=27) and intact mice (n=15), respectively (day -30). Mice with AR-KO cell injections were divided into two groups randomly when palpable tumors were detected (day 0). Mice with AR⁺ cell injections were castrated and were divided into two groups randomly when palpable tumors were detected (day 0). Enzalutamide (10 mg/kg t.i.w.) was given in experimental groups and vehicle treatment (100 μ L 2.5% DMSO in corn oil, t.i.w.) was given in the control groups.

B. Tumor volumes measured twice per week in animals implanted with AR⁺ (AR-30 and AR-31) LNCaP cells (mean \pm SD). The red line represents the enzalutamide treatment group (n=8), and the black line represents the control group (n=7).

C. Images of endpoint tumors generated from AR⁺ (AR-30 and AR-31) LNCaP cells, and corresponding tumor weight and tumor incidence with *P*-values indicated.

D. Tumor volumes measured twice per week in animals implanted with AR-KO (KO-03 and KO-16) LNCaP cells (mean \pm SD). The red line represents the enzalutamide treatment group (n=14), and the black line represents the control group (n=13).

E. Images of endpoint tumors generated from AR-KO (KO-03 and KO-16) LNCaP cells and corresponding tumor weight and tumor incidence with *P*-values indicated. *P*-values of tumor weight and tumor incidence were calculated using unpaired Student's *t*-test and Chi-squared test, respectively.

5.4. Discussion and perspectives

Primary PCa is largely a hormone-dependent disease as the majority of tumor cells express AR and are highly androgen-dependent. Based on this observation, serum levels of PSA, a transcriptional target of AR, are routinely screened for early disease detection and disease progression, and androgen signaling remains the main therapeutic target in PCa treatment [116]. The current clinical treatment plan for PCa starts with prostatectomy and/or radiation. When post treatment serum PSA levels rise, patients are treated with first-line hormonal therapy gonadotropin-releasing hormone (GnRH) analogs. A subsequent rise in PSA level is indicative of primary CRPC (castration resistant) disease and the patient is then put on second-line castration regimens to suppress AR function (e.g., enzalutamide) and/or adrenal androgen (e.g., abiraterone). Inevitably, secondary and tertiary CRPCs will occur with shorter intervals.

Strikingly, an increase in AR⁻ tumor cells and/or tumors have been reported in metastatic and treatment failed PCa patients [2, 117]. Due to the lack of tools enabling the separation of AR⁺ and AR⁻ tumor cells, the intrinsic differences between the two subsets of PCa cells, in terms of tumor initiation and treatment response, remain to be fully understood. In an effort to overcome this deficit, we utilized recent breakthrough gene editing techniques to develop an optimized protocol for the generation of isogenic AR⁺ and AR-KO LNCaP PCa cell populations. By using ZFN and CRISPR-cas9 technology, we successfully generated AR⁺ LNCaP clonal cells harboring one tagRFP integrated *AR* allele and one wild type *AR* allele, and six AR-KO LNCaP clones. These isogenic LNCaP models, for the first time, facilitated a thorough analysis of AR heterogeneity including systematic comparisons of AR⁺ and AR⁻ PCa cell tumorigenicity

under different androgen levels, as well as treatment responses to AR antagonists *in vitro* and *in vivo*.

In an androgen-supplemented environment, AR⁺ LNCaP cells exhibited a significantly greater capacity in generating tumors than AR-KO LNCaP cells. In addition, when both cell lines were combined and implanted in androgen-proficient mice, the AR⁺ LNCaP population quickly became dominant in AD tumors, resulting in almost undetectable levels of AR-KO LNCaP cells. This observation was not surprising as LNCaP cell proliferation is largely androgen dependent. On the other hand, this data also suggested that testosterone may inhibit AR^{-/-} PCa cell proliferation through an unknown pathway. A Phase II clinical trial of Bipolar Androgen Therapy (BAT), in which metastatic CRPC patients one year post ADT were treated with superphysiologic doses of testosterone and etoposide, showed promising results in controlling CRPC progression [118]. However, the molecular mechanism behind the tumor-inhibitory effects of androgen in PCa cells remains to be fully understood.

To mimic ADT in the clinic, we further interrogated the intrinsic differences in tumor initiation capacities between the AR⁺ and AR⁻ PCa cells in castrated hosts. Approximately 40% of the AR⁺ LNCaP cells maintained the ability to initiate tumors in a 4-month span in castrated hosts (AI), compared to approximately 100% in AD hosts (Figure 5-6). On one hand, this suggests that the AR⁺ LNCaP cells are sensitive to castration. On the other hand, some AR⁺ tumors (i.e. AR-30) were equal in weight to AR-KO tumors, indicating that the AR⁺ LNCaP tumor cells may have developed resistance to castration via alternative pathways including AR overexpression. Data from previous studies has shown that around 30% of human CRPC tumors harbored AR genomic

amplification, and AR overexpression alone may be sufficient for CRPC development [43, 119, 120]. Thus, results from these experiments provided the rationale for developing novel androgen signaling antagonists for AR⁺ CRPC treatment.

Despite the obvious importance of AR signaling even in androgen deprived environments, some data also suggest that AR⁻ CRPC represents a more aggressive subset of CRPC, which may be independent of androgen signaling and resistant to the second generation of androgen antagonists [117, 121]. The need for definitive evidence supporting the role of these aggressive AR⁻ PCa cells under castration and/or anti-AR treatment, is imperative. In our experiments, isogenic AR-KO LNCaP cells showed a significant growth advantage compared to AR⁺ clonal LNCaP cells in castrated hosts by generating significantly more tumors. In addition, in competition tumor assays, AR⁻ LNCaP cells remained the dominant cell population in tumors. Together, this data not only demonstrate intrinsic higher tumorigenicity in AR⁻ LNCaP cells in AI conditions than AR⁺ LNCaP cells, it also indicates that AR⁻ clones in CRPC may arise from pre-existing AR^{-/lo} cells in primary tumors.

Further, we illustrated differential responses to treatment with enzalutamide, an AR antagonist, in AR⁺ and AR-KO LNCaP cells. As expected, AR⁺ LNCaP cells were highly sensitive, while AR-KO LNCaP cells showed non-responsiveness *in vitro* and *in vivo*. Various cell-signaling pathways accounting for AR⁻ CRPC development have been proposed. High glucocorticoid receptor (GR) was shown in enzalutamide resistant human PCa and activation of GR in LNCaP cells conferred strong resistance to enzalutamide [122]. *MYCN* gene amplification has also been noted in the AR⁻ CRPC [123]. N-myc overexpression in androgen-dependent LNCaP cells was shown to repress

AR expression, and promote neuroendocrine differentiation in tumor cells [123]. Additionally, epigenetic regulators including EZH2 [124] and SOX2 [125] were shown to facilitate the transition of AR⁺ PCa cells to AR⁻ PCa cells and promote treatment resistance. Collectively, our current research on CRPC, as well as studies from other groups, urges drug development targeting both AR⁺ and AR⁻ CRPC cells. However, there is no drug available for targeting AR⁻ cells in CRPC treatment.

The main significance of my research is, by using newly developed genetically matched AR⁺ and AR-KO PCa cell clones, to demonstrate, for the first time, the intrinsic biological and tumorigenic differences between the two PCa cell subpopulations. As AR-KO cells are refractory to anti-androgen treatment, my work suggests that the AR^{-/lo} PCa cells pre-existing in untreated tumors will likely be selected for by ADT, that AR^{-/lo} PCa cells in CRPC will evade further castration treatment, and that the real impact in treating CRPC will come from strategies to co-target both AR⁺ and AR^{-/lo} PCa cells. In the future, we aim to uncover novel therapeutics that specifically target AR⁻ PCa cells. We propose to utilize the isogenic PCa cells for large-scale small molecule and/or CRISPR-cas9 screening for potential drug targets. At the same time, we wish to answer the questions raised from current data: 1) what are potential mechanisms of the androgen induced repression of AR⁻ PCa cells? 2) How is a subset of AR⁺ PCa cells able to initiate tumors in castrated animals? 3) What pathways allow the AR-KO cells to be highly tumorigenic in castrated hosts? To answer these questions, we propose to perform RNA-seq analysis on *in vitro* culturing AR-KO and AR⁺ LNCaP cells and xenograft tumor tissues generated from the cells in AD and AI conditions. Together, we wish to shed light on the role of AR heterogeneity in CRPC and on developing novel PCa therapeutics.

Bibliography

1. Deng, Q. and Tang, D.G., *Androgen receptor and prostate cancer stem cells: biological mechanisms and clinical implications*. Endocr Relat Cancer, 2015. **22**(6): p. T209-20.
2. Liu, X., Chen, X., Rycaj, K., Chao, H.P., Deng, Q., Jeter, C., Liu, C., Honorio, S., Li, H., Davis, T., Suraneni, M., Laffin, B., Qin, J., Li, Q., Yang, T., Whitney, P., Shen, J., Huang, J., and Tang, D.G., *Systematic dissection of phenotypic, functional, and tumorigenic heterogeneity of human prostate cancer cells*. Oncotarget, 2015. **6**(27): p. 23959-86.
3. Cooper, C.S., Eeles, R., Wedge, D.C., Van Loo, P., Gundem, G., Alexandrov, L.B., Kremeyer, B., Butler, A., Lynch, A.G., Camacho, N., Massie, C.E., Kay, J., Luxton, H.J., Edwards, S., Kote-Jarai, Z., Dennis, N., Merson, S., Leongamornlert, D., Zamora, J., Corbishley, C., Thomas, S., Nik-Zainal, S., Ramakrishna, M., O'Meara, S., Matthews, L., Clark, J., Hurst, R., Mithen, R., Bristow, R.G., Boutros, P.C., Fraser, M., Cooke, S., Raine, K., Jones, D., Menzies, A., Stebbings, L., Hinton, J., Teague, J., McLaren, S., Mudie, L., Hardy, C., Anderson, E., Joseph, O., Goody, V., Robinson, B., Maddison, M., Gamble, S., Greenman, C., Berney, D., Hazell, S., Livni, N., Group, I.P., Fisher, C., Ogden, C., Kumar, P., Thompson, A., Woodhouse, C., Nicol, D., Mayer, E., Dudderidge, T., Shah, N.C., Gnanapragasam, V., Voet, T., Campbell, P., Futreal, A., Easton, D., Warren, A.Y., Foster, C.S., Stratton, M.R., Whitaker, H.C., McDermott, U., Brewer, D.S., and Neal, D.E., *Analysis of the genetic phylogeny of multifocal prostate cancer identifies multiple independent*

clonal expansions in neoplastic and morphologically normal prostate tissue. Nat Genet, 2015. **47**(4): p. 367-72.

4. Berger, M.F., Lawrence, M.S., Demichelis, F., Drier, Y., Cibulskis, K., Sivachenko, A.Y., Sboner, A., Esgueva, R., Pflueger, D., Sougnez, C., Onofrio, R., Carter, S.L., Park, K., Habegger, L., Ambrogio, L., Fennell, T., Parkin, M., Saksena, G., Voet, D., Ramos, A.H., Pugh, T.J., Wilkinson, J., Fisher, S., Winckler, W., Mahan, S., Ardlie, K., Baldwin, J., Simons, J.W., Kitabayashi, N., MacDonald, T.Y., Kantoff, P.W., Chin, L., Gabriel, S.B., Gerstein, M.B., Golub, T.R., Meyerson, M., Tewari, A., Lander, E.S., Getz, G., Rubin, M.A., and Garraway, L.A., *The genomic complexity of primary human prostate cancer. Nature*, 2011. **470**(7333): p. 214-20.
5. Haffner, M.C., Mosbruger, T., Esopi, D.M., Fedor, H., Heaphy, C.M., Walker, D.A., Adejola, N., Gurel, M., Hicks, J., Meeker, A.K., Halushka, M.K., Simons, J.W., Isaacs, W.B., De Marzo, A.M., Nelson, W.G., and Yegnasubramanian, S., *Tracking the clonal origin of lethal prostate cancer. J Clin Invest*, 2013. **123**(11): p. 4918-22.
6. Grasso, C.S., Wu, Y.M., Robinson, D.R., Cao, X., Dhanasekaran, S.M., Khan, A.P., Quist, M.J., Jing, X., Lonigro, R.J., Brenner, J.C., Asangani, I.A., Ateeq, B., Chun, S.Y., Siddiqui, J., Sam, L., Anstett, M., Mehra, R., Prensner, J.R., Palanisamy, N., Ryslik, G.A., Vandin, F., Raphael, B.J., Kunju, L.P., Rhodes, D.R., Pienta, K.J., Chinnaiyan, A.M., and Tomlins, S.A., *The mutational landscape of lethal castration-resistant prostate cancer. Nature*, 2012. **487**(7406): p. 239-43.
7. Qin, J., Liu, X., Laffin, B., Chen, X., Choy, G., Jeter, C.R., Calhoun-Davis, T., Li, H., Palapattu, G.S., Pang, S., Lin, K., Huang, J., Ivanov, I., Li, W., Suraneni, M.V., and

- Tang, D.G., *The PSA(-/lo) prostate cancer cell population harbors self-renewing long-term tumor-propagating cells that resist castration*. Cell Stem Cell, 2012. **10**(5): p. 556-69.
8. Kreso, A. and Dick, J.E., *Evolution of the cancer stem cell model*. Cell Stem Cell, 2014. **14**(3): p. 275-91.
 9. Yang, T., Rycaj, K., Liu, Z.M., and Tang, D.G., *Cancer stem cells: constantly evolving and functionally heterogeneous therapeutic targets*. Cancer Res, 2014. **74**(11): p. 2922-7.
 10. Rycaj, K. and Tang, D.G., *Cell-of-Origin of Cancer versus Cancer Stem Cells: Assays and Interpretations*. Cancer Res, 2015. **75**(19): p. 4003-11.
 11. Rybak, A.P., Bristow, R.G., and Kapoor, A., *Prostate cancer stem cells: deciphering the origins and pathways involved in prostate tumorigenesis and aggression*. Oncotarget, 2015. **6**(4): p. 1900-19.
 12. Chen, X., Rycaj, K., Liu, X., and Tang, D.G., *New insights into prostate cancer stem cells*. Cell Cycle, 2013. **12**(4): p. 579-86.
 13. Kroon, P., Berry, P.A., Stower, M.J., Rodrigues, G., Mann, V.M., Simms, M., Bhasin, D., Chettiar, S., Li, C., Li, P.K., Maitland, N.J., and Collins, A.T., *JAK-STAT blockade inhibits tumor initiation and clonogenic recovery of prostate cancer stem-like cells*. Cancer Res, 2013. **73**(16): p. 5288-98.

14. Patrawala, L., Calhoun, T., Schneider-Broussard, R., Zhou, J., Claypool, K., and Tang, D.G., *Side population is enriched in tumorigenic, stem-like cancer cells, whereas ABCG2+ and ABCG2- cancer cells are similarly tumorigenic*. Cancer Res, 2005. **65**(14): p. 6207-19.
15. Huss, W.J., Gray, D.R., Greenberg, N.M., Mohler, J.L., and Smith, G.J., *Breast cancer resistance protein-mediated efflux of androgen in putative benign and malignant prostate stem cells*. Cancer Res, 2005. **65**(15): p. 6640-50.
16. Collins, A.T., Berry, P.A., Hyde, C., Stower, M.J., and Maitland, N.J., *Prospective identification of tumorigenic prostate cancer stem cells*. Cancer Res, 2005. **65**(23): p. 10946-51.
17. Patrawala, L., Calhoun-Davis, T., Schneider-Broussard, R., and Tang, D.G., *Hierarchical organization of prostate cancer cells in xenograft tumors: the CD44+alpha2beta1+ cell population is enriched in tumor-initiating cells*. Cancer Res, 2007. **67**(14): p. 6796-805.
18. Patrawala, L., Calhoun, T., Schneider-Broussard, R., Li, H., Bhatia, B., Tang, S., Reilly, J.G., Chandra, D., Zhou, J., Claypool, K., Coghlan, L., and Tang, D.G., *Highly purified CD44+ prostate cancer cells from xenograft human tumors are enriched in tumorigenic and metastatic progenitor cells*. Oncogene, 2006. **25**(12): p. 1696-708.
19. Liu, C., Kelnar, K., Liu, B., Chen, X., Calhoun-Davis, T., Li, H., Patrawala, L., Yan, H., Jeter, C., Honorio, S., Wiggins, J.F., Bader, A.G., Fagin, R., Brown, D., and

- Tang, D.G., *The microRNA miR-34a inhibits prostate cancer stem cells and metastasis by directly repressing CD44*. Nat Med, 2011. **17**(2): p. 211-5.
20. Li, H., Chen, X., Calhoun-Davis, T., Claypool, K., and Tang, D.G., *PC3 human prostate carcinoma cell holoclones contain self-renewing tumor-initiating cells*. Cancer Res, 2008. **68**(6): p. 1820-5.
21. Domingo-Domenech, J., Vidal, S.J., Rodriguez-Bravo, V., Castillo-Martin, M., Quinn, S.A., Rodriguez-Barrueco, R., Bonal, D.M., Charytonowicz, E., Gladoun, N., de la Iglesia-Vicente, J., Petrylak, D.P., Benson, M.C., Silva, J.M., and Cordon-Cardo, C., *Suppression of acquired docetaxel resistance in prostate cancer through depletion of notch- and hedgehog-dependent tumor-initiating cells*. Cancer Cell, 2012. **22**(3): p. 373-88.
22. Dubrovskaya, A., Kim, S., Salamone, R.J., Walker, J.R., Maira, S.M., Garcia-Echeverria, C., Schultz, P.G., and Reddy, V.A., *The role of PTEN/Akt/PI3K signaling in the maintenance and viability of prostate cancer stem-like cell populations*. Proc Natl Acad Sci U S A, 2009. **106**(1): p. 268-73.
23. Miki, J., Furusato, B., Li, H., Gu, Y., Takahashi, H., Egawa, S., Sesterhenn, I.A., McLeod, D.G., Srivastava, S., and Rhim, J.S., *Identification of putative stem cell markers, CD133 and CXCR4, in hTERT-immortalized primary nonmalignant and malignant tumor-derived human prostate epithelial cell lines and in prostate cancer specimens*. Cancer Res, 2007. **67**(7): p. 3153-61.

24. Rajasekhar, V.K., Studer, L., Gerald, W., Socci, N.D., and Scher, H.I., *Tumour-initiating stem-like cells in human prostate cancer exhibit increased NF-kappaB signalling*. Nat Commun, 2011. **2**: p. 162.
25. Quigley, C.A., De Bellis, A., Marschke, K.B., el-Awady, M.K., Wilson, E.M., and French, F.S., *Androgen receptor defects: historical, clinical, and molecular perspectives*. Endocr Rev, 1995. **16**(3): p. 271-321.
26. Kerkhofs, S., Denayer, S., Haelens, A., and Claessens, F., *Androgen receptor knockout and knock-in mouse models*. J Mol Endocrinol, 2009. **42**(1): p. 11-7.
27. Simanainen, U., Allan, C.M., Lim, P., McPherson, S., Jimenez, M., Zajac, J.D., Davey, R.A., and Handelsman, D.J., *Disruption of prostate epithelial androgen receptor impedes prostate lobe-specific growth and function*. Endocrinology, 2007. **148**(5): p. 2264-72.
28. Wu, C.T., Altuwaijri, S., Ricke, W.A., Huang, S.P., Yeh, S., Zhang, C., Niu, Y., Tsai, M.Y., and Chang, C., *Increased prostate cell proliferation and loss of cell differentiation in mice lacking prostate epithelial androgen receptor*. Proc Natl Acad Sci U S A, 2007. **104**(31): p. 12679-84.
29. Niu, Y., Altuwaijri, S., Lai, K.P., Wu, C.T., Ricke, W.A., Messing, E.M., Yao, J., Yeh, S., and Chang, C., *Androgen receptor is a tumor suppressor and proliferator in prostate cancer*. Proc Natl Acad Sci U S A, 2008. **105**(34): p. 12182-7.
30. Ruizeveld de Winter, J.A., Trapman, J., Brinkmann, A.O., Boersma, W.J., Mulder, E., Schroeder, F.H., Claassen, E., and van der Kwast, T.H., *Androgen receptor*

heterogeneity in human prostatic carcinomas visualized by immunohistochemistry.

J Pathol, 1990. **160**(4): p. 329-32.

31. Masai, M., Sumiya, H., Akimoto, S., Yatani, R., Chang, C.S., Liao, S.S., and Shimazaki, J., *Immunohistochemical study of androgen receptor in benign hyperplastic and cancerous human prostates.* Prostate, 1990. **17**(4): p. 293-300.
32. Chodak, G.W., Kranc, D.M., Puy, L.A., Takeda, H., Johnson, K., and Chang, C., *Nuclear localization of androgen receptor in heterogeneous samples of normal, hyperplastic and neoplastic human prostate.* J Urol, 1992. **147**(3 Pt 2): p. 798-803.
33. van der Kwast, T.H., Schalken, J., Ruizeveld de Winter, J.A., van Vroonhoven, C.C., Mulder, E., Boersma, W., and Trapman, J., *Androgen receptors in endocrine-therapy-resistant human prostate cancer.* Int J Cancer, 1991. **48**(2): p. 189-93.
34. Sadi, M.V., Walsh, P.C., and Barrack, E.R., *Immunohistochemical study of androgen receptors in metastatic prostate cancer. Comparison of receptor content and response to hormonal therapy.* Cancer, 1991. **67**(12): p. 3057-64.
35. Ruizeveld de Winter, J.A., Janssen, P.J., Sleddens, H.M., Verleun-Mooijman, M.C., Trapman, J., Brinkmann, A.O., Santerse, A.B., Schroder, F.H., and van der Kwast, T.H., *Androgen receptor status in localized and locally progressive hormone refractory human prostate cancer.* Am J Pathol, 1994. **144**(4): p. 735-46.
36. Sadi, M.V. and Barrack, E.R., *Image analysis of androgen receptor immunostaining in metastatic prostate cancer. Heterogeneity as a predictor of response to hormonal therapy.* Cancer, 1993. **71**(8): p. 2574-80.

37. Shah, R.B., Mehra, R., Chinnaiyan, A.M., Shen, R., Ghosh, D., Zhou, M., Macvicar, G.R., Varambally, S., Harwood, J., Bismar, T.A., Kim, R., Rubin, M.A., and Pienta, K.J., *Androgen-independent prostate cancer is a heterogeneous group of diseases: lessons from a rapid autopsy program*. Cancer Res, 2004. **64**(24): p. 9209-16.
38. Davis, J.N., Wojno, K.J., Daignault, S., Hofer, M.D., Kuefer, R., Rubin, M.A., and Day, M.L., *Elevated E2F1 inhibits transcription of the androgen receptor in metastatic hormone-resistant prostate cancer*. Cancer Res, 2006. **66**(24): p. 11897-906.
39. Zhau, H.Y., Chang, S.M., Chen, B.Q., Wang, Y., Zhang, H., Kao, C., Sang, Q.A., Pathak, S.J., and Chung, L.W., *Androgen-repressed phenotype in human prostate cancer*. Proc Natl Acad Sci U S A, 1996. **93**(26): p. 15152-7.
40. Li, Z.G., Mathew, P., Yang, J., Starbuck, M.W., Zurita, A.J., Liu, J., Sikes, C., Multani, A.S., Efstathiou, E., Lopez, A., Wang, J., Fanning, T.V., Prieto, V.G., Kundra, V., Vazquez, E.S., Troncoso, P., Raymond, A.K., Logothetis, C.J., Lin, S.H., Maity, S., and Navone, N.M., *Androgen receptor-negative human prostate cancer cells induce osteogenesis in mice through FGF9-mediated mechanisms*. J Clin Invest, 2008. **118**(8): p. 2697-710.
41. Ellwood-Yen, K., Graeber, T.G., Wongvipat, J., Iruela-Arispe, M.L., Zhang, J., Matusik, R., Thomas, G.V., and Sawyers, C.L., *Myc-driven murine prostate cancer shares molecular features with human prostate tumors*. Cancer Cell, 2003. **4**(3): p. 223-38.

42. Wang, S., Gao, J., Lei, Q., Rozengurt, N., Pritchard, C., Jiao, J., Thomas, G.V., Li, G., Roy-Burman, P., Nelson, P.S., Liu, X., and Wu, H., *Prostate-specific deletion of the murine Pten tumor suppressor gene leads to metastatic prostate cancer*. Cancer Cell, 2003. **4**(3): p. 209-21.
43. Robinson, D., Van Allen, E.M., Wu, Y.M., Schultz, N., Lonigro, R.J., Mosquera, J.M., Montgomery, B., Taplin, M.E., Pritchard, C.C., Attard, G., Beltran, H., Abida, W., Bradley, R.K., Vinson, J., Cao, X., Vats, P., Kunju, L.P., Hussain, M., Feng, F.Y., Tomlins, S.A., Cooney, K.A., Smith, D.C., Brennan, C., Siddiqui, J., Mehra, R., Chen, Y., Rathkopf, D.E., Morris, M.J., Solomon, S.B., Durack, J.C., Reuter, V.E., Gopalan, A., Gao, J., Loda, M., Lis, R.T., Bowden, M., Balk, S.P., Gaviola, G., Sougnez, C., Gupta, M., Yu, E.Y., Mostaghel, E.A., Cheng, H.H., Mulcahy, H., True, L.D., Plymate, S.R., Dvinge, H., Ferraldeschi, R., Flohr, P., Miranda, S., Zafeiriou, Z., Tunariu, N., Mateo, J., Perez-Lopez, R., Demichelis, F., Robinson, B.D., Schiffman, M., Nanus, D.M., Tagawa, S.T., Sigaras, A., Eng, K.W., Elemento, O., Sboner, A., Heath, E.I., Scher, H.I., Pienta, K.J., Kantoff, P., de Bono, J.S., Rubin, M.A., Nelson, P.S., Garraway, L.A., Sawyers, C.L., and Chinnaiyan, A.M., *Integrative clinical genomics of advanced prostate cancer*. Cell, 2015. **161**(5): p. 1215-28.
44. Finones, R.R., YeARGIN, J., Lee, M., Kaur, A.P., Cheng, C., Sun, P., Wu, C., Nguyen, C., Wang-Rodriguez, J., Meyer, A.N., Baird, S.M., Donoghue, D.J., and Haas, M., *Early human prostate adenocarcinomas harbor androgen-independent cancer cells*. PLoS One, 2013. **8**(9): p. e74438.

45. Isaacs, J.T. and Coffey, D.S., *Adaptation versus selection as the mechanism responsible for the relapse of prostatic cancer to androgen ablation therapy as studied in the Dunning R-3327-H adenocarcinoma*. Cancer Res, 1981. **41**(12 Pt 1): p. 5070-5.
46. Gu, G., Yuan, J., Wills, M., and Kasper, S., *Prostate cancer cells with stem cell characteristics reconstitute the original human tumor in vivo*. Cancer Res, 2007. **67**(10): p. 4807-15.
47. Schroeder, A., Herrmann, A., Cherryholmes, G., Kowolik, C., Buettner, R., Pal, S., Yu, H., Muller-Newen, G., and Jove, R., *Loss of androgen receptor expression promotes a stem-like cell phenotype in prostate cancer through STAT3 signaling*. Cancer Res, 2014. **74**(4): p. 1227-37.
48. Jeter, C.R., Badeaux, M., Choy, G., Chandra, D., Patrawala, L., Liu, C., Calhoun-Davis, T., Zaehres, H., Daley, G.Q., and Tang, D.G., *Functional evidence that the self-renewal gene NANOG regulates human tumor development*. Stem Cells, 2009. **27**(5): p. 993-1005.
49. Jeter, C.R., Liu, B., Liu, X., Chen, X., Liu, C., Calhoun-Davis, T., Repass, J., Zaehres, H., Shen, J.J., and Tang, D.G., *NANOG promotes cancer stem cell characteristics and prostate cancer resistance to androgen deprivation*. Oncogene, 2011. **30**(36): p. 3833-45.

50. Linn, D.E., Yang, X., Sun, F., Xie, Y., Chen, H., Jiang, R., Chen, H., Chumsri, S., Burger, A.M., and Qiu, Y., *A role for OCT4 in tumor initiation of drug-resistant prostate cancer cells*. Genes Cancer, 2010. **1**(9): p. 908-16.
51. Kregel, S., Kiriluk, K.J., Rosen, A.M., Cai, Y., Reyes, E.E., Otto, K.B., Tom, W., Paner, G.P., Szmulewitz, R.Z., and Vander Griend, D.J., *Sox2 is an androgen receptor-repressed gene that promotes castration-resistant prostate cancer*. PLoS One, 2013. **8**(1): p. e53701.
52. Bisson, I. and Prowse, D.M., *WNT signaling regulates self-renewal and differentiation of prostate cancer cells with stem cell characteristics*. Cell Res, 2009. **19**(6): p. 683-97.
53. Park, I.K., Qian, D., Kiel, M., Becker, M.W., Pihalja, M., Weissman, I.L., Morrison, S.J., and Clarke, M.F., *Bmi-1 is required for maintenance of adult self-renewing haematopoietic stem cells*. Nature, 2003. **423**(6937): p. 302-5.
54. Lessard, J. and Sauvageau, G., *Bmi-1 determines the proliferative capacity of normal and leukaemic stem cells*. Nature, 2003. **423**(6937): p. 255-60.
55. Molofsky, A.V., Pardal, R., Iwashita, T., Park, I.K., Clarke, M.F., and Morrison, S.J., *Bmi-1 dependence distinguishes neural stem cell self-renewal from progenitor proliferation*. Nature, 2003. **425**(6961): p. 962-7.
56. Lukacs, R.U., Memarzadeh, S., Wu, H., and Witte, O.N., *Bmi-1 is a crucial regulator of prostate stem cell self-renewal and malignant transformation*. Cell Stem Cell, 2010. **7**(6): p. 682-93.

57. Loughran, S.J., Kruse, E.A., Hacking, D.F., de Graaf, C.A., Hyland, C.D., Willson, T.A., Henley, K.J., Ellis, S., Voss, A.K., Metcalf, D., Hilton, D.J., Alexander, W.S., and Kile, B.T., *The transcription factor Erg is essential for definitive hematopoiesis and the function of adult hematopoietic stem cells*. Nat Immunol, 2008. **9**(7): p. 810-9.
58. Ng, A.P., Loughran, S.J., Metcalf, D., Hyland, C.D., de Graaf, C.A., Hu, Y., Smyth, G.K., Hilton, D.J., Kile, B.T., and Alexander, W.S., *Erg is required for self-renewal of hematopoietic stem cells during stress hematopoiesis in mice*. Blood, 2011. **118**(9): p. 2454-61.
59. Taoudi, S., Bee, T., Hilton, A., Knezevic, K., Scott, J., Willson, T.A., Collin, C., Thomas, T., Voss, A.K., Kile, B.T., Alexander, W.S., Pimanda, J.E., and Hilton, D.J., *ERG dependence distinguishes developmental control of hematopoietic stem cell maintenance from hematopoietic specification*. Genes Dev, 2011. **25**(3): p. 251-62.
60. Tomlins, S.A., Rhodes, D.R., Perner, S., Dhanasekaran, S.M., Mehra, R., Sun, X.W., Varambally, S., Cao, X., Tchinda, J., Kuefer, R., Lee, C., Montie, J.E., Shah, R.B., Pienta, K.J., Rubin, M.A., and Chinnaiyan, A.M., *Recurrent fusion of TMPRSS2 and ETS transcription factor genes in prostate cancer*. Science, 2005. **310**(5748): p. 644-8.
61. Mosquera, J.M., Perner, S., Genega, E.M., Sanda, M., Hofer, M.D., Mertz, K.D., Paris, P.L., Simko, J., Bismar, T.A., Ayala, G., Shah, R.B., Loda, M., and Rubin, M.A., *Characterization of TMPRSS2-ERG fusion high-grade prostatic intraepithelial*

- neoplasia and potential clinical implications*. Clin Cancer Res, 2008. **14**(11): p. 3380-5.
62. Mosquera, J.M., Mehra, R., Regan, M.M., Perner, S., Genega, E.M., Bueti, G., Shah, R.B., Gaston, S., Tomlins, S.A., Wei, J.T., Kearney, M.C., Johnson, L.A., Tang, J.M., Chinnaiyan, A.M., Rubin, M.A., and Sanda, M.G., *Prevalence of TMPRSS2-ERG fusion prostate cancer among men undergoing prostate biopsy in the United States*. Clin Cancer Res, 2009. **15**(14): p. 4706-11.
 63. Casey, O.M., Fang, L., Hynes, P.G., Abou-Kheir, W.G., Martin, P.L., Tillman, H.S., Petrovics, G., Awwad, H.O., Ward, Y., Lake, R., Zhang, L., and Kelly, K., *TMPRSS2- driven ERG expression in vivo increases self-renewal and maintains expression in a castration resistant subpopulation*. PLoS One, 2012. **7**(7): p. e41668.
 64. Polson, E.S., Lewis, J.L., Celik, H., Mann, V.M., Stower, M.J., Simms, M.S., Rodrigues, G., Collins, A.T., and Maitland, N.J., *Monoallelic expression of TMPRSS2/ERG in prostate cancer stem cells*. Nat Commun, 2013. **4**: p. 1623.
 65. Wang, Q., Li, W., Zhang, Y., Yuan, X., Xu, K., Yu, J., Chen, Z., Beroukhim, R., Wang, H., Lupien, M., Wu, T., Regan, M.M., Meyer, C.A., Carroll, J.S., Manrai, A.K., Janne, O.A., Balk, S.P., Mehra, R., Han, B., Chinnaiyan, A.M., Rubin, M.A., True, L., Fiorentino, M., Fiore, C., Loda, M., Kantoff, P.W., Liu, X.S., and Brown, M., *Androgen receptor regulates a distinct transcription program in androgen-independent prostate cancer*. Cell, 2009. **138**(2): p. 245-56.

66. Craft, N., Chhor, C., Tran, C., Beldegrun, A., DeKernion, J., Witte, O.N., Said, J., Reiter, R.E., and Sawyers, C.L., *Evidence for clonal outgrowth of androgen-independent prostate cancer cells from androgen-dependent tumors through a two-step process*. Cancer Res, 1999. **59**(19): p. 5030-6.
67. Germann, M., Wetterwald, A., Guzman-Ramirez, N., van der Pluijm, G., Culig, Z., Cecchini, M.G., Williams, E.D., and Thalmann, G.N., *Stem-like cells with luminal progenitor phenotype survive castration in human prostate cancer*. Stem Cells, 2012. **30**(6): p. 1076-86.
68. Jiao, J., Hindoyan, A., Wang, S., Tran, L.M., Goldstein, A.S., Lawson, D., Chen, D., Li, Y., Guo, C., Zhang, B., Fazli, L., Gleave, M., Witte, O.N., Garraway, I.P., and Wu, H., *Identification of CD166 as a surface marker for enriching prostate stem/progenitor and cancer initiating cells*. PLoS One, 2012. **7**(8): p. e42564.
69. Wang, X., Kruithof-de Julio, M., Economides, K.D., Walker, D., Yu, H., Halili, M.V., Hu, Y.P., Price, S.M., Abate-Shen, C., and Shen, M.M., *A luminal epithelial stem cell that is a cell of origin for prostate cancer*. Nature, 2009. **461**(7263): p. 495-500.
70. Litvinov, I.V., Antony, L., Dalrymple, S.L., Becker, R., Cheng, L., and Isaacs, J.T., *PC3, but not DU145, human prostate cancer cells retain the coregulators required for tumor suppressor ability of androgen receptor*. Prostate, 2006. **66**(12): p. 1329-38.

71. Cheng, H., Snoek, R., Ghaidi, F., Cox, M.E., and Rennie, P.S., *Short hairpin RNA knockdown of the androgen receptor attenuates ligand-independent activation and delays tumor progression*. Cancer Res, 2006. **66**(21): p. 10613-20.
72. Snoek, R., Cheng, H., Margiotti, K., Wafa, L.A., Wong, C.A., Wong, E.C., Fazli, L., Nelson, C.C., Gleave, M.E., and Rennie, P.S., *In vivo knockdown of the androgen receptor results in growth inhibition and regression of well-established, castration-resistant prostate tumors*. Clin Cancer Res, 2009. **15**(1): p. 39-47.
73. Puisieux, A., Brabletz, T., and Caramel, J., *Oncogenic roles of EMT-inducing transcription factors*. Nat Cell Biol, 2014. **16**(6): p. 488-94.
74. Tam, W.L. and Weinberg, R.A., *The epigenetics of epithelial-mesenchymal plasticity in cancer*. Nat Med, 2013. **19**(11): p. 1438-49.
75. Jacob, S., Nayak, S., Fernandes, G., Barai, R.S., Menon, S., Chaudhari, U.K., Kholkute, S.D., and Sachdeva, G., *Androgen receptor as a regulator of ZEB2 expression and its implications in epithelial-to-mesenchymal transition in prostate cancer*. Endocr Relat Cancer, 2014. **21**(3): p. 473-86.
76. Jennbacken, K., Tesan, T., Wang, W., Gustavsson, H., Damber, J.E., and Welen, K., *N-cadherin increases after androgen deprivation and is associated with metastasis in prostate cancer*. Endocr Relat Cancer, 2010. **17**(2): p. 469-79.
77. Sun, Y., Wang, B.E., Leong, K.G., Yue, P., Li, L., Jhunjunwala, S., Chen, D., Seo, K., Modrusan, Z., Gao, W.Q., Settleman, J., and Johnson, L., *Androgen deprivation*

- causes epithelial-mesenchymal transition in the prostate: implications for androgen-deprivation therapy. Cancer Res, 2012. 72(2): p. 527-36.*
78. Sun, F., Chen, H.G., Li, W., Yang, X., Wang, X., Jiang, R., Guo, Z., Chen, H., Huang, J., Borowsky, A.D., and Qiu, Y., *Androgen receptor splice variant AR3 promotes prostate cancer via modulating expression of autocrine/paracrine factors. J Biol Chem, 2014. 289(3): p. 1529-39.*
79. Tanaka, H., Kono, E., Tran, C.P., Miyazaki, H., Yamashiro, J., Shimomura, T., Fazli, L., Wada, R., Huang, J., Vessella, R.L., An, J., Horvath, S., Gleave, M., Rettig, M.B., Wainberg, Z.A., and Reiter, R.E., *Monoclonal antibody targeting of N-cadherin inhibits prostate cancer growth, metastasis and castration resistance. Nat Med, 2010. 16(12): p. 1414-20.*
80. Wu, K., Gore, C., Yang, L., Fazli, L., Gleave, M., Pong, R.C., Xiao, G., Zhang, L., Yun, E.J., Tseng, S.F., Kapur, P., He, D., and Hsieh, J.T., *Slug, a unique androgen-regulated transcription factor, coordinates androgen receptor to facilitate castration resistance in prostate cancer. Mol Endocrinol, 2012. 26(9): p. 1496-507.*
81. Celia-Terrassa, T., Meca-Cortes, O., Mateo, F., Martinez de Paz, A., Rubio, N., Arnal-Estape, A., Ell, B.J., Bermudo, R., Diaz, A., Guerra-Rebollo, M., Lozano, J.J., Estaras, C., Ulloa, C., Alvarez-Simon, D., Mila, J., Vilella, R., Paciucci, R., Martinez-Balbas, M., de Herreros, A.G., Gomis, R.R., Kang, Y., Blanco, J., Fernandez, P.L., and Thomson, T.M., *Epithelial-mesenchymal transition can suppress major attributes of human epithelial tumor-initiating cells. J Clin Invest, 2012. 122(5): p. 1849-68.*

82. Fleischmann, A., Rocha, C., Schobinger, S., Seiler, R., Wiese, B., and Thalmann, G.N., *Androgen receptors are differentially expressed in Gleason patterns of prostate cancer and down-regulated in matched lymph node metastases*. Prostate, 2011. **71**(5): p. 453-60.
83. Ford, O.H., 3rd, Gregory, C.W., Kim, D., Smitherman, A.B., and Mohler, J.L., *Androgen receptor gene amplification and protein expression in recurrent prostate cancer*. J Urol, 2003. **170**(5): p. 1817-21.
84. Lu-Yao, G.L., Albertsen, P.C., Moore, D.F., Shih, W., Lin, Y., DiPaola, R.S., and Yao, S.L., *Fifteen-year survival outcomes following primary androgen-deprivation therapy for localized prostate cancer*. JAMA Intern Med, 2014. **174**(9): p. 1460-7.
85. Minner, S., Enodien, M., Sirma, H., Luebke, A.M., Krohn, A., Mayer, P.S., Simon, R., Tennstedt, P., Muller, J., Scholz, L., Brase, J.C., Liu, A.Y., Schluter, H., Pantel, K., Schumacher, U., Bokemeyer, C., Steuber, T., Graefen, M., Sauter, G., and Schlomm, T., *ERG status is unrelated to PSA recurrence in radically operated prostate cancer in the absence of antihormonal therapy*. Clin Cancer Res, 2011. **17**(18): p. 5878-88.
86. Tamburrino, L., Salvianti, F., Marchiani, S., Pinzani, P., Nesi, G., Serni, S., Forti, G., and Baldi, E., *Androgen receptor (AR) expression in prostate cancer and progression of the tumor: Lessons from cell lines, animal models and human specimens*. Steroids, 2012. **77**(10): p. 996-1001.

87. Kakarala, M. and Wicha, M.S., *Implications of the cancer stem-cell hypothesis for breast cancer prevention and therapy*. J Clin Oncol, 2008. **26**(17): p. 2813-20.
88. Li, T., Su, Y., Mei, Y., Leng, Q., Leng, B., Liu, Z., Stass, S.A., and Jiang, F., *ALDH1A1 is a marker for malignant prostate stem cells and predictor of prostate cancer patients' outcome*. Lab Invest, 2010. **90**(2): p. 234-44.
89. Liu, C. and Tang, D.G., *MicroRNA regulation of cancer stem cells*. Cancer Res, 2011. **71**(18): p. 5950-4.
90. Jin, M., Zhang, T., Liu, C., Badeaux, M.A., Liu, B., Liu, R., Jeter, C., Chen, X., Vlassov, A.V., and Tang, D.G., *miRNA-128 suppresses prostate cancer by inhibiting BMI-1 to inhibit tumor-initiating cells*. Cancer Res, 2014. **74**(15): p. 4183-95.
91. Dubrovskaya, A., Elliott, J., Salamone, R.J., Kim, S., Aimone, L.J., Walker, J.R., Watson, J., Sauveur-Michel, M., Garcia-Echeverria, C., Cho, C.Y., Reddy, V.A., and Schultz, P.G., *Combination therapy targeting both tumor-initiating and differentiated cell populations in prostate carcinoma*. Clin Cancer Res, 2010. **16**(23): p. 5692-702.
92. Rycak, K., Cho, E.J., Liu, X., Chao, H.P., Liu, B., Li, Q., Devkota, A.K., Zhang, D., Chen, X., Moore, J., Dalby, K.N., and Tang, D.G., *Longitudinal tracking of subpopulation dynamics and molecular changes during LNCaP cell castration and identification of inhibitors that could target the PSA-/lo castration-resistant cells*. Oncotarget, 2016. **7**(12): p. 14220-40.

93. Yu, D., Chen, D., Chiu, C., Razmazma, B., Chow, Y.H., and Pang, S., *Prostate-specific targeting using PSA promoter-based lentiviral vectors*. Cancer Gene Ther, 2001. **8**(9): p. 628-35.
94. Takane, K.K. and McPhaul, M.J., *Functional analysis of the human androgen receptor promoter*. Mol Cell Endocrinol, 1996. **119**(1): p. 83-93.
95. Cai, C., He, H.H., Chen, S., Coleman, I., Wang, H., Fang, Z., Chen, S., Nelson, P.S., Liu, X.S., Brown, M., and Balk, S.P., *Androgen receptor gene expression in prostate cancer is directly suppressed by the androgen receptor through recruitment of lysine-specific demethylase 1*. Cancer Cell, 2011. **20**(4): p. 457-71.
96. Doetschman, T., Gregg, R.G., Maeda, N., Hooper, M.L., Melton, D.W., Thompson, S., and Smithies, O., *Targetted correction of a mutant HPRT gene in mouse embryonic stem cells*. Nature, 1987. **330**(6148): p. 576-8.
97. Elliott, B., Richardson, C., Winderbaum, J., Nickoloff, J.A., and Jasin, M., *Gene conversion tracts from double-strand break repair in mammalian cells*. Mol Cell Biol, 1998. **18**(1): p. 93-101.
98. Hsu, P.D., Lander, E.S., and Zhang, F., *Development and Applications of CRISPR-Cas9 for Genome Engineering*. Cell, 2014. **157**(6): p. 1262-1278.
99. Kim, B.K., Boika, A., Kim, J., Dick, J.E., and Bard, A.J., *Characterizing emulsions by observation of single droplet collisions--attoliter electrochemical reactors*. J Am Chem Soc, 2014. **136**(13): p. 4849-52.

100. Urnov, F.D., Rebar, E.J., Holmes, M.C., Zhang, H.S., and Gregory, P.D., *Genome editing with engineered zinc finger nucleases*. Nature reviews. Genetics, 2010. **11**(9): p. 636-46.
101. Sanchez-Rivera, F.J. and Jacks, T., *Applications of the CRISPR-Cas9 system in cancer biology*. Nat Rev Cancer, 2015. **15**(7): p. 387-95.
102. Urnov, F.D., Rebar, E.J., Holmes, M.C., Zhang, H.S., and Gregory, P.D., *Genome editing with engineered zinc finger nucleases*. Nat Rev Genet, 2010. **11**(9): p. 636-46.
103. Szymczak, A.L., Workman, C.J., Wang, Y., Vignali, K.M., Dilioglou, S., Vanin, E.F., and Vignali, D.A., *Correction of multi-gene deficiency in vivo using a single 'self-cleaving' 2A peptide-based retroviral vector*. Nat Biotechnol, 2004. **22**(5): p. 589-94.
104. Kim, J.H., Lee, S.R., Li, L.H., Park, H.J., Park, J.H., Lee, K.Y., Kim, M.K., Shin, B.A., and Choi, S.Y., *High cleavage efficiency of a 2A peptide derived from porcine teschovirus-1 in human cell lines, zebrafish and mice*. PLoS One, 2011. **6**(4): p. e18556.
105. Yang, S., Cohen, C.J., Peng, P.D., Zhao, Y., Cassard, L., Yu, Z., Zheng, Z., Jones, S., Restifo, N.P., Rosenberg, S.A., and Morgan, R.A., *Development of optimal bicistronic lentiviral vectors facilitates high-level TCR gene expression and robust tumor cell recognition*. Gene Ther, 2008. **15**(21): p. 1411-23.
106. Koefler, H.P. and Golde, D.W., *Human myeloid leukemia cell lines: a review*. Blood, 1980. **56**(3): p. 344-50.

107. Elliott, B. and Jasin, M., *Repair of double-strand breaks by homologous recombination in mismatch repair-defective mammalian cells*. Mol Cell Biol, 2001. **21**(8): p. 2671-82.
108. Sardana, G., Jung, K., Stephan, C., and Diamandis, E.P., *Proteomic analysis of conditioned media from the PC3, LNCaP, and 22Rv1 prostate cancer cell lines: discovery and validation of candidate prostate cancer biomarkers*. J Proteome Res, 2008. **7**(8): p. 3329-38.
109. Wright, A.V., Nunez, J.K., and Doudna, J.A., *Biology and Applications of CRISPR Systems: Harnessing Nature's Toolbox for Genome Engineering*. Cell, 2016. **164**(1-2): p. 29-44.
110. Ran, F.A., Hsu, P.D., Wright, J., Agarwala, V., Scott, D.A., and Zhang, F., *Genome engineering using the CRISPR-Cas9 system*. Nat Protoc, 2013. **8**(11): p. 2281-308.
111. Shi, J., Wang, E., Milazzo, J.P., Wang, Z., Kinney, J.B., and Vakoc, C.R., *Discovery of cancer drug targets by CRISPR-Cas9 screening of protein domains*. Nat Biotechnol, 2015. **33**(6): p. 661-7.
112. Yu, J., Yu, J., Mani, R.S., Cao, Q., Brenner, C.J., Cao, X., Wang, X., Wu, L., Li, J., Hu, M., Gong, Y., Cheng, H., Laxman, B., Vellaichamy, A., Shankar, S., Li, Y., Dhanasekaran, S.M., Morey, R., Barrette, T., Lonigro, R.J., Tomlins, S.A., Varambally, S., Qin, Z.S., and Chinnaiyan, A.M., *An integrated network of androgen receptor, polycomb, and TMPRSS2-ERG gene fusions in prostate cancer progression*. Cancer Cell, 2010. **17**(5): p. 443-54.

113. Bhatia-Gaur, R., Donjacour, A.A., Sciavolino, P.J., Kim, M., Desai, N., Young, P., Norton, C.R., Gridley, T., Cardiff, R.D., Cunha, G.R., Abate-Shen, C., and Shen, M.M., *Roles for Nkx3.1 in prostate development and cancer*. Genes Dev, 1999. **13**(8): p. 966-77.
114. Liao, X., Tang, S., Thrasher, J.B., Griebeling, T.L., and Li, B., *Small-interfering RNA-induced androgen receptor silencing leads to apoptotic cell death in prostate cancer*. Mol Cancer Ther, 2005. **4**(4): p. 505-15.
115. Fu, Y., Foden, J.A., Khayter, C., Maeder, M.L., Reyon, D., Joung, J.K., and Sander, J.D., *High-frequency off-target mutagenesis induced by CRISPR-Cas nucleases in human cells*. Nat Biotechnol, 2013. **31**(9): p. 822-6.
116. Watson, P.A., Arora, V.K., and Sawyers, C.L., *Emerging mechanisms of resistance to androgen receptor inhibitors in prostate cancer*. Nat Rev Cancer, 2015. **15**(12): p. 701-11.
117. Beltran, H., Prandi, D., Mosquera, J.M., Benelli, M., Puca, L., Cyrta, J., Marotz, C., Giannopoulou, E., Chakravarthi, B.V., Varambally, S., Tomlins, S.A., Nanus, D.M., Tagawa, S.T., Van Allen, E.M., Elemento, O., Sboner, A., Garraway, L.A., Rubin, M.A., and Demichelis, F., *Divergent clonal evolution of castration-resistant neuroendocrine prostate cancer*. Nat Med, 2016. **22**(3): p. 298-305.
118. Schweizer, M.T., Antonarakis, E.S., Wang, H., Ajiboye, A.S., Spitz, A., Cao, H., Luo, J., Haffner, M.C., Yegnasubramanian, S., Carducci, M.A., Eisenberger, M.A., Isaacs, J.T., and Denmeade, S.R., *Effect of bipolar androgen therapy for*

asymptomatic men with castration-resistant prostate cancer: results from a pilot clinical study. Sci Transl Med, 2015. **7**(269): p. 269ra2.

119. Visakorpi, T., Hyytinen, E., Koivisto, P., Tanner, M., Keinanen, R., Palmberg, C., Palotie, A., Tammela, T., Isola, J., and Kallioniemi, O.P., *In vivo amplification of the androgen receptor gene and progression of human prostate cancer.* Nat Genet, 1995. **9**(4): p. 401-6.
120. Chen, C.D., Welsbie, D.S., Tran, C., Baek, S.H., Chen, R., Vessella, R., Rosenfeld, M.G., and Sawyers, C.L., *Molecular determinants of resistance to antiandrogen therapy.* Nat Med, 2004. **10**(1): p. 33-9.
121. Beltran, H., Rickman, D.S., Park, K., Chae, S.S., Sboner, A., MacDonald, T.Y., Wang, Y., Sheikh, K.L., Terry, S., Tagawa, S.T., Dhir, R., Nelson, J.B., de la Taille, A., Allory, Y., Gerstein, M.B., Perner, S., Pienta, K.J., Chinnaiyan, A.M., Wang, Y., Collins, C.C., Gleave, M.E., Demichelis, F., Nanus, D.M., and Rubin, M.A., *Molecular characterization of neuroendocrine prostate cancer and identification of new drug targets.* Cancer Discov, 2011. **1**(6): p. 487-95.
122. Arora, V.K., Schenkein, E., Murali, R., Subudhi, S.K., Wongvipat, J., Balbas, M.D., Shah, N., Cai, L., Efstathiou, E., Logothetis, C., Zheng, D., and Sawyers, C.L., *Glucocorticoid receptor confers resistance to antiandrogens by bypassing androgen receptor blockade.* Cell, 2013. **155**(6): p. 1309-22.
123. Lee, J.K., Phillips, J.W., Smith, B.A., Park, J.W., Stoyanova, T., McCaffrey, E.F., Baertsch, R., Sokolov, A., Meyerowitz, J.G., Mathis, C., Cheng, D., Stuart, J.M.,

- Shokat, K.M., Gustafson, W.C., Huang, J., and Witte, O.N., *N-Myc Drives Neuroendocrine Prostate Cancer Initiated from Human Prostate Epithelial Cells*. Cancer Cell, 2016. **29**(4): p. 536-47.
124. Ku, S.Y., Rosario, S., Wang, Y., Mu, P., Seshadri, M., Goodrich, Z.W., Goodrich, M.M., Labbe, D.P., Gomez, E.C., Wang, J., Long, H.W., Xu, B., Brown, M., Loda, M., Sawyers, C.L., Ellis, L., and Goodrich, D.W., *Rb1 and Trp53 cooperate to suppress prostate cancer lineage plasticity, metastasis, and antiandrogen resistance*. Science, 2017. **355**(6320): p. 78-83.
125. Mu, P., Zhang, Z., Benelli, M., Karthaus, W.R., Hoover, E., Chen, C.C., Wongvipat, J., Ku, S.Y., Gao, D., Cao, Z., Shah, N., Adams, E.J., Abida, W., Watson, P.A., Prandi, D., Huang, C.H., de Stanchina, E., Lowe, S.W., Ellis, L., Beltran, H., Rubin, M.A., Goodrich, D.W., Demichelis, F., and Sawyers, C.L., *SOX2 promotes lineage plasticity and antiandrogen resistance in TP53- and RB1-deficient prostate cancer*. Science, 2017. **355**(6320): p. 84-88.

Vita

Qu Deng was born in Songzi, Hubei, China on February 4th 1989, the daughter of Quanmin Deng and Yun Zhang. After completing her work at Shiyan High School, Songzi, Hubei, China in 2005, she entered Anhui Medical University in Anhui, Hefei, China. She received the degree of Bachelor of Medicine in July 2010. During the following year, she worked as a research assistant in the Center for Disease Control and Prevention, Hubei, China. In August 2011, Qu came to the United States and was admitted to the Graduate School of Biomedical Sciences (GSBS) at the University of Texas Health Science Center at Houston and the University of Texas MD Anderson Cancer Center. Qu pursued her PhD thesis research work in the laboratory of Dr. Dean Tang at the University of Texas MD Anderson Cancer Center, Science Park, Department of Epigenetics and Molecular Carcinogenesis in Smithville, Texas.

Permanent address:

Lexiang Road 67, 2nd Building 602

Sanmeng Xiaoqu,

Xinjiangkou, Hubei, China, 434200